

# The role of Extracellular Matrix in Zebrafish Cardiac Development and Regeneration

---



Dissertation  
zur Erlangung des Doktorgrades  
der Naturwissenschaften

vorgelegt beim Fachbereich 15  
der Johann Wolfgang Goethe Universität  
in Frankfurt am Main

von  
Srinath Ramkumar  
aus Chennai, Indien

Frankfurt 2022  
(D30)



vom Fachbereich Biowissenschaften (FB15) der  
Johann Wolfgang Goethe Universität  
als Dissertation angenommen.

Dekan: Prof. Dr. Sven Klimpel

Gutachter: Prof. Dr. Didier Y. R. Stainier  
Prof. Dr. Amparo Acker-Palmer

Datum der Disputation:



**Reviewers**

**Prof. Dr. Didier Y. R. Stainier, Ph.D.**

**Department of Developmental Genetics**

**Max Planck Institute for Heart and Lung Research**

**Bad Nauheim, Germany**

**&**

**Prof. Dr. Amparo Acker-Palmer, Ph.D.**

**Department of Molecular and Cellular Neuroscience**

**Institute of Cell Biology and Neuroscience**

**Johann Wolfgang Goethe University**

**Frankfurt am Main, Germany**



DEDICATED TO THE MEMORY OF MY  
DEAREST LATE GRANDFATHER  
Prof. A.K.RANGANATHAN (1933 - 2022)

Your belief and confidence in me has been a  
true source of motivation and inspiration.





# Contents

<b>DEUTSCHE ZUSSAMMENFASSUNG</b> .....	<b>1</b>
<b>ENGLISH SUMMARY</b> .....	<b>8</b>
<b>Populärwissenschaftliche Zusammenfassung</b> .....	<b>14</b>
<b>Popular Scientific Summary</b> .....	<b>15</b>
<b>CHAPTER 1 - INTRODUCTION</b> .....	<b>17</b>
<b>1.1. Development from single cell to a complex organism</b> .....	<b>17</b>
1.1.1. Cell division and growth .....	17
1.1.1.1. Cell differentiation .....	18
1.1.2. Directional Migration of cells .....	19
1.1.3. Cardiac morphogenesis and development.....	20
1.1.3.1. Early cardiovascular development .....	21
1.1.3.2. Cardiogenesis and cardiomyocyte differentiation .....	22
1.1.3.3. Looping morphogenesis and chamber ballooning .....	24
1.1.3.4. Trabeculation and Valvulogenesis.....	25

<b>1.2. Extracellular Matrix</b> .....	<b>27</b>
1.2.1. Distinction of Extracellular Matrix regions and components .....	27
1.2.1.1. Basement Membrane.....	27
1.2.2. ECM in Heart Development .....	30
1.2.2.1. Cardiac Jelly composition and structure.....	30
1.2.2.2. Laminins in the Cardiac Jelly.....	31
1.2.2.3. Hyaluronan in the Cardiac Jelly .....	32
1.2.2.4. Proteoglycans of the cardiac jelly.....	34
1.2.3. ECM Proteoglycans and signaling molecules.....	36
1.2.3.1. Agrin – a trigger for cardiomyocyte proliferation.....	36
1.2.3.2. Decorin – a jack of all trades in the Matrix.....	38
1.2.3.3. Proline Arginine Rich End Leucine Rich Repeat Protein .....	40
1.2.3.4. Bone Morphogenic Protein - 3 ( <i>bmp3</i> ).....	42
 <b>CHAPTER 2 - AIMS</b> .....	 <b>43</b>
 <b>CHAPTER 3 - MATERIALS AND METHODS</b> .....	 <b>45</b>
 <b>3.1. Materials</b> .....	 <b>45</b>
3.1.1. Organisms .....	45
3.1.1.1. Strain of Microorganism .....	45
3.1.1.2. Established Zebrafish lines used in this thesis.....	45
3.1.1.3. Zebrafish lines established in this thesis work .....	46
3.1.1.4. Zebrafish diet.....	46
3.1.2. Laboratory equipment and Consumables .....	46
3.1.2.1. Antibiotics.....	46
3.1.2.2. Antibodies .....	47
3.1.2.3. Buffers and solutions.....	48
3.1.2.4. Centrifuges .....	50
3.1.2.5. Chemicals.....	50
3.1.2.6. Enzymes.....	53

3.1.2.7. Growth Medium.....	54
3.1.2.8. Readymade kits purchased for utilization in this thesis.....	55
3.1.2.9. Common Laboratory Supplies utilized in this thesis .....	56
3.1.2.10. Microscopes .....	57
3.1.2.11. Assorted and Miscellaneous Lab Equipments.....	57
3.1.3. Oligonucleotides.....	59
3.1.3.1. Long Oligos for CRISPR/Cas9 guide mRNA .....	59
3.1.3.2. Oligos for genotyping and plasmid generation .....	60
3.1.3.3. Oligos for qPCR and sequencing .....	62
3.1.4. Plasmids .....	63
3.1.5. Softwares .....	63
3.1.6. External Services .....	64
3.1.7. Databases .....	65
<b>3.2. Methods.....</b>	<b>66</b>
3.2.1. Combinatorial analysis and identification of candidates .....	66
3.2.2. Genome Editing.....	66
3.2.2.1. Generation of zebrafish mutants using CRISPR/Cas9 mediated mutagenesis .....	66
3.2.2.2. Generation of <i>myl7:prelp-p2a-EGFP</i> Transgenic line .....	68
3.2.3. Breeding, handling and experimentation with Zebrafish.....	69
3.2.3.1. Authorization and maintenance of Zebrafish lines .....	69
3.2.3.2. Zebrafish mating and breeding .....	70
3.2.3.3. Handling and Staging of Zebrafish embryos.....	70
3.2.3.4. Microinjections of the zygote and embryos.....	71
3.2.3.5. Anesthesia and cryoinjury of adult zebrafish .....	72
3.2.3.6. Non-Invasive Echocardiography of Adult Zebrafish .....	73
3.2.3.7. Termination and humane endpoints .....	74
3.2.3.8. Adult heart dissection .....	74
3.2.4. Molecular biology and Histology.....	76

3.2.4.1. Extraction and isolation of genomic DNA.....	76
3.2.4.2. Extraction and isolation of RNA and cDNA.....	77
3.2.4.3. Agarose Gel Electrophoresis.....	78
3.2.4.4. <i>in-vitro</i> transcription for mRNA injections.....	79
3.2.4.5. PCR, qPCR and HRM.....	79
3.2.4.6. Immunofluorescence assays on whole embryos.....	81
3.2.4.7. Immunohistochemistry on heart sections.....	81
3.2.4.8. <i>in-situ</i> hybridization of zebrafish embryos.....	83
3.2.4.9. Protein extraction and Western Blot.....	84
3.2.5. Transcriptomics analysis.....	85
3.2.5.1. Embryonic heart dissection and sample preparation.....	85
3.2.5.2. Bulk-mRNA sequencing.....	86
3.2.4.3. RNA-seq data interpretation.....	86
3.2.6. Microscopy and Image processing.....	86
3.2.6.1. Mounting for live embryo imaging.....	87
3.2.6.2. Mounting for fixed samples or immunostainings.....	88
3.2.6.3. Slide imaging.....	88
3.2.6.4. Image processing in ZEN and FIJI.....	89
3.2.6.5. Segmentation and image processing in IMARIS.....	89
3.2.6.6. Laminin and Sarcomere fluorescence intensity.....	89
3.2.6.7. Actin Orientation quantification.....	90
3.2.7. Miscellaneous methods.....	91
3.2.7.1. Protein Structure prediction using Alphafold2.....	91
3.2.7.2. Statistical analyses.....	91
<b>CHAPTER 4 - Results.....</b>	<b>93</b>
<b>4.1. Mutant alleles identified.....</b>	<b>93</b>
4.1.1. Mutant alleles of genes specific to the heart.....	93
4.1.1.1. Agrin.....	93

4.1.2. Mutant alleles of genes expressed in the heart and valve .....	94
4.1.2.1. Decorin ( <i>dcn</i> ) .....	94
4.1.2.2. Bone Morphogenic Protein – 3 ( <i>bmp3</i> ) .....	95
4.1.2.4. Proline Arginine Rich End Leucine Rich Repeat Protein ( <i>prelp</i> ) .....	96
<b>4.2. Agrin in Cardiac Regeneration .....</b>	<b>97</b>
4.2.1. Borderzone CM proliferation is reduced in <i>agrnp<sup>168</sup></i> mutants at 7 dpci .....	98
4.2.2. Borderzone CM dedifferentiation remains unchanged in <i>agrnp<sup>168</sup></i> mutants at 7 dpci .....	99
<b>4.3. Decorin in cardiac development and regeneration .....</b>	<b>100</b>
4.3.1. Decorin protein accumulates in collagen rich tissues and collagen rich scar post injury .....	100
4.3.2. Decorin overexpression leads to increased myocardium thickness .....	102
4.3.3. DN Decorin overexpression leads to cardiac looping defects .....	103
<b>4.4. The role of SLRP Prelp in heart development .....</b>	<b>104</b>
4.4.1. Prelp mutants exhibit reduced <i>prelp</i> mRNA and Prelp protein .....	105
4.4.2. Prelp mutants exhibit increased pericardial edema and exhibit vascular defects .....	106
4.4.3. Prelp mutants exhibit reduced heart rate and ventricular fractional shortening .....	107
4.4.4. Prelp mutants exhibit enlarged atria at 48 hpf .....	109
4.4.5. Prelp mutants exhibit an enlarged atrium and reduced ventricle size at 72 hpf .....	110
4.4.6. Cardiac contractility does not affect atrium size in <i>prelp</i> mutants .....	111
4.4.7. Prelp mutants exhibit increased number of atrial cardiomyocytes .....	112
4.4.8. Extracellular Laminin localization is disrupted in <i>prelp</i> mutants at 36 hpf .....	113
4.4.9. Cardiac Jelly thickness and volume is increased in <i>prelp</i> mutants at 48 hpf .....	114
4.4.10. Sarcomere distribution is irregular in <i>prelp</i> mutants at 48 hpf .....	116

4.4.11. Irregular sarcomere assembly can be attributed to impaired cardiac contractility in <i>prelp</i> mutants at 48 hpf.....	117
4.4.12. Actin fiber orientation is disrupted at 36 hpf in <i>prelp</i> mutants.....	118
4.4.13. Transcriptomics analysis on <i>prelp</i> mutants .....	119
4.4.14. Reactome analysis reveals multiple downregulated genes related to ECM..	120
4.4.15. KEGG Pathway and Gene Ontology analysis on <i>prelp</i> mutants reveals downregulated ECM-receptor interactions.....	121
4.4.16. Differentially regulated genes which potentially explain <i>prelp</i> mutant phenotypes.....	122
4.4.17. Cardiomyocytes in <i>prelp</i> mutants exhibit lack of apical polarization .....	124
4.4.18. Mutant cardiomyocytes exhibit increased sharp abluminal protrusions .....	125
4.4.19. Truncated forms of Prelp generated to identify domain specific roles of Prelp .....	126
4.4.20. Truncated forms of Prelp do not rescue pericardial edema exhibited by <i>prelp</i> mutants .....	128
4.4.21. N-terminal truncated <i>prelp</i> mRNA injections partially rescue basal lamina localization in <i>prelp</i> mutants .....	129
4.4.22. N-terminal truncated <i>prelp</i> mRNA injections rescue atrial cardiac jelly volume .....	131
4.4.23. Cardiomyocyte specific <i>prelp</i> expression rescues cardiac chamber morphology in <i>prelp</i> mutants .....	133
4.4.24. Adult <i>prelp</i> mutants exhibit reduced survival, pericardial edema, enlarged atrium and retrograde blood flow .....	135
4.4.25. Extracellular Laminin organization is disrupted in adult <i>prelp</i> mutants.....	137
<b>CHAPTER 5 - Discussion .....</b>	<b>139</b>
<b>5.1. Identifying new cardiac ECM components using a combined analysis of different datasets .....</b>	<b>139</b>

<b>5.2. Understanding the role of ECM proteoglycan Agrin in cardiac regeneration</b>	<b>141</b>
<b>5.3. Decorin as a modulator of cardiac collagen crosslinking during development and regeneration</b>	<b>143</b>
<b>5.4. ECM Small Leucine Rich Proteoglycan Prelp acts as a modulator of cardiac development through the basal lamina</b>	<b>145</b>
5.4.1. <i>prelp</i> expression correlates with tissues proximal to basement membrane	145
5.4.2. <i>prelp</i> contributes to maintaining cardiovascular integrity	147
5.4.3. Proliferation, Apoptosis or SHF could contribute to increased chamber size in <i>prelp</i> mutants	148
5.4.4. Delay of ECM maturation manifests as increased Cardiac Jelly volume and loss of Laminin localization	149
5.4.5. Outside-In signaling affects epithelial cell polarity	151
5.4.6. Identification of direct binding partners of Prelp and modulators of the ECM in <i>prelp</i> mutants	153
<b>Conclusion</b>	<b>155</b>
<b>BIBLIOGRAPHY</b>	<b>156</b>
<b>APPENDIX</b>	<b>172</b>
<b>I. List of Abbreviations</b>	<b>172</b>
<b>II. Acknowledgements</b>	<b>175</b>
<b>III. Curriculum Vitae</b>	<b>178</b>





# DEUTSCHE ZUSSAMMENFASSUNG

## Einleitung

Zelle in den frühen Entwicklungsstadien eines Organismus weisen Pluripotenz auf, und im Laufe der Entwicklung des Organismus beginnen diese Zellen, sich zu differenzieren und zu wandern. Die Differenzierung ermöglicht es den Zellen, spezifische Funktionen zu entwickeln, die von den Geweben benötigt werden, und die Migration sorgt dafür, dass sich diese Zellen zum richtigen Entwicklungszeitpunkt an der richtigen Stelle befinden. Diese Prozesse sind für die Gesamtentwicklung eines mehrzelligen Organismus von entscheidender Bedeutung. Die verschiedenen Keimblätter wandern über einen Gradienten von Genexpressionslandschaften. Es hat sich gezeigt, dass die Zell-Zell-Interaktion auf verschiedene Weise erfolgt, z. B. durch autokrine, parakrine oder juxtakrine Signalübertragung, um die Zellmigration zu erleichtern. Diese Signalinteraktionen zwischen Zellen in verschiedenen Schichten erfordern Interaktionen über eine extrazelluläre Region, die als extrazelluläre Matrix (ECM) bekannt ist. Zell-ECM-Interaktionen spielen eine entscheidende Rolle bei der Gestaltung der Form des Embryos während der frühen morphogenetischen Ereignisse. Jüngste Studien haben gezeigt, dass diese Zell-ECM-Interaktionen und der anschließende gezielte Abbau der ECM verschiedene Signalwege modulieren und zur Steuerung der gerichteten Migration des embryonalen Ektoderms beitragen können (Dzamba & DeSimone, 2018; Jayadev & Sherwood, 2017; Kyprianou et al., 2020; Wu et al., 2016). Der Schlüsselfaktor für diese Prozesse ist das Vorhandensein einer spezialisierten ECM, der sogenannten Basalmembran (BM), die sich in reifem Gewebe an der Basalseite der Epithelzelle befindet und diese von der darunter

## DEUTSCHE ZUSSAMMENFASSUNG

liegenden Bindegewebsschicht trennt (Rozario & DeSimone, 2010). Die Entwicklung des Herzens erfordert eine ähnliche Interaktion zwischen den Vorläuferzellen der Kardiomyozyten und der ECM. Eine optimale Entwicklung des kardiovaskulären Systems ist für mehrzellige Organismen, insbesondere für Organismen höherer Ordnung wie Wirbeltiere, entscheidend. Herzvorläufer in Wirbeltieren wie dem Zebrafisch wandern nach der Differenzierung aus dem Epiblast über eine Schicht extrazellulärer Basalmembran zur Mittellinie (Bakkers, 2011; Rosenthal & Harvey, 2010). Diese Vorläufer bilden eine Herzscheibe an der Mittellinie, die sich zum linearen Herzschlauch ausdehnt. Es hat sich gezeigt, dass extrazelluläre Basalmembranproteine wie Fibronectin diese sehr frühen Migrationsprozesse der Kardiomyozytenvorläufer modulieren (Trinh & Stainier, 2004). In der weiteren Entwicklung des Herzens besteht die lineare Herzhöhle aus Herzmuskelzellen mit einer inneren Endokardzellauskleidung, die durch eine Schicht aus einer dicken geleeartigen Substanz, dem so genannten "Cardiac Jelly" (CJ), getrennt ist. Es hat sich gezeigt, dass die CJ, die auch als kardiale Basalmembran bezeichnet wird, verschiedene Entwicklungsereignisse während der Kardiogenese reguliert. Diese frühe CJ enthält Komponenten der Basallamina wie Laminine, Fibronectin, Hyaluronan sowie Kollagene wie Kollagen IV (Little et al., 1989).

In dieser Studie wollte ich relativ unbekannte Gene der kardialen Basalmembran identifizieren, um die Mechanismen und die Rolle von bisher unbeschriebenen ECM-Molekülen bei der Modulation der Herzentwicklung zu verstehen. Außerdem wollte ich prüfen, ob diese aus Entwicklungsdatensätzen identifizierten Gene auch im erwachsenen Herzen exprimiert werden und zu

## DEUTSCHE ZUSSAMMENFASSUNG

Prozessen wie der Herzregeneration beitragen, wobei ich den Zebrafisch als Modellsystem verwendete.

### **Ergebnisse**

Anhand verschiedener Datensätze identifizierte ich Gene, die zum Zebrafisch-Matrisom gehören und die während der Herzentwicklung exprimiert werden, und verglich sie mit Regenerationsdatensätzen. Ich erstellte eine Liste von ECM-Genen, die für die Mutagenese und das anschließende phänotypische Screening und die Analyse in Frage kommen (*agnr*, *dcn*, *bmp3*, *prelp*). Ich führte eine CRISPR/Cas9 sgRNA-vermittelte Mutagenese an diesen Genen durch, die auf verschiedene Loci abzielte. Die daraus resultierenden Mutanten wurden auf potenzielle kardiovaskuläre Entwicklungsphänotypen untersucht. Darüber hinaus beschaffte ich auch veröffentlichte Mutanten für *agnr*, die keine offensichtlichen Entwicklungsphänotypen aufwiesen, um sie für Studien zur Herzregeneration bis zum Erwachsenenalter aufzuziehen. Mit diesen Mutanten wollte ich einzigartige und unterschiedliche Rollen für diese ECM-Gene bei der Entwicklung und Regeneration des Zebrafischherzens identifizieren und aufklären.

Agrin-Mutanten, die auf die Dystroglykan-Bindungsdomäne abzielen, wiesen während der Herzentwicklung keine offensichtlichen groben morphologischen Defekte auf und waren im adulten Stadium lebensfähig. Diese Mutanten wurden bis zum Erwachsenenalter aufgezogen und kryo-verletzt. Die Herzen der Mutanten wiesen eine verringerte Proliferation der Kardiomyozyten auf, aber keinen signifikanten Unterschied in der Dedifferenzierung der Kardiomyozyten, was auf eine mögliche Rolle bei Prozessen hindeutet, die

## DEUTSCHE ZUSSAMMENFASSUNG

sich von dem durch Agrin modulierten Prozess der Herzregeneration bei Mäusen unterscheiden (Bassat et al., 2017).

Um die Rolle von Decorin zu untersuchen, wurden mittels CRISPR/Cas9-Mutagenese Mutanten erzeugt. Zusätzliche Überexpressionswerkzeuge wie WT *dcn* und Dominant Negative *dcn* (DN *dcn*) mRNA wurden verwendet, um kardiovaskuläre Entwicklungsphänotypen zu bewerten. Die Überexpression von Decorin zeigte eine erhöhte Myokardwanddicke und die mRNA-Injektion von DN *dcn* einen Verlust der kardialen Schlingenbildung während der frühen Entwicklung. Parallel dazu zeigte die Färbung mit *Dcn*-Antikörpern eine Anhäufung von Proteinen in kollagenreichen Herzgeweben, was auf eine mögliche Rolle von *Dcn* bei der Modulation von Kollagenen während der Herzregeneration hindeutet.

Prelp, ein kleines leucinreiches Proteoglykan, erwies sich als der vielversprechendste Kandidat für die Untersuchung der Rolle von ECM-SLRPs in der kardiovaskulären Morphogenese. Prelp-Mutanten wurden mithilfe der CRISPR/Cas9-Mutagenese erzeugt und etabliert. Die *prelp*-Mutanten wiesen in frühen Entwicklungsstadien ein erhöhtes Perikardödem und eine Verringerung der Hirngefäße auf. Bei näherer Betrachtung der Herzen der *prelp*-Mutanten wurden eine verringerte Herzfrequenz und eine verminderte fraktionierte Verkürzung des Ventrikels festgestellt, was auf mögliche Defekte im kardialen Erregungsleitungssystem schließen lässt. Bei der Analyse der Herzkammergröße zeigten *prelp*-Mutanten im Vergleich zu ihren WT- und Heterozygoten-Geschwistern einen vergrößerten Vorhof bei 48 hpf und 72 hpf sowie eine reduzierte Ventrikelgröße bei 72 hpf. Die

## DEUTSCHE ZUSSAMMENFASSUNG

Kammergröße in den Mutantenherzen war unabhängig von der Kontraktilität des Herzens vergrößert, weshalb die Größe und Anzahl der Kardiomyozyten genauer untersucht wurde. Die Mutanten wiesen eine erhöhte Anzahl von Vorhof-Kardiomyozyten auf, aber keine Veränderung des mittleren Internukleus-Abstandes, was auf eine normale Zellgröße, aber eine erhöhte Zellanzahl schließen lässt. Auf molekularer Ebene wurde das Augenmerk auf extrazelluläre Basalmembrankomponenten wie Laminine und Hyaluronan gerichtet. Die Lokalisierung von Laminin war in den prelp-Mutanten gestört, während gleichzeitig die Dicke und das Volumen der CJ zunahmen, was auf eine mögliche kompensatorische Rolle oder die Beibehaltung der Unreife der CJ in den prelp-Mutanten schließen lässt. In den prelp-Mutanten wurden kontraktilitätsabhängige Störungen der Sarkomerverteilung sowie Defekte der Aktfaserorientierung beobachtet. An den Herzen der prelp-Mutanten wurde im Vergleich zu ihren WT-Geschwisterherzen eine Transkriptomanalyse durchgeführt. Die mRNA-Sequenzierung des gesamten Herzens ergab eine Herunterregulierung von ECM-bezogenen Genen in den Mutanten. Die Gene-Ontology-Analyse der prelp-Mutanten ergab eine verstärkte MAPK-Signalübertragung und Zytokin-Zytokin-Interaktion in den Herzen der prelp-Mutanten sowie eine reduzierte ECM-Rezeptor-Interaktion. Interessanterweise wurden Gene, die mit dem Abbau von kardialem HA und der Reifung des CJ zusammenhängen, herunterreguliert, während Gene, die mit der epithelialen Identität der Kardiomyozyten zusammenhängen, hochreguliert wurden. Die Analyse der mutierten Herzen mit Einzelzellauflösung ergab eine erhöhte Anzahl von Mutanten, die abgerundete Kardiomyozyten und einen Verlust von apikalem Podocalyxin aufwiesen. Die Herzen der Mutanten wiesen auch eine vermehrte Ausdehnung langer

## DEUTSCHE ZUSSAMMENFASSUNG

Ausstülpungen auf, was auf einen möglichen Verlust der epithelialen Identität hindeutet, den ich als mögliche sekundäre Auswirkung des Verlusts der Basallamina-Lokalisierung und Adhäsion auf die Kardiomyozyten annahm. Abgeschnittene Formen von Prelp wurden erzeugt, um domänenspezifische Rollen für Prelp zu identifizieren, und die Wiedereinführung von N-terminal abgeschnittenem Prelp in die Mutanten rettete die Phänotypen der Basallamina-Lokalisierung und des kardialen Gallertvolumens. Eine myokardspezifische Wiederherstellung der Prelp-Expression führte zu einer deutlichen Rettung des kardiovaskulären Phänotyps der Mutante. Diese Daten deuten darauf hin, dass eine gewebespezifische Expression von Prelp nicht erforderlich ist, solange Prelp in das CJ sekretiert wird.

### **Schlussfolgerung**

Auf der Grundlage der kombinierte Analyse von verschiedene Datensätze wurden mehrere ECM-Gene identifiziert, die möglicherweise eine Rolle in der extrazellulären Mikroumgebung spielen. Dieser Ansatz zur Identifizierung und Ausrichtung von Genen für genetische Manipulationen erweist sich als wertvoller Ansatz für künftige Studien über die kardialen Entwicklungsprozesse des Zebrafisches. Ich habe festgestellt, dass die Manipulation und Interpretation von ECM-Genen aufgrund der Vielzahl extrazellulärer Interaktionen, die bei der Erzeugung mutierter Formen potenziell außer Kraft gesetzt werden könnten, besonders kompliziert ist. Ich habe auch beobachtet, dass prelp LOF-Mutanten deutliche Unterschiede in der kardialen Basalmembran aufweisen und die Reifung der CJ durch Modulation einer Vielzahl von Prozessen beeinflussen. Ich habe festgestellt, dass die Wiedereinführung der N-terminalen basischen Domäne von Prelp ausreicht,

## DEUTSCHE ZUSSAMMENFASSUNG

um den starken Verlust der Basallamina-Lokalisierung und die Veränderungen des Volumens der CJ zu lindern, was darauf hindeutet, dass die Basallamina-Lokalisierung möglicherweise aufgrund von ECM-Rezeptor-Interaktionen verloren geht, die in den Prelp-Mutanten transkriptionell herunterreguliert werden. Ich beobachtete einen Verlust der Polarität in den Kardiomyozyten, der auch das Ergebnis von Signalprozessen von außen nach innen sein könnte, und zwar durch die Interaktion der Basallamina mit Zelloberflächenrezeptoren wie Integrinen. Mit diesen Daten habe ich neue Einblicke in die Rolle der SLRP Prelp bei der Modulation der Laminin-vermittelten Herzkammermorphogenese gewonnen..

# ENGLISH SUMMARY

## **Introduction**

Cells in early developmental stages of an organism exhibit pluripotency and as the organism develops, these cells begin to undergo the processes of differentiation and migration. Differentiation enables cells to develop specific functions which are required by the tissues, and migration enables these cells to be present in the correct location at the correct developmental time. These processes are crucial to the overall development of a multicellular organism. The different germ layers migrate over a gradient of gene expression landscapes. It has been shown that cell-cell interaction occurs through various manners such as autocrine, paracrine or juxtacrine signaling to facilitate cell migration. These signaling interactions between cells in different layers require interactions over an extracellular region known as the Extracellular Matrix (ECM). Cell-ECM interactions play a crucial role in sculpting the shape of the embryo during early morphogenic events. Recent studies have shown that these cell-ECM interactions and subsequent targeted degradation of the ECM modulates various signaling pathways and acts towards guiding directional migration of the embryonic ectoderm (Dzamba & DeSimone, 2018; Jayadev & Sherwood, 2017; Kyprianou et al., 2020; Wu et al., 2016). The key factor to these processes is the presence of a specialized ECM known as the Basement Membrane (BM) which, in mature tissues, is located to the basal side of the epithelial cell separating it from the underlying connective tissue layer (Rozario & DeSimone, 2010). Development of the heart requires similar interaction between the precursor cells of cardiomyocytes and the ECM. Optimal development of the cardiovascular system is crucial to multicellular



## ENGLISH SUMMARY

organisms especially to higher order organisms such as vertebrates. Cardiac progenitors in vertebrates such as the zebrafish, migrate over to the midline after differentiation from the epiblast over a layer of extracellular basement membrane (Bakkers, 2011; Rosenthal & Harvey, 2010). These progenitors form a cardiac disc at the midline which elongates into the linear heart tube. Extracellular basement membrane proteins such as Fibronectin have been shown to modulate these very early migration processes of the cardiomyocyte progenitors (Trinh & Stainier, 2004). As the heart develops further, the linear heart tube is composed of myocardial cells with an inner endocardial cell lining separated by a layer of thick jelly like substance called the cardiac jelly. The cardiac jelly also called the cardiac basement membrane, has been shown to regulate distinct developmental events during cardiogenesis. This early CJ contains components of the basal lamina such as laminins, fibronectin, hyaluronan as well as non-fibrillar collagens such as Collagen IV (Little et al., 1989).

In this study, I aimed to identify relatively obscure genes of the cardiac basement membrane to understand the mechanisms and roles for previously undescribed ECM molecules in modulation of cardiac development. I also aimed to test whether these genes identified from developmental datasets are expressed in adult hearts and would contribute to processes such as cardiac regeneration using the zebrafish as my model system.

### **Results**

I identified genes belonging to the Zebrafish Matrisome expressed in cardiac developmental timepoints using various datasets and cross-referenced them

## ENGLISH SUMMARY

with regeneration datasets and generated a list of ECM genes as candidates for mutagenesis and subsequent phenotypic screening and analysis (*agrn*, *dcn*, *bmp3*, *prelp*). I performed CRISPR/Cas9 sgRNA mediated mutagenesis to these genes targeting different loci. The resultant mutants were screened for potential cardiovascular developmental phenotypes. In addition to this, I also procured published mutants for *agrn*, which exhibited no obvious developmental phenotypes to raise to adulthood for studies in cardiac regeneration. With these mutants, I planned to identify and elucidate unique and distinct roles for these ECM genes in development and regeneration of the Zebrafish heart.

Agrin mutants targeting the Dystroglycan binding domain exhibited no obvious gross morphology defects during cardiac development and were adult viable. These mutants were raised to adulthood and cryo-injured. Mutant hearts exhibited reduced cardiomyocyte proliferation, but no significant difference in cardiomyocyte dedifferentiation, suggesting a potential role in processes different from the murine cardiac regeneration process modulated by Agrin (Bassat et al., 2017).

To study the role of Decorin, mutants were generated using CRISPR/Cas9 mutagenesis. Additional overexpression tools such as WT *dcn* and Dominant Negative *dcn* mRNA were used to assess cardiovascular developmental phenotypes. Decorin overexpression showed increased myocardial wall thickness and mRNA injections of DN *dcn* showed loss of cardiac looping during early development. In parallel, Dcn antibody staining revealed protein

## ENGLISH SUMMARY

accumulation in cardiac collagen rich tissues, suggesting a potential role for Dcn in modulating collagens during cardiac regeneration.

Prelp, a small leucine rich proteoglycan turned out to be the most promising candidate for assessment of the role of ECM SLRPs in cardiovascular morphogenesis. Prelp mutants were generated and established using CRISPR/Cas9 mutagenesis. The *prelp* mutants revealed increased pericardial edema and reduction of brain vasculature during early developmental stages. Closer observation of *prelp* mutant hearts revealed a reduced heart rate and impaired fractional shortening of the ventricle, suggesting potential defects in the cardiac conduction system. Upon analysis of the cardiac chamber size, *prelp* mutants exhibited an enlarged atrium at 48 hpf and 72 hpf as well as a reduced ventricle size at 72 hpf compared to their WT and Heterozygous siblings. Chamber size in the mutant hearts were enlarged irrespective of contractility of the heart, and hence a closer attention was paid to size and number of cardiomyocytes. Mutants showed an increased number of Atrial cardiomyocytes, but no change in the mean internuclear distance, suggesting normal cell size, but increased number of cells. On the molecular level, attention was paid to extracellular basement membrane components such as Laminins and Hyaluronan. Laminin localization was disrupted in the *prelp* mutants along with an increase in thickness and volume of the cardiac jelly suggesting a potential compensatory role, or retention of immaturity of the cardiac jelly in the *prelp* mutants. Contractility dependent disruption of sarcomere distribution as well as actin fiber orientation defects were observed in the *prelp* mutants. Transcriptomics analysis was performed on the *prelp* mutant hearts in comparison to their WT sibling hearts. Whole heart mRNA

## ENGLISH SUMMARY

sequencing revealed downregulation of ECM related genes in the mutants. Gene Ontology analysis on *prelp* mutants revealed increased MAPK signaling and cytokine-cytokine interaction in the *prelp* mutant hearts and reduced ECM-Receptor interactions. Interestingly, genes related to degradation of cardiac HA and maturation of cardiac jelly were downregulated, and genes related to epithelial identity of cardiomyocytes were upregulated. Analysis of the mutant hearts at single cell resolution revealed increased number of mutants exhibiting rounded up cardiomyocytes and loss of apical Podocalyxin. Mutant hearts also revealed increased extension of long protrusions, suggesting a potential loss of epithelial identity, which I hypothesized to be a potential secondary effect on the cardiomyocytes from the loss of basal lamina localization and adhesion. Truncated forms of *prelp* were generated to identify domain specific roles for Prelp, and reintroduction of N-terminal truncated Prelp into the mutants rescued the basal lamina localization and cardiac jelly volume phenotypes. Myocardium specific re-establishment of *prelp* expression revealed a marked rescue of the mutant cardiovascular phenotype. These data suggest that tissue specific expression of *prelp* is not required so long as Prelp is secreted into the CJ .

### **Conclusion**

Based on the combined analysis of different datasets, multiple ECM genes were identified with potential roles in the extracellular microenvironment. This approach to identification and targeting of genes for genetic manipulation proves to be a valuable approach for future studies on zebrafish cardiac developmental processes. I observed that *prelp* LOF mutants shows marked differences to the cardiac basement membrane and impacts maturation of

## ENGLISH SUMMARY

cardiac jelly, through modulation of a plethora of processes. I noted that reintroduction of the N-terminal basic domain of the Prelp is sufficient to alleviate severe loss of basal lamina localization and changes to cardiac jelly volume, suggesting that the basal lamina localization is potentially lost due to ECM-receptor interactions, which are transcriptionally downregulated in the *prelp* mutants. Additionally, I observed a loss of polarity in cardiomyocytes, which could also be a result of outside-in signaling processes through the activity of the basal lamina on cell surface receptors such as Integrins. With these data, I have provided novel insights into the role of SLRP Prelp in modulating laminin mediated cardiac chamber morphogenesis.

## **Populärwissenschaftliche Zusammenfassung**

Unsere physische Umgebung beeinflusst uns und unsere Stimmung. Wenn es ein kalter Regentag ist, halten wir uns lieber drinnen mit einer warmen Tasse heißer Schokolade auf, und wenn es ein sonniger Tag ist, gehen wir lieber nach draußen, um etwas Sonnenlicht zu erhaschen. Genau wie wir und unsere physische Umgebung sind auch die Zellen in unserem Körper in eine Mikroumgebung eingebettet, die extrazelluläre matrix (ECM).

In dieser Studie versuche ich zu verstehen, wie Proteine in dieser ECM bei Prozessen wie der Entwicklung und möglicherweise der Regeneration des Herzens eine Rolle spielen können. Das Herz ist ein muskuläres Organ, das für alle lebenden Organismen, die einen Blutkreislauf und die Verteilung von Nährstoffen benötigen, lebenswichtig ist. Die Fähigkeit des Herzens, als konstante und ununterbrochene Pumpe zu fungieren, unterscheidet es von anderen Organen des Körpers. Die Art und Weise, wie sich das Herz entwickelt, ist rätselhaft und beinhaltet viele Prozesse in den Zellen des Herzens sowie in der ECM.

Ich habe festgestellt, dass einige Proteine dieser ECM in verschiedenen Stadien der Herzentwicklung exprimiert werden, und ich habe diese Proteine so mutiert, dass ihnen möglicherweise die Funktion der nativen Formen dieser Proteine fehlt. Mit diesem Ansatz konnte ich feststellen, dass ein solches Protein, Prelp heißt, die Reifung der extrazellulären Matrix kontrolliert und die Stimmung der Muskelzellen im Herzen während des Entwicklungsprozesses reguliert.

Mit dieser Studie zeige ich, dass die Modulation der extrazellulären Mikroumgebung die Zellen des Herzens beeinflusst, und diese Methode liefert Anhaltspunkte für weitere Studien, auf denen potenzielle therapeutische Ansätze für Patienten mit angeborenen Herzentwicklungsstörungen aufbauen können.

## **Popular Scientific Summary**

Our physical environment influences us and our mood. If it's a cold rainy day, we prefer to be indoors with a warm cup of hot chocolate, and if it's a sunny day, we prefer to go outside to catch some sunlight. Just like us and our physical environment, the cells in our body are embedded in a micro-environment called the extracellular matrix (ECM).

In this study, I attempt to understand how proteins in this ECM can play a role on the cells of the heart during processes such as development and potentially regeneration of the heart. The heart is a muscular organ vital for all living organisms which require blood circulation and nutrient distribution. The heart's ability to act as a constant and non-stopping pump differentiates it from other organs in the body. The way the heart develops is mysterious and involves many processes from the cells of the heart, as well as from the ECM.

I identified that some proteins of this ECM are expressed during different stages of the development of the heart, and I mutated these proteins such that they would potentially lack the function of their native forms. With this approach, I identified that one such protein expressed during the development of the heart called Prelp, controls the maturation of the extracellular matrix and regulates the mood of the muscle cells in the heart during the developmental process.

With this study, I show that modulation of the extracellular micro-environment influences the cells of the heart, and this method provides cues for further studies to build upon as potential therapeutic approaches for patients exhibiting congenital heart developmental defects.





# CHAPTER 1 - INTRODUCTION

## 1.1. Development from single cell to a complex organism

### 1.1.1. Cell division and growth

All complex multicellular organisms start their development as a single cell. A single cell of totipotency which undergoes successive divisions (cleavages) in a patterned manner to give rise to a cluster of cells (Fig. 1.1). These cells grow in number to reach a critical mass of cells while maintaining the pluripotency, until it forms the morula. As successive divisions take place, the cells start to migrate from the animal pole towards the vegetal pole, to form a Blastocyst, which eventually undergoes invagination in a process called gastrulation.

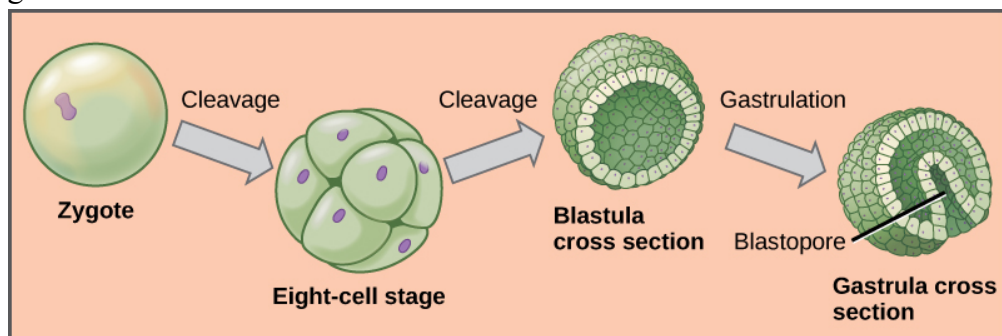


**Figure 1.1** Stages of Embryonic Development. Reprint under Creative Commons Attribution License, CC BY 4.0 (CNX OpenStax, Wikimedia Commons)

Along these processes, the pluripotent cell loses its ability to contribute to all cell layers and starts to express specific genes in a process called differentiation.

### 1.1.1.1. Cell differentiation

Differentiation enables cells to develop specific functions thereby increasing the efficiency of the organism becoming the master of one task, instead of having to be the jack-of-all-trades. As these cells specialize, they form precursor cells to major organs and tissues. Most vertebrate organisms have three major germ layers, called endoderm, mesoderm and ectoderm. The endoderm gives rise to the inner layer of the organism in tissues belonging to the digestive tract. The mesoderm gives rise to tissues belonging to the circulatory system such as the heart, blood vessels, etc. Whereas the ectoderm gives rise to the epidermis, such as skin, hair etc.

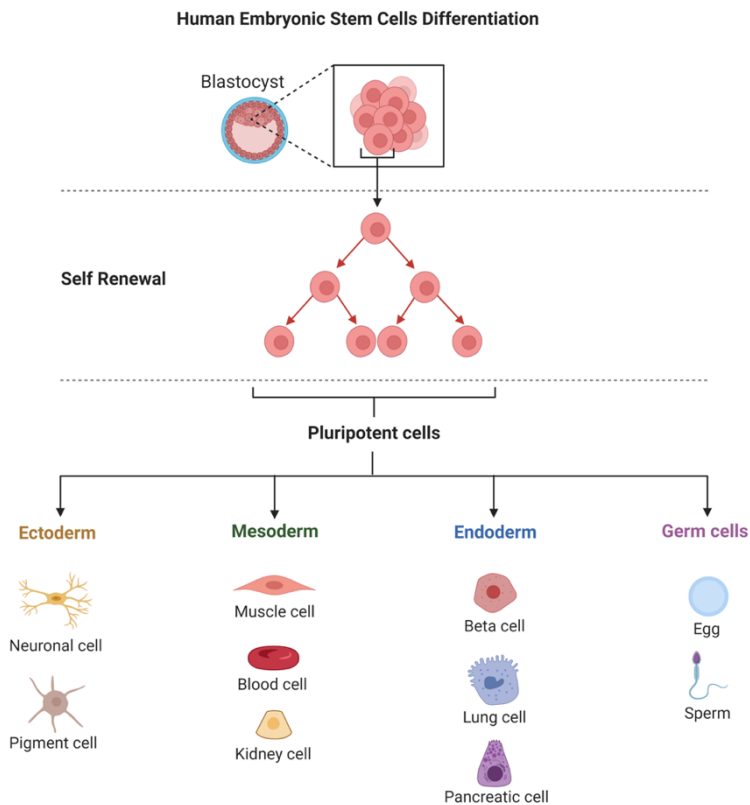


**Figure 1.2.** Human embryonic Stem cell differentiation and germ layers of the developing embryo. Created with BioRender.com. Publication License No. BU24H4X44U.

Along these processes of development, an important gradient of molecules provide directionality to the mass of cells. This gradient enables the breakage of symmetry which is an essential process in the transformation from a mass of cells to a functional embryo (Rosenthal & Harvey, 2010; Wittig & Münsterberg, 2016) .

### **1.1.2. Directional Migration of cells**

As the mass of cells migrate, they are guided by a variety of extracellular cues providing by a gradient of proteins and their respective receptors being expressed in the corresponding neighboring cell layers. These cell-cell interactions can occur through cell surface motifs, or secreted motifs. The establishment of these protein gradients provides directionality to the cells and acts as a beacon for the migrating cells (Arrington & Yost, 2009). The migration process occurs along the different axes of the embryo based on the molecular gradients and this enables the embryonic stem cells to be present in the correct location and undergo differentiation to contribute to organogenesis (Ribeiro et al., 2003). Vertebrates such as zebrafish are excellent models to study development and organogenesis due to the transparency of the embryo during these early developmental stages. The importance of directional migration during cardiogenesis has been studied in the zebrafish using genetic mutants such as mil (miles apart), bon (bonnie and clyde), nat(natter). In the mil mutant, the mutated gene is the sphingosine 1 phosphate receptor 2 (s1pr2), which binds to extracellular Sphingosine 1 phosphate and enables activation of various signaling pathways such as the PI3K-AKT signaling and NF-kb signaling pathways which enable the migration of cardiac precursors towards the midline ((J. N. Chen et al., 1996; Haffter et al., 1996; Kupperman et al.,

2000a; Stainier et al., 1996). Similarly, a mutant for a secreted ECM gene fibronectin 1a was identified to exhibit incomplete migration of myocardium precursors (Glicman Holtzman et al., 2007; Stainier et al., 1996; Trinh & Stainier, 2004; Zhao et al., 2001). These studies highlight the necessity of extracellular molecular cues, which enable and modulate the directional migration of cells to enable the formation of organs.

### **1.1.3. Cardiac morphogenesis and development**

Cardiac development is a complex and dynamic process. In terms of function, the heart is a very simple organ as it is basically a muscular pump which beats continuously throughout the lifetime of the organism. Morphogenesis and development of this simple muscular pump is nevertheless intricate and highly complex. The heart is a necessary evolutionary acquisition, as its role in distributing nutrients is a particular requirement for multicellular organisms. The heart appears morphologically different between animals in different evolutionary and taxonomical Phyla. And not too long ago, the general impression of the scientific community was that this pumping organ was acquired independently across metazoans (Rosenthal & Harvey, 2010). Only quite recently, it was established that many species across the developmental landscape share a conserved set of genes involved in the formation and organization of the body plan, and similar pathways and network of genes regulate these processes (Komuro & Izumo, 1993; Lints et al., 1993; Waardenberg et al., 2014) such as the *Csx*, and the *Nkx* homeobox domains containing genes. These evolutionarily conserved information in terms of genes and regulatory networks provide the building blocks to study the

increasingly complex structure of the pump as we move to higher Order organisms.

### 1.1.3.1. Early cardiovascular development

Early cardiovascular development hinges on the key process of cell migration as previously described. To start the process of cardiogenesis, primitive groups of cells migrate towards a midline after differentiation from the epiblast. These cells are called the cardiac progenitor cells, and they contribute to the formation of the primordium of the tubular heart (Wittig & Münsterberg, 2016). Not surprisingly, the chick embryo has been the most studied model for early cardiogenesis, due to its easy amenability to ex-ovo and in-ovo analyses of development as well as similarity to the mammalian heart (Wittig & Münsterberg, 2016, 2020).

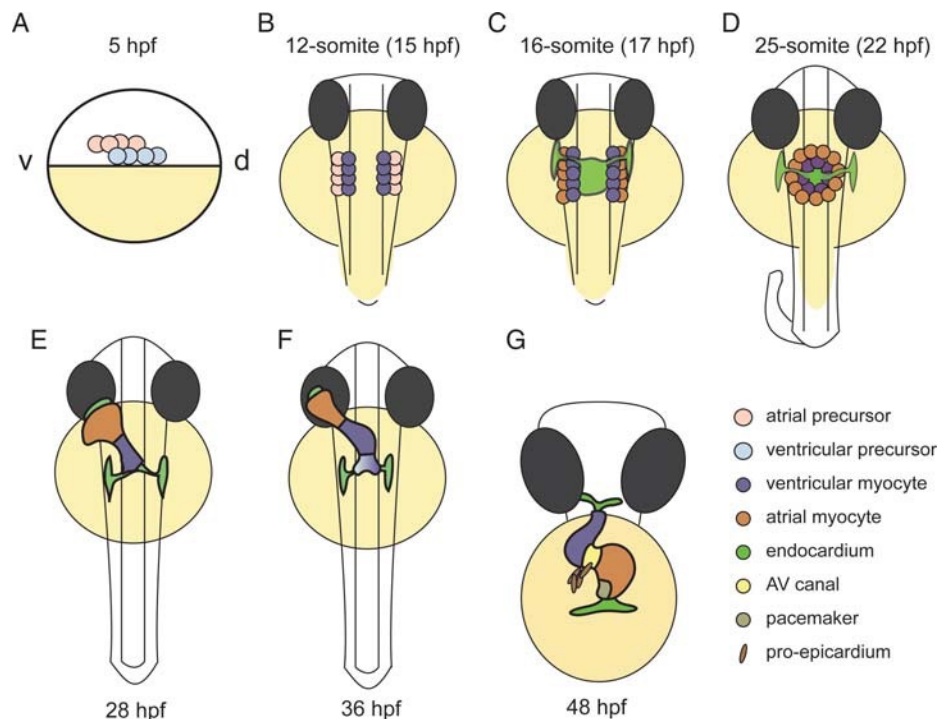


**Figure 1.4.** Stages of Cardiac development in the zebrafish ( Image reprint with permission from (Bakkers, 2011) without modification. Copyright License No: 5394290271647, Dated Sept 22, 2022)

The zebrafish as a model to study heart development offers compelling advantages due to the transparency of the embryos, ease of maintenance and

high clutch size. Unlike the chick and mammalian embryos, the zebrafish cardiac progenitors migrate to form a cardiac disc first (Fig. 1.4 D) (Bakkers, 2011; J. N. Chen et al., 1996; Stainier et al., 1996). The cardiac disc further expands into the linear heart tube as observed in mammals (Rosenthal & Harvey, 2010). In the zebrafish, progenitors of atrial and ventricular cardiomyocytes are present in the epiblast at around 5 hours post fertilization (hpf). These progenitors are present between the dorsal-ventral axis, with the atrial precursors slightly more dorsal to the ventricular precursors, as identified by cell-labelling studies (Keegan et al., 2004; Stainier et al., 1993). Identification of this group of progenitors, made this developmental stage an ideal timepoint to perform transplantation experiments, to study cell autonomous and non-autonomous properties.

### **1.1.3.2. Cardiogenesis and cardiomyocyte differentiation**

As the embryo develops, and somitogenesis begins, the progenitors migrate towards the lateral line in what is called the Anterior Lateral Plate Mesoderm (ALPM) (Fig. 1.4. B, C). These cells, expressing *nkx2.5* activated through the BMP signaling pathway start to differentiate further and express the sarcomeric myosin gene *myosin light chain polypeptide 7* (*myl7*) which was formerly known as *cmlc2* (Fig. 1.5) (Yelon et al., 1999). Interestingly, the differentiation of ventricular myocytes (expressing *vmhc* – *ventricle myosin heavy chain*) precedes the differentiation of atrial myocytes (expressing *amhc* – *atrial myosin heavy chain*) and these populations somehow maintain these properties based on a time dependent manner (Berdougo et al., 2003). At 16 somites, the cardiogenic differentiation of these cells occurs and they eventually form the cardiac disc, with the endocardial cells lining what will eventually form the

lumen of the heart (Fig. 1.4 C, D). This cardiac disc extends into the linear heart tube around prim-5 which is just after 24 hpf (Fig. 1.4 D, E).

### Cardiomyocyte Differentiation Markers

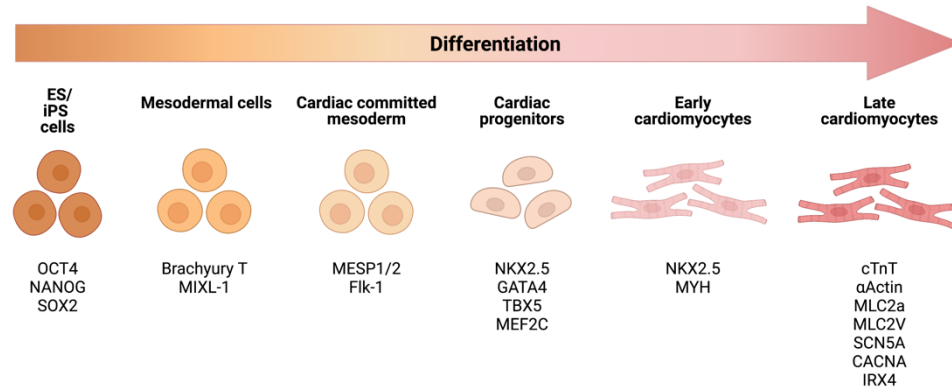


**Figure 1.5.** Cardiomyocyte differentiation markers during development. Created with BioRender.com. Publication License No. NY24H5AS23.

The migration and fusion of cardiac progenitors are influenced by neighboring tissues such as the yolk-syncytial layer (Sakaguchi et al., 2006) which was shown to secrete the ligand Sphingosine 1 Phosphate (*s1p*) which binds to the S1pr2 receptor, and enables the secretion of the ECM glycoprotein Fibronectin (*fn*) (Kupperman et al., 2000b; Osborne et al., 2008). Similarly, an ECM Proteoglycan Syndecan 2 (*sdc2*) is also required for the migration of these cells towards the midline, and a knockdown of this gene causes a reduction in Fibronectin at the extracellular space between the cardiac progenitors and the yolk-syncytial layer, thereby affecting the differentiation and polarity of these myocardial cells (Arrington & Yost, 2009). The process of migration and cardiac disk formation is symmetrical, whereas the subsequent processes such as formation and rotation of the linear heart tube, involve breaking this left-right symmetry into a dorsal-ventral organization merged with anterior-posterior axis. As a result, the cardiac tube forms maintaining its arterial pole at the midline, whereas the venous pole extends more towards the anterior side

of the embryo on top of the yolk. During this process, the epithelial identity of the myocardial cells plays a crucial role, as losing polarity arrests the heart development at the disc stage (Rohr et al., 2006, 2008).

### **1.1.3.3. Looping morphogenesis and chamber ballooning**

The next major developmental process is the looping and ballooning of the cardiac chambers. As the heart tube forms, it forms a slight bend towards the right side of the embryo, such that the future atrium would be positioned to the left of the midline, whereas the future ventricle is positioned more towards the right of the embryo's midline (Fig. 1.4 E,F). The venous pole of the heart experiences an increased amount of rotation and torsion whereas the arterial pole does not exhibit much rotation. This difference alone has been hypothesized to drive dextral/sinistral looping of the heart, whereas molecular data on drivers of this process remain unclear (Maenner, 2009). As looping occurs, the chambers of the heart begin to exhibit distinct morphological features as they appear to develop this kidney-bean shaped appearance with a distinct outer curvature and inner curvature. This morphology is clearly observed as early as prim - 25 (36 hpf), but the molecular expression marker Natriuretic peptide (*nppa*) for the outer curvature is first detected much earlier at 28 hpf (Auman et al., 2007). Contractility of the heart as well as blood flow act as additional factors to promote the ballooning of the chambers as the cardiomyocytes develop a cuboidal and elongated shape along the axis of the outer curvature, and subsequently provides the necessary convex shape to the outer curvature of the ventricle of the heart (Auman et al., 2007).



### 1.1.3.4. Trabeculation and Valvulogenesis

As the organism grows, the requirement of blood and nutrients to peripheral tissues increases, which requires the heart to improve pumping efficiency. This is accomplished by the development of trabeculae and valves in the heart (Fig. 1.6 A, B). The onset of cardiac trabeculation enables the heart to pump blood with an increased amount of force and the atrioventricular valve enable unidirectional blood flow between the chambers of the heart.

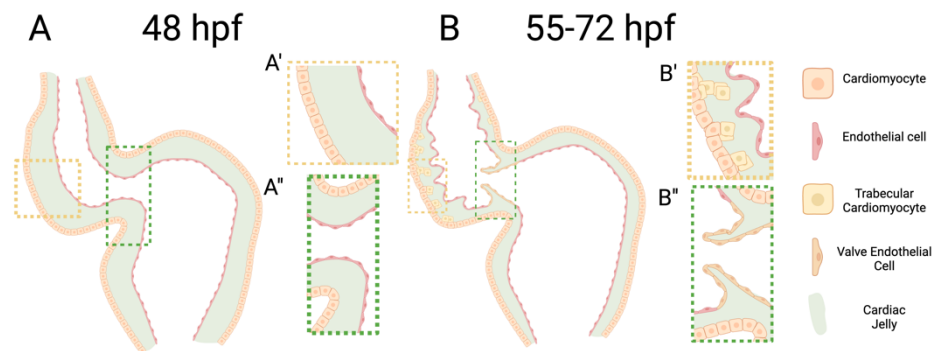


**Figure 1.6.** Diagrammatic representation of trabeculation and valvulogenesis of the zebrafish heart between 48 hpf (A) and 55-72 hpf (B). Created with BioRender.com. Publication license no: FB24H6RLVY.

The process of trabeculation is a key component of heart development and has some distinct differences between the mammalian models and vertebrate models (C. C. Chen et al., 2008; Wu, 2018). The onset of trabeculation is influenced by the activation of specific pathways in endocardium and myocardium, and this crosstalk is mediated by the cardiac jelly (Fig 1.6 A', B'). The onset of trabeculation is triggered by cardiac contractility, which triggers secretion of molecules by the activated endocardium such as *Nrg2a*, as they reach the myocardium and activate signaling pathways such as ErbB2 signaling (Rasouli & Stainier, 2017). Additionally, degradation of the cardiac jelly is required for endocardial cell to extrude protrusions modulated by Tie 2 and Apelin signaling to reach the myocardium to trigger the formation of trabecular units (Qi et al., 2022; Qu et al., 2019). The cardiomyocytes which

## CHAPTER 1 - INTRODUCTION

leave the myocardial epithelium, lose their apicobasal polarity and adhesion to their neighbors, and undergo an Epithelial to mesenchymal-like Transition to become trabecular cardiomyocytes (Jiménez-Amilburu et al., 2016; Jiménez-Amilburu & Stainier, 2019). Recent studies have also shown that some endocardium independent processes such as crowding of cardiomyocytes upon proliferation and the resultant onset of heterogenous tension in the myocardial wall trigger the delamination process of the cardiomyocytes (Priya et al., 2020). Additionally, maintaining the integrity of the myocardial wall requires activation of Fgf signaling downstream of flow responsive factors such as Klf2 (Rasouli et al., 2018) as well as suppression of intermediate filament genes, such as Desmins by EMT transcription factor Snail (Gentile et al., 2021). These studies elucidate the onset of various signaling pathways and molecular mechanisms crucial to the development of the heart. The onset of valvulogenesis further improves the efficiency of the beating heart by preventing retrograde blood flow (Fig 1.6 A'', B''). This process regulated by shear stress on endocardium of the atrioventricular canal as a result of blood flow, as well the formation of the endocardial cushions (Camenisch et al., 2001; Steed et al., 2016). Furthermore, ECM mediated interaction with endocardial cell surface integrins to form focal adhesions drive valvulogenesis (Gunawan et al., 2019). These valves formed by specialized valve endothelial cells express transcription factors such as Nfatc1, which promotes an EndoMT like process to form the valve interstitial cells (Gunawan et al., 2020), which enables the maturation of the valve leaflets as the heart grows (Hulin et al., 2019).

## **1.2. Extracellular Matrix**

Extracellular matrix is a complex and dynamic environment. Previously, the ECM was considered a passive conduit providing structural support, anchoring of cells and acting as a hub for various growth factors(Hynes, 2009). Only recently, direct and active roles for various components of the ECM have been uncovered (Frantz et al., 2010; Hocking et al., 1998; Lockhart et al., 2011; Naba et al., 2016; Neill et al., 2012; Rienks et al., 2014).

### **1.2.1. Distinction of Extracellular Matrix regions and components**

The ECM is also distinct and unique in composition, as it exhibits a stratified layering of different proteins, each with specific function and crosstalk across the different layers. The ECM found in different tissues exhibit different types of stratifications. This stratified nature of ECM permits these extracellular layers found next to epithelial tissues to be subcategorized as basement membrane and interstitial matrix.

#### **1.2.1.1. Basement Membrane**

The basement membrane is as the name suggest a membrane like dense ECM layer found to the basal side of the epithelial tissues. It is a unique ECM which is renowned to separate any epithelial cell layer from its neighboring connective tissue layer. It is composed of various types of laminins, collagens and nidogens which interact with large cell membrane receptors such as integrins, dystroglycans as well as smaller transmembrane receptors such as Fibronectin Leucine Rich transmembrane Proteins (FLRTs). Proteomics studies of the Basal Lamina has been limited and curtailed due to severe limitations which arise due to dynamic range of quantification of these

extracellular components due to their large size (Calve et al., 2020; de Sá Schiavo Matias et al., 2022; Li et al., 2022; Pokhilko et al., 2021).

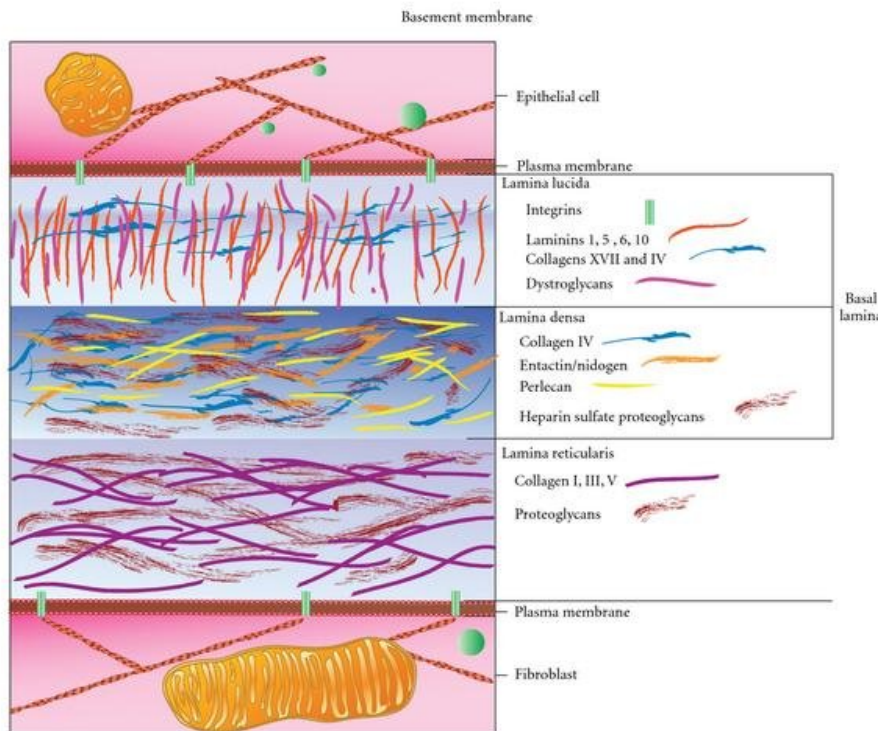


**Figure 1.7 Basement Membrane distinction and components.** Figure reprinted under a Creative Commons Attribution License from (Menter & Dubois, 2012)

The basement membrane is further subdivided into the basal lamina (BL) and the reticular lamina (RL). The BL consists of the lamina lucida and the lamina densa, each distinguished by the proximity of the region to the neighboring epithelial cell and composition of laminins and specific collagens (Zhang et al., 2021).

The lamina lucida typically consists of laminins forming heterotrimers and assembling into a mesh like structure called the laminin lattice (Colognato & Yurchenco, 2000). The existence of lamina lucida as a distinct layer of the BL has come under scrutiny due to limitations of microscopy techniques, nevertheless, for the sake of this study, we continue to use the established terminology (Chan & Inoue, 1994).

## CHAPTER 1 - INTRODUCTION

The lamina densa typically consists of various proteoglycans harboring heparan sulphate side chains, among which a major constituent being Perlecan. The lamina densa also consists of non-fibrillar collagens such as Collagen IV, commonly called basement membrane collagen (Mak & Mei, 2017). Various proteins of the lamina densa exhibit distinct laminin-binding properties and lead to maturation and stabilization of the laminin lattice (Charonis et al., 1985; Laurie et al., 1983).

The region of the basement membrane closest to connective tissues and farther away from the epithelial tissue is known as the reticular lamina, or *lamina reticularis*. This region contains large fibrillar structures formed by multimerization of Collagens such as Collagen I and Collagen II, which provide the necessary rigidity and stability to the tissue through cross linking (Exposito et al., 2010; Pakshir et al., 2019). As shown by various expression datasets, genes of this regions are expressed in increased amounts from the connective tissue cells such as fibroblasts as opposed to epithelial tissues (Pakshir et al., 2019).

### **1.2.2. ECM in Heart Development**

Heart development like any major developmental process relies heavily on intricate coordination of various processes. These processes include distinct modulation of various signaling pathways which are activated and deactivated in a time dependent manner. These signaling interactions are expertly controlled and regulated through tissue interaction and crosstalk through the developing cardiac ECM known as the cardiac jelly.

#### **1.2.2.1. Cardiac Jelly composition and structure**

The early developing cardiac ECM or cardiac jelly (CJ) is a fluidic entity with a high degree of affinity towards water and rich in growth factors and signaling molecules (Männer & Yelbuz, 2019; Thureson-Klein & Klein, 1971). This fluidity manifests in a jelly like morphology which was originally observed in the avian developmental model and named cardiac jelly nearly a 100 years ago by Davis C.L. in 1924, in the Anatomical Record (Davis CL, 1924). Further studies began to show the functional significance of the cardiac jelly (Barry, 1948). As technology developed and electron microscopy techniques began to gain popularity, studies emerged attempting to show the ultrastructure of various molecules in the cardiac jelly based on distribution of charged Sodium and magnesium ions (Thureson-Klein & Klein, 1971). Researchers further attempted to dissect the cardiac jelly from the embryonic heart, to understand its potential influence on the shape and structure of the heart (Nakamura & Manasek, 1978, 1981).

These studies conducted over 50 years ago began to establish the importance of CJ as a regulator of heart development. These studies proceeded to encourage future researchers to question the protein composition of the CJ and

provided potential ideas to manipulate these individual components to further our understanding of cardiac development.

Limitations due to lack of suitable technologies prevented detailed studies of these processes until closer to the turn of the century (Little et al., 1989; Nakajima et al., 1997). Eventually researchers regained interest in the CJ upon widespread adoption of advanced light microscopy techniques (del Monte-Nieto et al., 2018; Derrick et al., 2022; Grassini et al., 2018; K. H. Kim et al., 2018; Männer & Yelbuz, 2019). These publications began to exhibit interesting new modulators of the CJ such as Notch1 and Nrg1, as well as elucidated tissue specific activation or repression of signaling pathways through extracellular Angiopoetin1 and Hapln1a which controlled CJ dynamics during heart development (Derrick et al., 2022; K. H. Kim et al., 2018).

A lack of cardiac jelly enriched proteomics studies shows that albeit interest in modulation of the jelly exists, primary focus has been on large previously discovered components such as Hyaluronan, Fibronectin, Laminins and Collagens.

### **1.2.2.2. Laminins in the Cardiac Jelly**

Laminins form a mesh facing both endocardium and myocardium in the cardiac basement membrane during early development. They are found as heterotrimers consisting of Alpha chains, Beta chains and Gamma chains encoded by the *lama(s)*, *lamb(s)* and *lamc(s)* genes in vertebrates. In mammals, five alpha chains (LAMA1, 2, 3, 4, 5) four beta chains (LAMB1, 2, 3, 4) and three gamma chains (LAMC1, 2, 3) have been detected. These subunits form heterotrimers where the Alpha chain provides tissue specificity as it interacts directly with the epithelial tissue surface integrins and laminin receptors using its C-Terminal globular domain (Laminin-G domain), whereas

the Beta and Gamma chains enable multimerization and stabilization (Fig. 1.8). The multimerization and self-assembly processes occur extracellularly and is assumed to be independent of external factors except pH (Freire & Coelho-Sampaio, 2000).

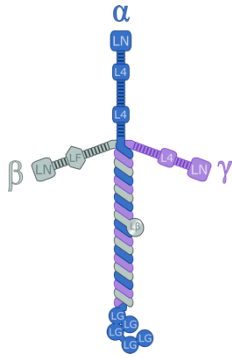


**Figure 1.8** Laminin heterotrimer consisting of an  $\alpha$  chain in blue,  $\beta$  chain in pale green and  $\gamma$  chain in lavender. Image reprint under CC-BY 4.0 license, (Gad Armony, 2017)

In the zebrafish heart, expression datasets show expression of four alpha subunits (*lama1*, *lama2*, *lama4*, *lama5*), three beta subunits (*lamb1*(*lamb1a*, *lamb1b*), *lamb2*, *lamb4*) and all three gamma subunits (*lamc1*, *lamc2*, *lamc3*) (this study). A recent study has claimed tissue specific expression of laminins in the heart where *lama4* and *lamb1b* are expressed specifically in the endocardium, *lama5* and *lamb2* are expressed specifically in the myocardium and *lamb1a* and *lamc1* are expressed in a pan-cardiac manner (Derrick et al., 2021) based on fluorescence *in-situ* hybridization data. The same study also showed that mutating *lamb1a* increased SHF addition to the venous pole of the heart in a contractility dependent manner suggesting that specific laminins may have different and distinct roles in the cardiac jelly during developmental processes.

### 1.2.2.3. Hyaluronan in the Cardiac Jelly

Alongside large proteins such as Laminins and Collagens, Hyaluronan also known as Hyaluronic Acid is a key component of the CJ. It is responsible for various unique physical properties exhibited by the CJ. HA is a Glycosaminoglycan (GAG) and is produced by specific enzymes located on the plasma membrane called Hyaluronan Synthases (Has). Since HA is not synthesized like proteins in vesicles, it does not have a protein core, and hence



## CHAPTER 1 - INTRODUCTION

to detect HA in the cardiac jelly, special proteins are used as proxies, known as Hyaluronan binding proteins. Neurocan is an example of a protein with a Hyaluronan binding domain, which was cloned and tagged to detect extracellular HA in zebrafish (Grassini et al., 2018).

The HA found in cardiac jelly is secreted by the Enzyme encoded by the gene *has2*. It has been shown that the secreted HA takes part in creating an environment with high affinity towards water and promotes the formation of a matrix with lower resistance such that cells embedded in this HA rich matrix have higher ability to be motile (Pang et al., 2021). This water retention property of Hyaluronan is key for various developmental processes such as the formation of the endocardial cushions and valvulogenesis (Rosenthal & Harvey, 2010). Has2 mediated HA synthesis is responsible for various processes in the embryonic heart including processes such as EMT (Camenisch et al., 2000). Another enzyme responsible for HA synthesis in zebrafish is the uridine 5'-diphosphate(UDP)-glucose dehydrogenase and the mutant of this enzyme called *Jekyll* exhibits defects with valvulogenesis suggesting a major role for the biosynthesis and activity of HA in the cardiac jelly (Walsh & Stainier, 2001). Interestingly, timely degradation and reduction of HA is also important during early development (de Angelis et al., 2017; Grassini et al., 2018). This reduction of cardiac HA enables increased proximity and signaling crosstalk between the endocardium and myocardium(Camenisch et al., 2001; de Angelis et al., 2017; del Monte-Nieto et al., 2018; Hällgren et al., 1990; Totong et al., 2011).

### 1.2.2.4. Proteoglycans of the cardiac jelly

A third and major group of proteins found in the ECM are Proteoglycans (PG). PGs are found both in the basal lamina and reticular lamina of the basement membrane. In the Reticular Lamina (RL), many proteoglycans are found which are associated with fibrillar collagens such as Class I Small Leucine Rich Proteoglycans (SLRPs) (Decorin, Biglycan, Lumican, etc.) (Fig. 1.9).

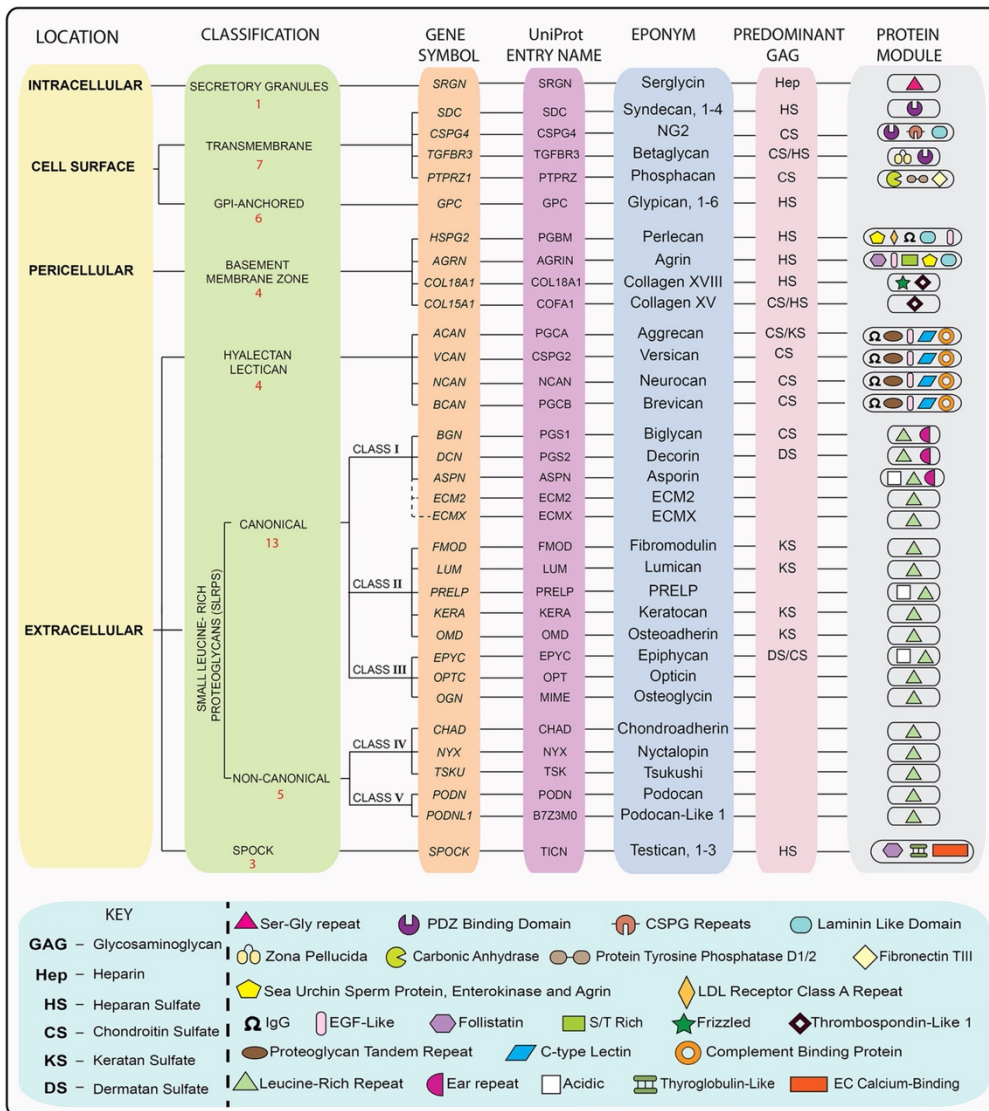


**Figure 1.9** Comprehensive nomenclature of Proteoglycans from “Proteoglycans form and function: A comprehensive nomenclature of proteoglycans” (Iozzo & Schaefer, 2015). Reuse authorized under a Creative Commons attribution license CC-BY 4.0.

These RL proteoglycans exhibit an increased association to Chondroitin Sulphate (CS), and Dermatan Sulphate (DS) side chains of large PGs. Large

## CHAPTER 1 - INTRODUCTION

proteoglycans found in the RL include CS PGs such as Versican, Aggrecans and Neurocans (Fig. 1.9). Additionally, smaller Proteoglycans such as Fibromodulin and Lumican are also present in the Reticular Lamina with association to Keratan Sulphate (KS) side chains. The different glycosaminoglycans (GAGs) associated with these Proteoglycans enable easier classification of the various extracellular players (Fig. 1.9).

In the Basal Lamina, an increasing number of Proteoglycans are detected which exhibit association with Heparan Sulphate (HS) as opposed to CS, DS or KS (Fig. 1.9). Key players in the Basal Lamina are the large HSPGs known as Perlecan and Agrin. Perlecan, known as HSPG2, is a major contributor to the Basal Lamina and exhibits associations with cell surface integrins, as well as Collagens of the Lamina Densa. Perlecan has been described to exhibit activity related to Angiogenesis, Fibroblast Growth Factor (FGF) sequestration, as well as promoting mitogenesis (Aviezer et al., 1994; Costell et al., 1999; Ocken et al., 2020). Additionally, Perlecan exhibits direct binding activity to Laminins, as well as the Class II SLRP, PRELP (Bengtsson et al., 2002; Laurie et al., 1983).

In the CJ, the exact composition, location and associations of the different PGs has not yet been studied in a detailed manner. Hypotheses about the roles of PGs in the CJ range from potential modulators of crosstalk, potential regulators of Basement Membrane integrity and anchoring, as well as potential orchestrators of tissue maturation through enhancing ligand-receptor interactions, or through inhibition of ligand-receptor interactions (D. Chen et al., 2020; Iozzo & Schaefer, 2015; Moorehead et al., 2019). Additional hypotheses about CJ maturation and degradation can also be made based on activity of proteoglycans in the other tissues and developmental models. But

at the moment, there is a paucity of knowledge about specific Proteoglycan interactions and activity in the cardiac jelly during cardiac morphogenesis.

### 1.2.3. ECM Proteoglycans and signaling molecules

At the outset of this study, various cardiac specific genes were identified with potential roles in both development and regeneration. Identification and modulation of genes belonging to the matrisome were prioritized. Detailed introduction to these genes are provided below as emphasis.

#### 1.2.3.1. Agrin – a trigger for cardiomyocyte proliferation

The ECM PG Agrin is one of the few large Proteoglycans involved in the basement membrane of the heart. Agrin consists of an N-Terminal domain which exhibits laminin binding activity, and a C-Terminal part containing Laminin Globular (LG) domains which exhibit binding with cell surface Laminin receptors such as Dystroglycan and Agrin receptors (Fig. 1.10).

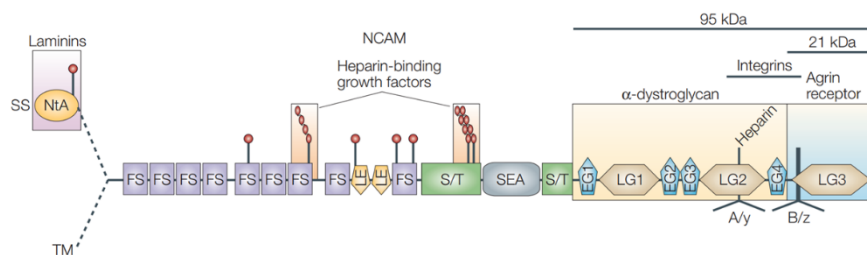


**Figure 1.10** Graphical representation of Agrin and its various domains. Reprint in this thesis under copyright License no. 5397850364228 from *Nat. Rev. Mol. Cell. Biol.*

Agrin is highly expressed by neurons forming neuromuscular junctions (NMJs) and acts as a key regulator of Acetylcholine receptor (AChR) clustering in the NMJ, by binding to LRP4/MuSK complex (Hopf & Hoch, 1996; Walker et al., 2021). Additionally, Agrin also has very detailed description of roles in synaptic development and formation of neuromuscular synapses (Bezakova &

## CHAPTER 1 - INTRODUCTION

Ruegg, 2003; Choi et al., 2013; Daniels, 2012; Tezuka et al., 2014). In the heart, the existence of neuromuscular junctions is debated, but innervation of the heart is key in regulation of the cardiac conduction system(Fukuda et al., 2015). Recent surprising findings have shown that Agrin promotes cardiomyocyte proliferation in the murine and porcine hearts post myocardial infarction(Baehr et al., 2020; Bassat et al., 2017). Agrin binding to cardiomyocyte cell surface receptor Dystroglycan leads to increased proliferation of cardiomyocytes through increased YAP nuclear translocation and Dystrophin mediated disassembly of the contractile units of the cardiomyocyte (Bassat et al., 2017). In the zebrafish, Agrin's role has been primarily studied to understand motor axon growth and neuromuscular synapse formation (M. J. Kim et al., 2007; Walker et al., 2021). Although *agrln* is expressed in high amounts in the heart as well as other tissues during development, studies with morpholinos have focused preliminarily on gross morphological defects related to posterior elongation of the embryos (M. J. Kim et al., 2007). A recent short publication showed an increased expression of Agrin the adult zebrafish heart post cryo-injury and claimed induction of transient p53 mediated epicardial senescence (Sarig et al., 2019). The role of Agrin in modulating zebrafish cardiovascular development or regeneration is still not clear.

### 1.2.3.2. Decorin – a jack of all trades in the Matrix

Decorin is a Class I SLRP which gains its name by the way it “decorates” fibrillar collagen at a regular interval of about 67nm (J. E. Scott, 1988). The reason Decorin has been called a jack of all trades is due to the variety of extracellular roles described for Decorin in various contexts.



**Figure 1.11.** Crystal Structure of Dcn from RCSB PDB (rcsb.org) of PDB 1XEC deposited by P. G. Scott et al., 2004.

A preliminary reason for the high number of published literature describing different roles for Decorin is the early discovery, high survival and mild phenotype of the Decorin null mutant mice, which was originally described to exhibit abnormal sub-cutaneous collagen morphology and skin fragility (Danielson et al., 1997). Since then, using this null Decorin mutant mice, many studies have come out showcasing the role of Decorin as a modulator of collagen fibril formation (Rühland et al., 2007), as a regulator of angiogenesis and promoter of wound healing (Järveläinen et al., 2006), as a controller of inflammation (Merline et al., 2011), as a regulator of embryonic fibroblast migration, and controller of fibroblast adhesion and proliferation (Ferdous et al., 2010). Multiple studies have also suggested various roles for Decorin in remodeling the extracellular microenvironment post myocardial infarction reviewed by Weis et al. in 2005. Expression of Murine *Dcn* has also been shown to occur downstream of TNF $\alpha$  signaling in some contexts, and to have notable involvement in various signaling pathways through sequestering Tgf $\beta$  ligand and direct interaction with Vegf receptors, etc. (Gubbiotti et al., 2016; Järveläinen et al., 2015; Järvinen & Prince, 2015; Mauviel et al., 1995; Neill et al., 2012, 2016; Schönherr et al., 2001).

## CHAPTER 1 - INTRODUCTION

Not surprisingly, zebrafish Decorin has also been shown to regulate the non-canonical Wnt-Signaling and play a role in the convergent extension during development (Zoeller et al., 2009).

An interesting role for Decorin in Congenital Stromal Corneal Dystrophy occurring in a hereditary manner in human patients showed a unique mutation to *DCN*, leading to loss of the C-Terminal ear repeat of DCN. This mutation was hypothesized to elicit a dominant negative activity of the mutant protein (S. Chen et al., 2011). This was further characterized by the discovery that the mutant form of Decorin gets retained intracellularly and causes stress in the Endoplasmic Reticulum (Bredrup et al., 2005; S. Chen et al., 2011, 2013; J. H. Kim et al., 2011). A zebrafish model expressing this mutant form of Decorin has not been described. Based on the above information, it I feel it is fair to call Decorin “A jack of all trades” in the ECM.

### 1.2.3.3. Proline Arginine Rich End Leucine Rich Repeat Protein

PRELP is a Class II SLRP, also known as Prolargin. Its unique name arises from the fact that the N-terminus of PRELP is enriched with amino acids exhibiting basic properties (Bengtsson et al., 1995). The basicity of the N-Terminus of PRELP, enables it to bind to heparin and heparan sulphate. Additionally, this basicity leads to unique ability to interact with Tyrosine-sulfate rich domains of Class III SLRPs such as Fibromodulin and Osteoadherin (Heinegård, 2009). Initial discovery of Prealp was in the collagen rich articular cartilage extracts (Heinegård et al., 1986), and it was noted to be distinctly present in the matrix surrounding chondrocytes, called territorial matrix.

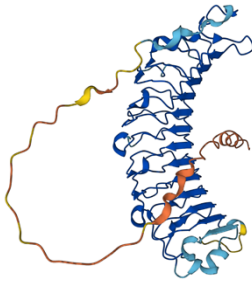


**Figure 1.12** Predicted 3D structure of zebrafish Prealp by AlphaFold used under CC-BY4.0 license. (Jumper et al., 2021; Varadi et al., 2022).

However, later studies have shown tissue specific and context dependent localization of PRELP, in different regions of the ECM. PRELP expression has been observed in hepatic tissue, cardiovascular system, renal tissue, as well as in the basement membrane of skeletal muscles (Heinegård, 2009). These data along with interaction of N-Terminus of PRELP with HS chains on the N-terminus of Perlecan, suggest a potential structural role for PRELP in anchoring the basal lamina with fibrillar collagen in the surrounding reticular lamina. This also suggest a link between fibrillar collagen of the RL and Laminins in the BL through the PRELP-HSPG2 bridging axis suggesting



## CHAPTER 1 - INTRODUCTION

increased cross-talk of components within the ECM (Bengtsson et al., 2000, 2002; Heinegård, 2009).

An interesting role for PRELP has been its ability to inhibit the formation of complement membrane attack complex (MAC). This particular role for PRELP has been hypothesized to reduce the activity of the complement system in atherosclerotic conditions of the vascular endothelium, thereby reducing chronic inflammation in disease conditions such as Rheumatoid Arthritis. The MAC inhibition activity is mediated by the basic N-terminal domain of PRELP (Birke et al., 2014; Grover & Roughley, 2001; Happonen et al., 2012; Lewis, 2003; Liu et al., 2017). The N-terminal domain is positively charged and is able to inhibit Nf- $\kappa$ b signaling thereby attenuating the formation of bone resorptive osteoclasts (Rucci et al., 2009). More recent studies have also shown PRELP acting as an inhibitor of differentiation of fibroblasts into myofibroblasts in dilated and hypertrophic cardiomyopathies in humans (Chaffin et al., 2022). PRELP also exhibits tumor inhibitive activity, which could potentially be mediated through recent novel interactions identified with IGF1-R (Kosuge et al., 2021).

#### **1.2.3.4. Bone Morphogenic Protein - 3 (*bmp3*)**

Bone Morphogenic Protein 3, (*bmp3*) is a signaling protein expressed in bony and cartilaginous tissues and a member of the Tgf $\beta$  superfamily (Gamer et al., 2008). BMP3 expression has also been detected in the central nervous system (Yamashita et al., 2016) and variations in expression of Bmp3 induces differences during skull morphogenesis (Schoenebeck et al., 2012). Additionally, zebrafish morphants for *bmp3* exhibit severe pericardial edema and craniofacial defects (Schoenebeck et al., 2012). In osteoblasts, BMP3 expression is regulated by canonical Wnt signaling and acts as a noggin independent inhibitor of BMP signaling pathway (Kokabu & Rosen, 2018).

## CHAPTER 2 - AIMS

The Extracellular Microenvironment of the developing heart is a highly dynamic and fluidic space with interactions between proteins secreted by various tissues and behaving in a cohesive and collaborative manner. A lot has been described about the cardiac jelly from chicken embryos prior to the turn of the century, but molecular data using modern imaging techniques and genetic manipulation techniques are still lacking. At the onset of this study, I started with two basic aims.

- 1. Identification of ECM genes expressed during early heart development and regeneration**
- 2. Genetic manipulation of the identified genes related to cardiovascular development and regeneration, to screen for potential cardiovascular phenotypes**

Based on preliminary data from the above aims, I proceeded to focus on a specific gene which showed a promising developmental phenotype and added a couple more aims.

- 1. Identification of the role of ECM proteoglycan Prelp during heart development**
- 2. Dissecting direct and indirect effects of Prelp loss of function**
- 3. Identification of active domains of Prelp in modulating extracellular matrix organization**

## CHAPTER 2 - AIMS

## CHAPTER 3 - MATERIALS AND METHODS

### 3.1. Materials

#### 3.1.1. Organisms

##### 3.1.1.1. Strain of Microorganism

*Escherichia coli* (*E.coli*) strain of DH5 $\alpha$  was used for all bacterial transformations as the choice of competent cells. The same strain was also used to amplify plasmids.

##### 3.1.1.2. Established Zebrafish lines used in this thesis

**Table 3.1: Previously established zebrafish lines in this thesis.**

Allele	Description	Reference
WT - AB	Oregon AB strain	
WT - TL	Tüpfel Longfin	
myl7:actnn3b-EGFP <sup>sd10</sup>	CM sarcomere reporter	(Wang et.al., 2011)
myl7:BFP-CAAX <sup>bns193</sup>	CM membrane reporter	(Guerra et al., 2018)
-5.1myl7:DsRed2-NLS <sup>f2</sup>	CM nuclear reporter	(Rottbauer et al., 2002)
myl7:EGFP-Hsa.HRAS <sup>s883</sup>	CM membrane reporter	(D'Amico et al., 2007)
myl7:EGFP <sup>twu26</sup>	CM cytosolic reporter	(Ho et al., 2007)
kdrl:EGFP <sup>s843</sup>	endothelial cell reporter	(Jin et al., 2005)
-0.2myl7:EGFP-podxl <sup>bns103</sup>	apical polarity reporter	(Jiménez-Amilburu et al., 2016)
ubb:SEC-Rno-Ncan-EGFP <sup>uq25bh</sup>	HA biosensor reporter	(Grassini et al., 2018)
agrnp <sup>p168</sup>	Mutant allele for Agrn	(Gribble et al., 2018)

### 3.1.1.3. Zebrafish lines established in this thesis work

**Table 3.2: Generated zebrafish alleles established for this thesis.**

Allele	Description	Reference
<i>bns416</i>	<i>prelp</i> mutant	This Thesis
<i>bns495</i>	<i>prelp</i> mutant	This Thesis
<i>bns496</i>	<i>prelp</i> mutant	This Thesis
<i>Tg(-0.2myl7:prelp-p2a-EGFP)<sup>T200511b_SR</sup></i>	myocardium specific <i>prelp</i> expression	This Thesis

### 3.1.1.4. Zebrafish diet

Zebrafish larvae were added to the system at 5 dpf. Fish were fed with Zebrafeed™ by SPAROS® starting from 5 dpf. Upto the age of 14 dpf, Zebrafeed with maximum diameter of 100µm was used, following which feed diameter was adjusted to 200µm upto 21 days. Subsequently, feed size was adjusted to 400/600µm from 1 month onwards depending on size of fish. Additionally, dry feed was supplemented with life brine shrimp (*Artemia salinaris*) from 14 dpf onwards.

## 3.1.2. Laboratory equipment and Consumables

### 3.1.2.1. Antibiotics

**Table 3.3. : List of Antibiotics and concentrations utilized for conducting experiments in this thesis.**

Antibiotics	Concentration	Supplier	Catalog #
<b>Ampicillin</b>	100 µg/ml	Merck	171254-25GM

**3.1.2.2. Antibodies****Table 3.4.: List of antibodies used in the thesis with their respective dilution and supplier.**

<b>Antibody</b>	<b>Raised in</b>	<b>Dilution</b>	<b>Supplier</b>	<b>Catalog #</b>
<b>Alexa Fluor 488 anti-Chicken</b>	Goat	1:500	Life Technologies	A11039
<b>Alexa Fluor 568 conjugated Phalloidin</b>	NA	1:200	Thermo Scientific	A12380
<b>Alexa Fluor 647 anti-Mouse</b>	Goat	1:500	Life Technologies	A21236
<b>Anti – Histone 3</b>	Rabbit	1:200	Abcam	ab18521
<b>Anti Prelp</b>	Rabbit	1:100	Genetex	GTX123359
<b>Anti-Dcn</b>	Mouse	1:100	DSHB	6D6
<b>Anti-DIG-AP, Fab fragments</b>	Sheep	1:10,000	Roche	11 093 274 910
<b>Anti-EGFP</b>	Chicken	1:500	Aves Lab	gfp-1020
<b>Anti-Laminin</b>	Rabbit	1:150	Sigma	L9393
<b>HRP Goat anti Rabbit</b>	Goat	1:500	Merck	12-348
<b>Living Colors DsRed</b>	Rabbit	1:200	Takara	632496
<b>Mef-2</b>	Rabbit	1:200	Santa Cruz	sc-313

## CHAPTER 3 - MATERIALS AND METHODS

<b>MYH (MHC)</b>	Mouse	1:200	DSHB	MF20
<b>MYH7</b>	Mouse	1:200	DSHB	n2.261
<b>PCNA</b>	Mouse	1:200	Santa Cruz	sc-56
<b>TagBFP-Nanobody</b>	NA	1:1000	NanoTag Biotechnologies	N0501

### 3.1.2.3. Buffers and solutions

**Table 3.5. List of buffers and solutions along with their composition.**

Buffer / Solution	Composition
<b>0.1% PBST</b>	0.1% Triton X-100 dissolved in 1X PBS
<b>0.3% PBST</b>	0.3% Triton X-100 dissolved in 1X PBS
<b>0.1% PBSTw</b>	0.1% Tween-20 dissolved in 1X PBS
<b>10X PBS</b>	10 PBS tablets (Sigma) in 200 mL distilled water
<b>10X TBE</b>	121 g Tris + 62 g Boric Acid + 7.4 g EDTA dissolved in 1 liter of distilled water
<b>1X PBDX</b>	0.1% Triton X-100 + 1% DMSO + 1% BSA dissolved in 1X PBS
<b>20X SSC</b> (Dilutions made per requirement)	175.3 g NaCl + 88.2 g Sodium citrate dissolved in 800 mL of distilled water – adjusted to pH 7, then filled to volume to 1000 mL with distilled water



CHAPTER 3 - MATERIALS AND METHODS

<b>5X MBS</b>	88mM NaCl + 1mM KCl + 2.4mM NaHCO <sub>3</sub> + 0.82mM MgSO <sub>4</sub> · 7 H <sub>2</sub> O + 0.33mM Ca(NO <sub>3</sub> ) <sub>2</sub> · 4 H <sub>2</sub> O + 0.41mM CaCl <sub>2</sub> · 2 H <sub>2</sub> O + 5mM HEPES adjusted to pH 7.4
<b>Alkaline Tris buffer</b>	100 mM Tris-HCl pH 9.5 + 100 mM NaCl + 0.1% Tween 20 dissolved in distilled water
<b>Blocking buffer (immunostaining)</b>	1X PBDX + 1.5% goat serum
<b>Blocking buffer (in situ)</b>	2 mg/mL BSA + 2% sheep serum in 0.1% PBST
<b>Egg water</b>	3 g Instant Ocean + 0.75 g Calcium sulfate dissolved in 10 liters of distilled water
<b>FISH fix (100 mL)</b>	100 mL FISH fix buffer – prewarmed at 60 °C - + 4 g PFA + 1 mL 1M NaOH adjusted to pH to 7.35 with HCl
<b>FISH fix buffer (100 mL)</b>	77 mL 0.1M Na <sub>2</sub> HPO <sub>4</sub> + 22.6 mL 0.1M NaH <sub>2</sub> PO <sub>4</sub> + 12 µL 1M CaCl <sub>2</sub> + 4 g sucrose + 4 g PFA in 1X PBS adjusted to pH 7.35 with HCl/NaOH
<b>Ginzburg Fish Ringer</b>	55mM NaCl, 1.8mM KCl, 1.25 mM NaHCO <sub>3</sub> dissolved in RNase free H <sub>2</sub> O
<b>HM (-) (in situ)</b>	50% Formamide + 5X SSC + 0.1% Tween 20 adjusted to pH 6 with 1M Citric acid

## CHAPTER 3 - MATERIALS AND METHODS

<b>HM (+) (in situ)</b>	HM (-) + Heparin 50 µg/mL + tRNA 500 µg/mL
<b>Laemml Buffer</b>	Purchased from Bio Rad 1610747
<b>Paraformaldehyde (4%)</b>	4% W/V solution of PFA in RNase free H <sub>2</sub> O

### 3.1.2.4. Centrifuges

**Table 3.6.: List of centrifuges**

Centrifuge model	Supplier
Centrifuge (1.5-2 mL tubes) 5425	Eppendorf
Centrifuge (1.5-2 mL tubes) 5424 R	Eppendorf
Centrifuge (8 strip - 100ul tubes) 5417 R	Eppendorf
GALAXY MINI Star <i>silverline</i> (8 strip - 100ul tubes, 1.5-2ml tubes)	VWR
Centrifuge (15 mL, 50 mL tubes) 5810Rf	Eppendorf

### 3.1.2.5. Chemicals

**Table 3.7.: List of chemicals used in the thesis with their respective suppliers**

Chemical	Supplier	Catalog #
1-Phenyl-2-thiourea (PTU)	Sigma	P7629
10X NEBuffer 2.1	NEB	B7202S
10X NEBuffer 3.1	NEB	B7203S

CHAPTER 3 - MATERIALS AND METHODS

<b>2-Dodecenylsuccinic acid anhydride (DDSA)</b>	Serva	20755.02
<b>2,4,6-Tris(dimethylaminomethyl)phenol (DMP)</b>	Serva	36975.01
<b>5-ethynyl-2'-deoxyuridine (EdU)</b>	Invitrogen	C10340
<b>Acetone, anhydrous</b>	VWR	83683.290
<b>Agarose</b>	Peqlab	35-1020
<b>Agarose, low gelling temperature</b>	Sigma	A9414
<b>Alexa Fluor 568 Phalloidin</b>	Thermo Scientific	A12380
<b>Aqua (water, endotoxin-free)</b>	B. Braun Melsungen AG	0082479E
<b>Azure II</b>	Carl Roth	7640.1
<b>BM Purple AP substrate</b>	Roche	11442074001
<b>Bovine serum albumin (BSA)</b>	Sigma	A2153
<b>Calcium chloride (CaCl<sub>2</sub>)</b>	Merck	10035-04-8
<b>Chloroform</b>	Merck	102445
<b>Citric acid</b>	Sigma	27109
<b>CutSmart buffer</b>	NEB	B7204S
<b>DAPT</b>	Merck	565770
<b>di-Sodium tetraborate (Borax, water free)</b>	Carl Roth	4403.1
<b>DIG RNA labeling mix (Sp6/T7)</b>	Roche	11277073910
<b>Dimethylsulfoxide (DMSO)</b>	Sigma	D4540
<b>DNA ladder (1 kb)</b>	Thermo Scientific	SM0311

CHAPTER 3 - MATERIALS AND METHODS

<b>DNA ladder (100 bp)</b>	Thermo Scientific	SM0241
<b>Ethanol</b>	Roth	K928.3
<b>FITC conjugated Dextran 40kDa</b>	Merck	FD-40
<b>Gel loading dye</b>	Thermo Scientific	R0611
<b>Gelatin (from Porcine Skin)</b>	Sigma	9000-70-8
<b>Glycid ether 100</b>	Serva	21045.02
<b>Goat serum</b>	Sigma	
<b>Heparin</b>	Sigma	136098-10-7
<b>Hydrochloridic acid (HCl)</b>	Sigma	H1758
<b>Hydrogen peroxide (H<sub>2</sub>O<sub>2</sub>)</b>	Sigma	7722-84-1
<b>Isopropanol</b>	Roth	6752,4
<b>Methanol</b>	Roth	4627.5
<b>Methylene blue</b>	Sigma	M9140
<b>Methylene blue</b>	Carl Roth	A514.1
<b>Methylnadic anhydride (MNA)</b>	Serva	29452.03
<b>Mineral oil</b>	Sigma	M8410
<b>Nuclease-free water</b>	Ambion	AM9938
<b>O-dianisidine</b>	Sigma	119-90-4
<b>Osmium tetroxide, 4% aqueous solution</b>	Science Services	E19190
<b>Paraformaldehyde (PFA)</b>	Sigma	P6148
<b>Paraformaldehyde, granulated</b>	Carl Roth	0335.3
<b>Phalloidin 568</b>	Invitrogen	A12380
<b>Phenol red</b>	Sigma	P0290

## CHAPTER 3 - MATERIALS AND METHODS

<b>Phosphate-buffered saline (PBS) tablets</b>	Sigma	P4417
<b>Pronase</b>	Roche	10165921001
<b>Proteinase K</b>	Roche	1092766
<b>Sheep serum</b>	Sigma	ABIN925265
<b>Sodium citrate</b>	Sigma	18996-35-5
<b>Sodium hydroxide (NaOH)</b>	Sigma	221465
<b>Sucrose</b>	Sigma	S0389
<b>SYBR safe</b>	Invitrogen	S33102
<b>T4 ligase buffer</b>	Takara	SD0267
<b>Tricaine (ethyl-m-aminobenzoate methanesulfonate)</b>	Pharmaq	NA
<b>Tris</b>	Sigma	5429.2
<b>Tris hydrochloride (Tris-HCl)</b>	Sigma	RES3098T-B701X
<b>Triton X-100</b>	Sigma	RES3103T-A101X
<b>Trizol</b>	Ambion	15596018
<b>tRNA</b>	Sigma	9014-25-9
<b>Tween-20</b>	Sigma	P1379
<b>Uranyl acetate·2H<sub>2</sub>O</b>	Serva	77870.01

### 3.1.2.6. Enzymes

**Table 3.8.: List of enzymes used in the thesis with their respective supplier.**

Enzyme	Supplier
--------	----------

CHAPTER 3 - MATERIALS AND METHODS

<b>AscI</b>	NEB
<b>BamHI-HF</b>	NEB
<b>BsmBI</b>	NEB
<b>ClaI</b>	NEB
<b>DNase I</b>	Qiagen
<b>EcoRI-HF</b>	NEB
<b>KAPA 2G fast DNA polymerase</b>	Kapa Biosystem
<b>Phusion High Fidelity DNA Pol</b>	New England Biolabs
<b>PrimeSTAR max DNA polymerase</b>	Takara
<b>Q5 – High Fidelity DNA Pol</b>	New England Biolabs
<b>RNasin ribonuclease inhibitor</b>	Promega
<b>SalI</b>	NEB
<b>SmaI</b>	NEB
<b>SYBR Green PCR master mix</b>	Thermo Scientific
<b>T4 DNA ligase</b>	Takara
<b>T7 RNA polymerase</b>	Promega
<b>XbaI</b>	NEB
<b>XhoI</b>	NEB

### 3.1.2.7. Growth Medium

Table 3.9.: List of growth media used in this thesis

<b>Growth medium</b>	<b>Composition</b>
<b>SOC medium</b>	Tryptone 2% + Yeast extract 0.5% + NaCl 0.05% + KCl 0.0186% dissolved in distilled water and

CHAPTER 3 - MATERIALS AND METHODS

	adjusted to a pH 7, then added MgCl <sub>2</sub> 10mM + D-glucose 20 mM and autoclaved
<b>LB agar</b>	Roth
<b>LB medium</b>	Roth

**3.1.2.8. Readymade kits purchased for utilization in this thesis**

**Table 3.10. List of kits used in this thesis**

<b>Kit</b>	<b>Supplier</b>	<b>Catalog #</b>
<b>Clarity Western ECL Substrate</b>	Bio-Rad	1705061
<b>Cold Fusion cloning kit</b>	System Biosciences	MC101A-1
<b>Criterion RGX Precast Gels</b>	Bio-Rad	5671093
<b>GeneJET gel extraction kit</b>	Thermo Scientific	K0691
<b>GeneJET PCR purification</b>	Thermo Scientific	K0701
<b>GeneJET plasmid miniprep</b>	Thermo Scientific	K0502
<b>High Capacity RNA-to-cDNA</b>	Applied Biosystem	4387406
<b>InFusion Cloning kit</b>	Takara Biosciences	638910
<b>Maxima first strand cDNA synthesis</b>	Thermo Fisher	K-1641
<b>MEGAscript T7 kit</b>	Ambion	AM1354
<b>miRNeasy micro kit</b>	Qiagen	217084
<b>mMESSAGE mMACHINE (T3)</b>	Ambion	AM1348
<b>mMESSAGE mMACHINE (T7)</b>	Ambion	AM1344
<b>pGEM-T-easy vector</b>	Promega	A1360
<b>Pierce BCA Protein Assay</b>	Thermo Fisher	23225

<b>RNA clean and concentrator</b>	Zymo Research	R1016
-----------------------------------	---------------	-------

### 3.1.2.9. Common Laboratory Supplies utilized in this thesis

**Table 3.11. Table of laboratory supplies**

<b>Laboratory supply</b>	<b>Supplier</b>
<b>Bacterial culture tube</b>	Sarstedt
<b>Beakers</b>	VWR
<b>Centrifuge tubes (1.5 mL, 2 mL)</b>	Sarstedt
<b>Conical flasks (100 mL, 500 mL)</b>	VWR
<b>Eyelash for fine mounting</b>	TedPella
<b>Falcons (15 mL, 50 mL)</b>	Greiner bio-one
<b>Forceps</b>	Dumont
<b>Glass bottles (50 mL, 100 mL, 250 mL, 500 mL, 1000 mL)</b>	Schott Duran
<b>Glass bottom dish</b>	MatTek
<b>Insulin syringes</b>	Terumo
<b>Laboratory film</b>	Parafilm
<b>Latex gloves</b>	Roth
<b>Microloader pipette tips</b>	Eppendorf
<b>MicroPipette (2 <math>\mu</math>L, 20 <math>\mu</math>L, 200 <math>\mu</math>L, 1000 <math>\mu</math>L)</b>	Gilson
<b>Nitrile gloves</b>	VWR
<b>Play-Doh®</b>	Mattel
<b>PCR tubes (200 <math>\mu</math>L)</b>	Sarstedt
<b>Petri dish (90 mm, 60 mm, 35 mm)</b>	Grainer bio-one
<b>Pipetboy</b>	Integra



<b>Pipette filter tips</b>	Grainer bio-one
<b>Pipette tips</b>	Grainer bio-one
<b>Scalpel</b>	Braun
<b>Serum pipette</b>	Grainer bio-one

### 3.1.2.10. Microscopes

**Table 3.12: Microscopes used in the thesis**

<b>Microscope</b>	<b>Provider</b>
<b>Confocal microscope LSM700</b>	Zeiss
<b>Confocal microscope LSM800 Examiner</b>	Zeiss
<b>Confocal microscope LSM800 Observer</b>	Zeiss
<b>Confocal microscope LSM880 w/Airyscan</b>	Zeiss
<b>Spinning Disk microscope, cell observer SD</b>	Zeiss
<b>Stereomicroscope SMZ18</b>	Nikon
<b>Stereomicroscope SMZ25</b>	Nikon
<b>Stereomicroscope Stemi 2000</b>	Zeiss

### 3.1.2.11. Assorted and Miscellaneous Lab Equipments

**Table 3.13. List of assorted and miscellaneous laboratory equipments**

<b>Equipment</b>	<b>Supplier</b>
<b>Bacterial incubator</b>	Heraeus
<b>Bacterial incubator shaker</b>	Infors HAT
<b>CFX connect real time PCR detection system</b>	Bio Rad
<b>Bio Rad Electrophoresis chamber</b>	Bio Rad

CHAPTER 3 - MATERIALS AND METHODS

<b>Dark reader transilluminator</b>	Clare chemical
<b>Eco Real-Time PCR System</b>	Illumina
<b>Electrophoresis power supply</b>	Bio Rad
<b>Fluostar Omega Plate Reader</b>	BMG Labtech
<b>Gel Doc EZ system</b>	Bio Rad
<b>Heating block</b>	VWR
<b>Injection micromanipulator</b>	World precision instruments
<b>LabChip Gx Touch 24</b>	Perkin Elmer
<b>Micropipette puller P-1000</b>	Sutter instruments
<b>Microscale</b>	Novex
<b>Microwave</b>	Bosh
<b>Nanodrop 2000c</b>	Thermo Scientific
<b>NextAdvance Bullet Blender® Homogenizer</b>	Scientific instrument services
<b>NextSeq500 instrument</b>	Illumina
<b>PCR mastercycler Pro</b>	Eppendorf
<b>Printer P95</b>	Mitsubishi
<b>Slot grid (Copper) 2x1mm</b>	Plano
<b>Trans Blot Turbo</b>	Bio Rad
<b>Leica CM3050S Cryostat</b>	Leica
<b>Vevo 2100 Ultrasound Imager</b>	VisualSonics
<b>Weighing balance</b>	Sartorius
<b>Zebrafish aqua culture system</b>	Tecniplast
<b>Zebrafish breeding tanks</b>	Tecniplast
<b>Zebrafish incubator</b>	Binder

### 3.1.3. Oligonucleotides

This section covers Oligonucleotides used throughout this thesis.

#### 3.1.3.1. Long Oligos for CRISPR/Cas9 guide mRNA

Table 3.14. Long Oligos for CRISPR/Cas9 guide mRNA synthesis

Oligonucleotide name	Sequence 5'-3'
<i>bmp3</i> Crispr 1	TAATACGACTCACTATAGGCTGATA TCGGCTGGAGCGAGTTTTAGAGCTA GAAATAGCAAG
<i>bmp3</i> Crispr 2	TAATACGACTCACTATAGGATCTTT TCGGGCACACAGCAGTTTTAGAGCT AGAAATAGCAAG
constant Oligo	AAAAGCACCGACTCGGTGCCACTTT TTCAAGTTGATAACGGACTAGCCTT ATTTAACTTGCTATTTCTAGCTCTA AAAC
<i>dcn</i> Crispr 1	TAATACGACTCACTATAGGACTTGA TACCACTCTCCTGTTTTAGAGCTAG AAATAGCAAG
<i>dcn</i> Crispr 2	TAATACGACTCACTATAGGCGACTT CAAAGGCCTGAAGTTTTAGAGCTA GAAATAGCAAG
<i>dcn</i> Crispr 3	TAATACGACTCACTATAGGCCTGTC TAAGAACCTCCTGAGTTTTAGAGCT AGAAATAGCAAG
LG- <i>agr</i> n Crispr 1	TAATACGACTCACTATAGGGACAC AGACCTTTTCATCGGAGTTTTAGAG CTAGAAATAGCAAG
LG- <i>agr</i> n Crispr 2	TAATACGACTCACTATAGGGAAAA TGCGGGTATCTCCGGAGTTTTAGAG CTAGAAATAGCAAG
Nt- <i>agr</i> n Crispr 1	TAATACGACTCACTATAGGGAAAA TGCGGGTATCTCCGGAGTTTTAGAG CTAGAAATAGCAAG
Nt- <i>agr</i> n Crispr 2	TAATACGACTCACTATAGGTACTCT CCGCAACTTGGAGGAGTTTTAGAG CTAGAAATAGCAAG
<i>prelp</i> Crispr 1	TAATACGACTCACTATAGGAGTTGT GGTTATTCACAAGTTTTAGAGCTAG AAATAGCAAG
<i>prelp</i> Crispr 2	TAATACGACTCACTATAGGCACTAT CAAGTAGACAGGAGTTTTAGAGCT AGAAATAGCAAG
<i>prelp</i> Crispr 3	TAATACGACTCACTATAGGAAGAC CTTTGTCACATAATGTTTTAGAGCTA GAAATAGCAAG

<i>prelp</i> Crispr 4	TAATACGACTCACTATAGGAAGCA CATAATGACATCTAGGTTTTAGAGC TAGAAATAGCAAG
<i>prelp</i> Crispr 5	TAATACGACTCACTATAGGAGTGAT TGCCATCCAAACGCGTTTTAGAGCT AGAAATAGCAAG

### 3.1.3.2. Oligos for genotyping and plasmid generation

Table 3.15. Oligos for genotyping mutants and generation of plasmid constructs

Oligonucleotide name	Sequence 5'-3'
<i>agrN</i> -NtA genotyping Forward	CGCTACCTGAAAGGCAAGAC
<i>agrN</i> -NtA genotyping Reverse	CAAGAGCGCTGTCCTACCA
<i>agrN</i> -LG genotyping Forward	CCATCCTTTGGTGGAAAGTC
<i>agrN</i> -LG genotyping Reverse	CTGAGCTCCACATATCCTTCAA
<i>prelp</i> <sup><i>bns416</i></sup> genotyping Forward	CCCCCTCACAATGTGCATGA
<i>prelp</i> <sup><i>bns416</i></sup> genotyping Reverse	TGCATGGAGGTGTCTAAAGCA
<i>dcn</i> Crispr genotyping Fw 1	CCGTGATCTTGTTGTTCTGCA
<i>dcn</i> Crispr genotyping Rev 1	AGGTCTGAAGACTGTTCCAGA
<i>dcn</i> Crispr genotyping Fw 2	AGTCGTTTTCTTTAATCTCCGTGA
<i>dcn</i> Crispr genotyping Rev 2	GTCTTTAAGGTCTGAAGACTGTTCC
<i>dcn</i> Crispr genotyping Fw 3	AGGAAAGGAGAGAGTGATTGAAA
<i>dcn</i> Crispr genotyping Rev 3	CCTGGACCTGCAGAACAACA
<i>dcn</i> Crispr genotyping Fw 4	AGTGATTGAAAACTCACTTGGAGAC
<i>dcn</i> Crispr genotyping Rev 4	TACCACTCTCCTGGACCTGC
<i>dcn</i> Overexpression Fw	TAAGCTTGGTACCGAGCTCGATGAAAT CGGCCTGTCTCTC

CHAPTER 3 - MATERIALS AND METHODS

<b><i>dcn</i> Overexpression Rev</b>	GAGAGACAGGCCGATTTTCATCGAGCTC GGTACCAAGCTTA
<b><i>DNdcn</i> Overexpression Fw</b>	AGGCCATGTATTCAGGCTAGAATTCTG CAGATATCCAGCA
<b><i>DNdcn</i> Overexpression Rev</b>	TGCTGGATATCTGCAGAATTCTAGCCT GAATACATGGCCT
<b><i>bmp3</i> genotyping Fw 1</b>	CTACATGGGATGAGGCCAGC
<b><i>bmp3</i> genotyping Rev 1</b>	GCGGGTTTCAGATGATTGGAA
<b><i>bmp3</i> genotyping Fw 2</b>	ATGGATCGCTGTCAGCGGCT
<b><i>bmp3</i> genotyping Rev 2</b>	CCGACAGGCGCAGGAGTCCA
<b><i>agrnp<sup>168</sup></i> genotyping Fw 1</b>	GCATTAACGGCAAAGACCCTG
<b><i>agrnp<sup>168</sup></i> genotyping Rev 1</b>	TGAGATGATGTTTGTGGCCT
<b><i>agrnp<sup>168</sup></i> genotyping Fw 2</b>	GGCCAGCAGAAAAGGAGAGA
<b><i>agrnp<sup>168</sup></i> genotyping Rev 2</b>	CAGAATATGCATAAGTTTGTCTCCT
<b><i>agrnp<sup>168</sup></i> genotyping Fw 3</b>	GGTCAGAAGACAGACGGCAA
<b><i>agrnp<sup>168</sup></i> genotyping Rev 3</b>	GGCAAGGGTTGGAACAGCTA
<b>Prelp for 02myl7 fw</b>	TATAATGGATCCCATCGATTCTGAATTA GATCTGTCGACCACCATGAAAGCTGGG CTTGCATA
<b>Prelp for 02myl7 p2a Reverse</b>	GCTTCAGCAGGCTGAAGTTAGTAGCTC CGCTTCCACGCGTTATCACTATTGCAT GGAGGT
<b>Prelp_ cterm_ Fw</b>	TAATACGACTCACTATAATGCCTGCGA ATATACCAA
<b>Prelp_ cterm_ rev</b>	TATCACTATTGCATGGAGGT

<b>Prelp_nterm_Fw2</b>	TAATACGACTCACTATAGGATGAAAGC TGGGCTTGCATA
<b>Prelp_cterm_Fw2</b>	TAATACGACTCACTATAGGATGCCTGC GAATATACCAAA

### 3.1.3.3. Oligos for qPCR and sequencing

**Table 3.16. Oligos for qRT-PCR and sequencing purposes**

<b>Oligonucleotide name</b>	<b>Sequence 5'-3'</b>
<b>dcn_qPCR_F1</b>	TTGAAAGACTTCCTATGATGCC
<b>dcn_qPCR_F2</b>	CTATTCCCAAAGGTCTGCC
<b>dcn_qPCR_R1</b>	CAAGATGAGCGTTTGGAGAC
<b>dcn_qPCR_R2</b>	TTCCAGGTGAAGTTCCTC
<b>EGFP_Fw</b>	AGGACGACGGCAACTACAAG
<b>EGFP_Rev</b>	AAGTCGATGCCCTTCAGCTC
<b>M13_Fw</b>	GTTGTAAAACGACGGCCAGT
<b>m13_pUC_Fw</b>	CCCAGTCACGACGTTGTAAAACG
<b>m13_pUC_Rev</b>	AGCGGATAACAATTCACACAGG
<b>M13_Rev</b>	ACACAGGAAACAGCTATGAC
<b>p168_qPCR_Dwn1_Fw</b>	GAAGGAATCGCTCTTTGTGG
<b>p168_qPCR_Dwn1_Rev</b>	GGACTTCTCAAATATTGTGTCTG
<b>p168_qPCR_Dwn2_Fw</b>	CAGCACACGGATCTCAATCTG
<b>p168_qPCR_Dwn2_Rev</b>	TCAAAGTAATCTTCTGAATGGCCC
<b>p168_qPCR_On1_Fw</b>	CTTAATGACGGCATCCTGGAG
<b>p168_qPCR_On1_Rev</b>	TCAAAGTAATCTTCTGAATGGCCC
<b>p168_qPCR_On2_Fw</b>	AAATCAAGCTGAACGAGTGGA
<b>p168_qPCR_On2_Rev</b>	CAAAGTAATCTTCTGAATGGCCC
<b>p168_qPCR_Up1_Fw</b>	TTCAGCATGACTATCGTTCTACTG
<b>p168_qPCR_Up1_Rev</b>	TTCTTTACTCCTAATGACAGCTGG
<b>p168_qPCR_Up2_Fw</b>	GTTCTACTGGCCAATGACTCC
<b>p168_qPCR_Up2_Rev</b>	TCTTTACTCCTAATGACAGCTGG
<b>prelp_qPCR_dn_f1</b>	CTAGAGATGCGTTTACACTGG

<b>prelp_qPCR_dn_r1</b>	GCGTATTGTTCCCTTATTTGTC
<b>prelp_qPCR_f1</b>	TGCATTTGGCCCATAACAAGC
<b>prelp_qPCR_r1</b>	TCATGCACATTGTGAGGGGG
<b>prelp_qPCR_up_f1</b>	GTTCCCTCTGTTCAACTCCGA
<b>prelp_qPCR_up_f2</b>	GGACTACTTCAAGAATTTTCGCA
<b>prelp_qPCR_up_r1</b>	ATCCAAACGCAGGTATCTCAG
<b>prelp_qPCR_up_r2</b>	ACGCAGGTATCTCAGTTTGG
<b>T7_Primer</b>	TAATACGACTCACTATAGGG

### 3.1.4. Plasmids

**Table 3.17. Plasmids used as templates in this thesis**

<b>Plasmid</b>	<b>Resistance</b>	<b>Source</b>	<b>Purpose</b>
<b>pCDNA3.1</b>	Ampicillin	Addgene	Vector for overexpression
<b>pGEM-T</b>	Ampicillin	Promega	Sequencing cloning
<b>pT3TS-nlsCas9nls vector</b>	Ampicillin	Addgene	CRISPR mutagenesis
<b>pT7-gRNA vector</b>	Ampicillin	Addgene	CRISPR mutagenesis
<b>pTol2-mRNA vector</b>	Ampicillin	Addgene	Transposase
<b>pcs2-myl7:snai1b-p2a-egfp</b>	Ampicillin	(Gentile et al., 2021)	Generation of prelp rescue plasmid

### 3.1.5. Softwares

**Table 3.18. Softwares used for the generation of this thesis**

<b>Softwares</b>	<b>Purpose</b>
<b>Adobe Photoshop, Illustrator, Inkscape</b>	Image formatting
<b>AlphaFold2 – DeepMind (Google Colab)</b>	Protein Structure Prediction
<b>ApE, SnapGene</b>	Sequence analysis, primer design

<b>Chop-Chop / IDT gRNA design tool</b>	Guide RNA identification for CRISPR/Cas9
<b>FastQC</b>	Bioinformatics analysis
<b>Gitools</b>	Bioinformatics analysis
<b>GraphPad Prism 8</b>	Statistical Analysis of data
<b>ImageJ, Imaris, Zen</b>	Microscopy image processing and segmentation
<b>Mendeley Desktop, Mendeley Cite and Browser extension</b>	Bibliography management
<b>Microsoft Office 365</b>	Writing, data analysis, image formatting
<b>OrientationJ for ImageJ</b>	Plugin for specialized image processing
<b>Primer3Plus, PerlPrimer</b>	Primer design
<b>PyMol (Education)</b>	3D Protein Visualization
<b>VevoLab Imaging and analysis software</b>	Echocardiography of adult zebrafish

### 3.1.6. External Services

Oligonucleotide synthesis and production was performed by SIGMA (Merck) and purchased under a PO license by Department III – MPIHLR, upon providing the required sequence.

Sanger sequencing for validation of plasmids and genomic sequences was performed through shipment of primer pre-mixed DNA samples to Microsynth Seqlab (Economy Tube) or Eurofins Genomics (previously known as GATC) using prepaid bar codes.



### 3.1.7. Databases

**Table 3.19. The following online databases were used in this thesis**

<b>Database</b>	<b>URL</b>
<b>Ensembl</b>	<a href="http://www.ensembl.org">www.ensembl.org</a>
<b>InterPro</b>	<a href="http://www.ebi.ac.uk/interpro/">www.ebi.ac.uk/interpro/</a>
<b>PubMed</b>	<a href="http://pubmed.ncbi.nih.gov">pubmed.ncbi.nih.gov</a>
<b>RefSeq</b>	<a href="http://www.ncbi.nlm.nih.gov/refseq/">www.ncbi.nlm.nih.gov/refseq/</a>
<b>Uniprot</b>	<a href="http://www.uniprot.org">www.uniprot.org</a>
<b>ZFIN</b>	<a href="http://zfin.org">zfin.org</a>
<b>Matrisome</b>	<a href="http://matrisome.org">matrisome.org</a>

## **3.2. Methods**

### **3.2.1. Combinatorial analysis and identification of candidates**

To identify ECM genes associated with cardiac development and regeneration, I cross referenced the Zebrafish Matrisome (Nauroy et al., 2018; Shao et al., 2020) with the genes from the following datasets.

1. Developing heart microarray – (52 hpf and 7 dpf) (Tsedeke et al., 2021)
2. Single cell RNAseq from whole developing zebrafish (0-24 hpf) (Wagner et al., 2018)
3. LCMseq adult zebrafish valve vs adult zebrafish remaining heart tissues (>3 mpf) (Bensimon-Brito et al., 2020)
4. LCMseq Adult zebrafish valve regeneration uninjured, 2 dpab and 21 dpab (Bensimon-Brito et al., 2020)
5. Cryoinjured hearts vs sham injured hearts in zebrafish and medaka (Lai et al., 2017)

ECM genes which exhibited a transcriptional upregulation during early stages of development, as well as upregulation in early stages of regeneration in both the heart and the valve datasets were identified, and considered for detailed analysis using genetic manipulation tools

### **3.2.2. Genome Editing**

#### **3.2.2.1. Generation of zebrafish mutants using CRISPR/Cas9 mediated mutagenesis**

The CRISPR/Cas9 technique was identified to be most reliable to generate double strand nicks in the genome, which made it an excellent tool for mutagenesis. CRISPR/Cas9 mediated mutagenesis was utilised to generate the

## CHAPTER 3 - MATERIALS AND METHODS

various mutants used in this thesis. Single guide RNAs were identified using Chop-Chop or the sgRNA design tool from Integrated DNA Technologies (IDT).

Long Oligonucleotides harboring the unique spacer sequence with PAM site were designed, procured and annealed with the Constant Oligonucleotide, followed by filling in the spaces with T4 DNA polymerase, followed by sgRNA synthesis using MEGAShortscript® T7 RNA Polymerase Kit.

pT3TS-nlsCas9nls vector was linearized and subjected to mRNA synthesis using the mMessage mMachine® T3 RNA Polymerase kit to produce *cas9* mRNA.

Synthesized RNAs were purified using Zymo-Research™ RNA Clean and Concentrator Kit. Concentration of purified RNAs were measured using a Nanodrop Spectrophotometer, following which an injection mixture with 300pg of Cas9 mRNA and 20-100pg of gRNA was prepared with 10% Phenol Red and injected into zebrafish zygotes at the single cell stage.

Embryos were raised up to 48 hours post fertilization, following which they were subjected to DNA extraction using 30µl of 50mM NaOH heated to 95°C for 10 minutes, and 3µl of 1M Tris-HCl was added to this. Resultant supernatant was used to perform genotyping analysis.

Injections were repeated with varying concentrations of sgRNA until satisfactory detection of mutation, following which these larvae were raised in the animal husbandry water system until adulthood under an authorized animal proposal for generation of genetically modified animals. Adult Founders (F0) were outcrossed for screening of germline transmission of mutation, and subsequently outcrossed into WT background for a minimum of three generations, to establish the mutant allele, which was evaluated and

documented according to local, national and international law for genetically modified organisms.

### **3.2.2.2. Generation of *myl7:prelp-p2a-EGFP* Transgenic line**

Wild Type adults were crossed, and larvae were collected at 72 hpf for RNA extraction and subsequent cDNA synthesis. PCR was performed using this cDNA as template, using primers with flanking sequence carrying homology to the previously published -0.2myl7:snail1b-p2a-EGFP plasmid (Gentile et al., 2021).

This plasmid was subjected to restriction digestion using Bam-HI and MluI enzymes using standard restriction digestion protocol from NEB<sup>®</sup>, and run on a gel to verify band size, following which the band was extracted using the Gel Extraction Kit.

The linearized plasmid and PCR product were mixed in a 3:1::insert : vector ratio along with 0.5µl of InFusion enzyme. This mixture was placed at 50°C for 2 minutes, followed by 20 min at room temperature, following which competent cells were added to the mixture and incubated on ice for 20 minutes. The incubation was followed by a heat-shock at 42°C for 45 seconds and then kept on ice for 2 minutes, following which 200µl of SOC medium was added to this and incubated with shaking at 37°C for 1 hour. These samples were then added and spread on an LB containing agarose plate with ampicillin and incubated at 37°C overnight.

Positive colonies were identified and validated using colony PCR, following which the positive colonies containing plasmid were grown in liquid culture, containing Ampicillin overnight with shaking at 37°C. Plasmids were extracted using GeneJet Miniprep kit for validation through sequencing. Once

validated, plasmids were extracted using Sigma-Aldrich Midiprep, with an additional endotoxin removal step. These plasmids were used for injections.

mRNA corresponding to the Tol2 Transposase enzyme was synthesized from the pTol2 plasmid, and subsequently purified. Purified transposase mRNA along with midi-prepped plasmid was injected into zebrafish zygote, and subsequent insertion and incorporation of the transgene was validated using microscopy as well as genotyping procedures.

### **3.2.3. Breeding, handling and experimentation with Zebrafish**

#### **3.2.3.1. Authorization and maintenance of Zebrafish lines**

All experiments in this thesis using zebrafish were performed under standard housing and maintenance conditions of zebrafish (Kimmel et al., 1995), and embryonic stages were measured based on previously described and published methods in the Zebrafish Book by Westerfield M.

All animal experimentation were within the conforms and guidelines of the European Parliament Directive 2010/63/EU on the protection and welfare of laboratory animals, and generation of mutant and transgenic alleles were performed after validation of clear scientific question and approved by the Animal Protection Commission (Tierschutzkommission) of the Regierungspräsidium (RP) Darmstadt under the authorized animal proposal numbers B2/1218, B2/1017, B2/2023, B2/1141, and B2/Anz. 1007.

### **3.2.3.2. Zebrafish mating and breeding**

Mating of Zebrafish were setup using mating tanks in the late afternoon, to reduce amount of time the fish are housed outside the circulating water system to ameliorate potential stressors. Males and females were separated by plastic divided which were removed in the mornings. Mating commences around the onset of daylight in the animal system, and post collection of eggs, animals were promptly returned to their home tanks to reduce stress. Egg collection was performed by filtering the water in the mating tanks through tea sieves, which were subsequently emptied into petri plates using egg water or transferred into falcon tubes for spillage-free transportation from the animal facility into the laboratory.

### **3.2.3.3. Handling and Staging of Zebrafish embryos**

Zygotes received from mating were split across multiple petri dishes and placed in fish incubator at 27.5-28.5°C with pre-warmed egg water. Plates of embryos were observed under a microscope within 12 hours post fertilization to identify and discard unfertilized eggs and to improve oxygen availability for the healthy embryos. Embryos were raised in an optimal density of 1 embryo per 1 mL of egg water (roughly 40 embryos per petri dish).

Embryos were staged based on expected morphology at 28.5°C, to prim-25 as 36 hpf and longpec as 48 hpf, based on the established zebrafish developmental timecourse. These timepoints were used extensively in this study.

Embryos were physically dechorionated using forceps, or enzymatically treated with pronase (200 µl of 30 mg/ml) for a maximum of 60 minutes. Additionally, embryos were treated with phenylthiourea (PTU) at a

concentration of 0.003% in egg water from 24 hpf onwards to delay the onset of pigmentation and to make them more amenable to live imaging using light microscopy.

Embryos were bleached with the chorion between 24 and 36 hpf and subsequently dechorionated to prevent the spread of diseases and therefore reducing stress. Free swimming larvae exhibiting fully developed swim bladders were returned to the running water facility (4-5 dpf).

### **3.2.3.4. Microinjections of the zygote and embryos**

Injection plates were prepared using plastic molds placed in petridishes containing melted 2% agarose in Egg Water. Upon cooling, the plastic molds were removed to reveal the grooves for positioning of zygotes. Matings were set up on the previous day and on the morning of the day of injections, the plastic divider was removed to permit the mating pairs to mate and lay eggs.

Pre-pulled injection needles were loaded using a micro-loader with premixed injection samples, with 10% Phenol Red as a pH indicator as well as to monitor the location of the injected bubble. Pre-calibrated settings were utilized on the micromanipulator using compressed air and using a timed release of gated air controlled by a floor pedal. The microinjection needle was mounted into the micromanipulator and a sample volume was injected into mineral oil droplet placed on top of cover slip placed on a microscale slide. Calibration of droplet size was performed by manipulation of ejection pressure or ejection time.

Within 10-15 minutes of removal of divider, the eggs spawned were collected and loaded into the injection plate along the grooves, and oriented facing the

injection needle using a blunt tipped metal poker stick. Using an injection stand, the microinjection needle was sharply thrust into the egg to pierce the chorion and subsequently enter the zygote through the yolk where the bubble of injection mixture was deposited under high pressure. This is validated by the observation of a pale red coloration of the bubble in the region of injection. This procedure was repeated for all the eggs loaded onto the injection plate and the injected eggs were subsequently rinsed off into a fresh petri plate.

Injected eggs were observed within 8 hours of injection under a stereo microscope to clean the unfertilized, dead or deformed embryos, and the good eggs were deposited into a fresh petri dish with pre warmed egg water to avoid unnecessary developmental delays in the embryonic development. The same procedure was followed for injections of morpholino, mRNA or plasmids.

For CCV injections of 30 hpf embryos, dechorionated embryos were placed in the same microinjection plate under a mild dosage of anesthesia. Microinjection needles were loaded with FITC-Dextran and thrust into the ccv until blood cells entered the needle tip, following which dextran was immediately injected into the embryos. Embryos were recovered in egg water and observed within 15 minutes for distribution of FITC-Dextran throughout the embryo.

### **3.2.3.5. Anesthesia and cryoinjury of adult zebrafish**

Adult zebrafish were exposed to 0.01% tricaine in system water in a small glass beaker to induce anaesthesia. FELASA guidelines regarding the achievement of the anaesthetic stage were observed in the adult zebrafish exposed to tricaine. The anaesthetized zebrafish were removed from the glass beaker and



## CHAPTER 3 - MATERIALS AND METHODS

placed in a supine position on a sponge with a slit dipped in the anaesthetic medium under a stereomicroscope with additional light from the top. The pericardial epidermis was pinched with forceps and an incision was made using a sterile surgical scissors. This incision was expanded using the scissor to reveal the beating ventricle of the adult zebrafish. A fine metal cryoprobe pre-chilled in liquid nitrogen was used to contact the apex of the adult zebrafish ventricle, for a specific time period of 30 seconds following which the cryoprobe was detached using addition of the anaesthetic mixture with the aid of a plastic pipette. The cryo-injured zebrafish were then returned to a beaker devoid of tricaine and containing only system water to recover.

Careful attention was paid to the status of the recovery. Any indication of Pain, Suffering or Harm to the fish manifesting in common stressed behaviour, led towards a humane endpoint using an overdose of tricaine, or ice water. Following which secondary killing techniques were utilized.

### **3.2.3.6. Non-Invasive Echocardiography of Adult Zebrafish**

The non-invasive imaging procedure of echocardiography was used to determine the cardiovascular phenotypes in adult zebrafish. Fish were anaesthetized in 0.01% tricaine in system water, in a glass beaker. Upon onset of anaesthesia, the fish were placed in a supine position on a mold made from Play-Doh® filled with the anaesthesia. These fish were placed under an MS700- 70 MHz MicroScan Ultrasound Transducer, with a frequency of 30-70 MHz in broadband. The Vevo 2100 system was used in B-mode and Color Doppler mode to visualize the anatomical properties of the cardiovascular system. The Color Doppler mode also revealed direction of cardiovascular

blood movement and mean velocity of blood flow, along the direction vertical to the orientation of the transducer. Additionally, pulsed wave doppler mode was used to quantify the blood flow and to identify potential onset of anterograde and retrograde blood flow in these hearts. Zebrafish were anesthetized one by one and returned to water devoid of tricaine for recovery. Due to the non-invasive process of echocardiography, this imaging modality generated only mild stress in the animals.

### **3.2.3.7. Termination and humane endpoints**

Zebrafish were killed with an overdose of anaesthesia (0.1% Tricaine) or through exposure to ice water without direct contact with ice at a maximum concentration of 10 fish per liter. Humane endpoints were followed on adult animals exhibiting Pain, Suffering or Harm (PSH). Secondary killing techniques were performed on cadavers to ensure non-recovery through decapitation.

### **3.2.3.8. Adult heart dissection**

To collect adult hearts, zebrafish were exposed to an overdose of anaesthesia (0.02% Tricaine), following which non recovery was judged using the lack of stimulus response. A secondary killing technique of decapitation was performed to ensure non-recovery. The dead fish were placed laterally and using one pair of forceps, the cleithrum was firmly caught underneath the operculum. Using a second pair of forceps to hold down the cadaver, the forceps holding the cleithrum was pulled outward like opening a book, revealing the pericardial space and the adult heart underneath. With one pair of forceps, the outlet of the bulbus was caught, and with the other pair of

## CHAPTER 3 - MATERIALS AND METHODS

forceps the inlet of the atrium was firmly caught. With the forceps holding the inlet of the atrium a slight tug severs the vein and using the grasp on the outlet of the BA, the heart is detached from the cadaver.

### **3.2.4. Molecular biology and Histology**

Detailed protocols for molecular biology using the kits mentioned are available from the manufacturer website of the respective kits. For the sake of simplicity, detailed protocols of the kits have been omitted in these portions of the Methods. I would request the reader to refer to the catalog number of the specific kit of interest mentioned in the methods to find the corresponding detailed protocol from the website of the manufacturer of these kits.

#### **3.2.4.1. Extraction and isolation of genomic DNA**

Quick and easy extraction of genomic DNA was performed using 50 mM NaOH. Embryos from 2-5 dpf were collected in PCR tubes containing 30  $\mu$ l of 50 mM NaOH. The tubes were heated to a temperature of 95°C for 10 minutes which chemically lyses the cells. After that the tubes are allowed to return to room temperature and then 3  $\mu$ l of 1M Tris-HCl at pH 8 is added to buffer the mixture. The DNA isolated using this protocol can be used immediately and stored at room temperature or at +4°C or frozen at -20°C for some time. Usually, the DNA extracted using the above method does not remain good for long periods of time. For longer term storage, it is advised to add Proteinase K to 10 mM Tris-HCl, or to use standard Elution buffer in place of 50 mM NaOH and incubate the biological samples overnight at 55°C with Proteinase K, followed by heat inactivation at 95°C for 10 minutes. This method generally provides gDNA with longer shelf life.

For adult samples from fin-swabs or fin clips, a higher volume of 50mM NaOH and 1M Tris-HCl mixed in the same ratio is recommended to enable better lysis of the cells in the tissue.

### **3.2.4.2. Extraction and isolation of RNA and cDNA**

For RNA isolation from live samples, specific tissues or whole embryos are collected in a 1.5 ml Eppendorf containing 200  $\mu$ l of Trizol reagent and small magnetic beads. The tissue is then homogenized and mixed for 3-5 minutes on a Bullet Blender at room temperature. The homogenized samples are transferred to a fresh 1.5 ml Eppendorf and 20  $\mu$ l of Chloroform is added to the tube. This ratio and volume of Trizol-Chloroform can be varied based on specific need and size of the tissue samples. The samples are then vortexed vigorously and then permitted to stand at room temperature for 10 minutes, followed by centrifugation at 4°C for 15 minutes at maximum speed. The phase separation leads to a clear aqueous phase floating on top of an organic phase. This aqueous phase is then transferred to another 1.5mL Eppendorf tube, and mixed with equal volume of isopropanol, following which it is transferred to the Zymo® IC RNA Clean and Concentrator kit spin column and the standard protocol of the kit is followed. After final elution of the RNA in Nuclease-Free water, the concentration is measured using a Nanodrop spectrophotometer.

This eluted and purified RNA is subjected to Reverse Transcription (cDNA synthesis) using the Maxima first strand cDNA Synthesis Kit preceded by incubation with Double Stranded DNase. This extracted RNA and subsequent cDNA can be used directly for molecular biology applications such as qPCRs, PCRs for cDNA to be used in cloning.

### **3.2.4.3. Agarose Gel Electrophoresis**

Agarose gels are prepared using 1x Tris, Boric Acid, EDTA (TBE) buffers ranging from 0.5% - 3% agarose based on the specific size of DNA of interest. Agarose is weighed and dissolved in the TBE by heating the agarose-TBE suspension in a microwave until boiling and dissolution of all agarose particles. This solution is then cooled in a chill water bath until warm to the touch (approx. 55-60°C). To this gel solution, DNA intercalating agent SYBR-Safe is added to enable visualization. The gel is then poured into agarose molds and a comb of required number of wells is inserted as the gel is still liquid. Once the gel has cooled sufficiently and solidified, it is transferred to an immersed gel-electrophoresis chamber filled with 1x TBE. The comb is removed, and DNA/RNA is added into the wells premixed with the loading dye containing glycerol to enable the sample to sink to the bottom of the well. The gels are then exposed to a constant voltage and current for 25-60 minutes depending on required resolution of the bands. The voltage settings vary from 120-160V depending on the particular use case and sample size. Post electrophoresis, the bands are observed under a UV-Vis light box, and imaged using BIO-RAD Gel-Doc. The UV-Vis light box provides a platform for isolation of specific bands from the gel which can be melted, and the DNA of the particular size can be extracted using the GeneJet™ Gel Extraction Kit. Extracted DNA is then eluted and quantified using a Nanodrop Spectrophotometer.

### **3.2.4.4. *in-vitro* transcription for mRNA injections**

To prepare capped mRNA, for injections and other purposes, a PCR or cloning is performed from a cDNA sample. For a PCR, forward primers are designed with either the T7 or SP6 viral promoters followed by a KOZAK sequence and an overhang of about 20nt 3' from the start codon of the cDNA. A PCR is performed using an enzyme with proof reading activity such as Phusion® or Q5® DNA polymerase to amplify the corresponding sequence.

For cloning, the PCR product can be used with the plasmid of choice provided existence of corresponding overhangs of the plasmid on the primer and proceeded as previously explained.

For direct mRNA synthesis, the PCR product can be isolated and purified and directly used as a template using the mMessage mMachin<sup>TM</sup> T7/SP6 kits [Depending on corresponding promoter overhangs]. The resultant mRNA is capped and stable and therefore can be subjected to Turbo DNase treatment to get rid of the template and purified using Zymo RNA Clean and Concentrator Kits. This purified mRNA can be quantified using a nanodrop spectrophotometer and run on an agarose gel to test quality. This mRNA can be directly injected in appropriate dilutions into the zygote.

### **3.2.4.5. PCR, qPCR and HRM**

PCR Primers are designed manually and verified using NCBI Primer BLAST. Sequence and annotation data for primer design is procured from Ensembl genome browser.

## CHAPTER 3 - MATERIALS AND METHODS

PCR primers melting temperature  $T_m$  is an important factor to pay attention to while designing the primers. It is important to pay attention to special requirements of specific polymerases/master mixes to be used for each specific reaction.

PCRs performed conform with the guidelines of the enzyme/master mix manufacturers and limitations of the enzymes were noted. For high fidelity application requiring proof reading activity, HF enzymes such as Q5 or Phusion Polymerases were used. For standard genotyping reactions, KAPA2G or PrimeSTAR Max master mixes were used in PCR volumes recommended by the respective manufacturers. An Eppendorf thermal cycler was used for all PCRs and samples were held at 4°C upon reaction completion.

For quantitative PCRs, a Bio-Rad™ CFX Real-Time qPCR Thermal Cycler was used. Flash SyBR Green qPCR master mix was used in 20 µl reactions and technical duplicates and biological triplicates. Quantification of real time amplification was acquired from the machine and fold change was calculated using the  $\Delta\Delta$ -Ct method.

For High Resolution Melt (HRM) analysis, Flash SyBR Green master mix was used in 10µl reactions and an Eco-HRM machine was used to perform the PCR and melt curve analysis. The melt curve was generated by annealing melted double stranded DNA and re-melting the annealed DNA to detect changes in loss of fluorescence during the melting process. HRM was used for genotyping all mutants in this thesis, except for the *prelp* mutant rescued using the *Tg(-0.2myl7:prelp-p2a-EGFP)*, for which PCR was used due to size of amplicon



required to genotype [to distinguish hets from mutants] . HRM analysis is optimal for amplicon sizes less than 100bp.

### **3.2.4.6. Immunofluorescence assays on whole embryos**

To perform immunohistochemistry on whole embryos, the embryos were dechorionated using Pronase as previously mentioned, and subsequently overdosed with anaesthesia and fixed using Paraformaldehyde (PFA) or Fish-Fix at 4°C overnight. (Exception for Laminin immunostainings – embryos fixed for 15 mins at RT).

Following fixation, embryos were washed in PBS-Tween (PBST), and permeabilized with 10µg/mL Proteinase K for varying amounts of time depending on developmental stage (36 hpf – 15 mins, 48 hpf – 30 mins) and then transferred to Blocking Buffer for a minimum of 2 hours. Following blocking, embryos were transferred to blocking buffer containing primary antibodies and left on a nutating shaker at 4°C overnight. Following morning, embryos were washed in PBST and transferred to blocking buffer containing secondary antibody conjugated with a fluorophore and left on a nutating shaker at RT for a minimum of 2 hours placed in the dark. The samples were then washed multiple times with PBST and then imaged using confocal microscopes. DAPI was included or not included along with the 2'Ab mix depending on fluorescence wavelength conflict.

### **3.2.4.7. Immunohistochemistry on heart sections**

Upon extraction of the adult cardiac tissues, the whole hearts were immersed into a 2mL Eppendorf tube containing PFA and left for fixation for 1 hour at RT or at 4°C overnight. Following which PFA was washed out using PBS and

## CHAPTER 3 - MATERIALS AND METHODS

replaced with 30%(w/v) Sucrose prepared in PBS in the same 2mL Eppendorf and incubated overnight, or until hearts sank completely. Samples were then transferred into 15% (w/v) Gelatin, 15% (w/v) Sucrose solution and placed in a water bath at 37°C for one hour, during which gelatin beds were prepared on cryo molds and placed in 4°C to solidify. Hearts were then mounted onto the gelatin beds to maintain the Atrium-Ventricle-Bulbus Arteriosus axis and more Gelatin was added on top of the hearts after mounting. Mounted gelatin molds were left at 4°C overnight. Blocks of gelatin encased hearts were prepared and mounted onto ball-point pen labelled pieces of cardboard, using OCT<sup>®</sup> containing Tissue-Tek compound. These mounted pieces were then immersed in isopentane pre-cooled using liquid N<sub>2</sub>, to provide gentle cooling gradient. Frozen samples were tested using a metal spatula to hear “tick-tick” sounds instead of “tock-tock” sounds and left to stabilize at -80°C. Mounted samples were transferred into a LEICA CM3050S cryostat and sectioned at 10 µm thickness onto an UltraFrost Plus glass slides. These sections were stored at -20 °C.

For IHC, sections were thawed to RT and placed in glass couplings with pre-heated PBS to 37 °C, in a water bath, to dissolve the gelatin. Sections were washed in PBS, and for samples requiring Antigen retrieval, slides were placed in Sodium Citrate buffer preheated to 95°C for 10 mins. Slides were then cooled and incubated at RT with 10% Glycine for 10 mins, followed by permeabilization using either Methanol at RT, or Acetone at -20°C for 10 mins. Following permeabilization, slides were washed with PBS – Triton X 10% and PBDX (PBS, BSA, DMSO, TritonX) thrice. Slides were then transferred into a humid box after outlining with a hydrophobic pen and incubated with Blocking Solution (PBDX + 15% Goat Serum) for a minimum of 2 hours.

Slides were then incubated overnight at 4°C with Primary antibody mix prepared in blocking solution covered with Parafilm, and the next morning washed with PBDX as much as possible, followed by either a short 2-hour incubation with Secondary antibody in blocking solution, or overnight incubation at 4°C. Slides were then washed with PBSTriton and stained with DAPI prepared in PBST. Slides were then washed successively and mounted using DAKO® antifade mounting medium. Mounted slides were imaged using confocal microscopes.

### **3.2.4.8. *in-situ* hybridization of zebrafish embryos**

To perform *in-situ* hybridization, RNA probes were designed using primers containing T7 overhangs over the *prelp* cDNA template. Antisense probes were synthesized using *in-vitro* transcription using T7 polymerase and DIG labelling kit. The ISH was performed using the protocol from Christine and Bernard Thisse.

Embryos were dechorionated, fixed and dehydrated using dilutions of methanol in PBSTween and stored at -20°C. Embryos were then successively rehydrated using the reverse dilutions of Methanol in PBSTw and washed thoroughly using PBSTw alone and permeabilized using 10 µg/mL Proteinase-K in PBSTw. Samples were postfixed in PFA and exposed to prehybridization using the Hybridization buffer at 65-70°C for 2-5 hours. Following this samples were hybridized with anti-sense probe mixed in HB at 1 µg/mL concentration overnight at 65-70°C. Following the O/N hybridization, the HB is exchanged with 2x SSC in successive dilutions, and then the 2x SSC is exchanged with 0.2x SSC in subsequent washes all performed at 65-70°C. Then the sample is allowed to cool to room temperature when the 0.2xSSC is

replaced with PBSTw in successive dilutions, and finally the embryos are transferred into the ISH blocking buffer. After blocking, the samples are transferred to primary anti-DIG antibody prepared in ISH blocking buffer at 4°C overnight left gently rotating. Samples are then washed the next morning with PBSTw many times, and then transferred into a multiwell plate and washed with PBS and Alkaline-Tris buffer. The BM purple substrate is prepared in Alkaline-Tris buffer and incubated with the sample with attention towards the developing staining intensity. After sufficient staining intensity is reached, the staining solution is replaced with PBSTween, and embryos can then be imaged on agarose coated plates under the Stereomicroscope Nikon SMZ25.

### **3.2.4.9. Protein extraction and Western Blot**

Dechorionated embryos were collected and treated with Ginzburg Fish Ringer with protease inhibitor and repeatedly parsed through a pipette tip with narrow opening, to facilitate deyolking. Deyolked embryos were centrifuged at 300g at 4°C for 30 seconds and supernatant was discarded. Pellet was washed and centrifuged, and supernatant was discarded again. The resulting pellet was snap frozen using Liquid N<sub>2</sub> for longer storage. Pellets were thawed and introduced to Lysis Buffer and homogenized using small metallic beads and the Bullet Blender. Homogenized samples were placed on a rotating plate for 30 mins at 4°C and then centrifuged for 10 minutes at 4°C at speeds >13000g. Supernatant was collected and protein quantification was carried out using Pierce BCA Protein assay kit and measured using a Fluostar Omega Plate Reader. Quantified Protein was normalized and mixed 3:1 in Laemmli buffer containing  $\beta$ -Mercaptoethanol. Proteins were added to the wells of a Criterion TGX precast gel and electrophoresed using Running buffer in a Bio Rad

protein electrophoresis apparatus. The acrylamide gel was transferred into a Transblot Turbo membrane using the Transblot Turbo apparatus. Membrane was successively washed with PBS, and 0.1%PBSTw and placed in Blocking buffer (0.1% PBSTw + 5%w/v BSA). The membrane was then transferred into plastic pouches with antibody mixture prepared in blocking solution and left rotating overnight at 4°C. The membrane was removed and washed using 0.1%PBSTw multiple times and then incubated with secondary antibody solution prepared in Blocking Buffer for a minimum of 2 hours at RT. Membrane was then washed with 0.1%PBSTw and then with PBS and exposed to Clarity Western Blot ECL substrate and visualized under Hi Resolution Chemiluminescence detection in BioRad Gel Doc.

### **3.2.5. Transcriptomics analysis**

Transcriptomics analysis was performed in close collaboration with the Bioinformatics and Deep Sequencing Core Facility at the MPIHLR and in large parts by Dr. Stefan Günther. Methods in this section of the thesis was not performed entirely and independently by me, and hence was written with input from Dr. Günther.

#### **3.2.5.1. Embryonic heart dissection and sample preparation**

I crossed adult heterozygous mutants for *prelp* and collected the embryos and raised them to 28 hpf, when I performed DNA collection from embryos using the zebrafish embryonic genotyper (ZEG), without killing the embryos. I isolated them into labelled 96 well dishes and performed HRM analysis to identify WT and mutant siblings. I then separated the embryos based on genotype and raised them to 36 hpf, when I manually dissected embryonic

hearts using an insulin syringe and No.55 forceps from WT and Mutant siblings. I collected 30 hearts per biological replicate with 3 replicates each for WT and Mutant hearts. I proceeded to extract the mRNA from these samples using the miRNeasy micro kit from Qiagen according to the protocol provided by the manufacturer. I also performed DNase digestion on the column and eluted the resultant mRNA.

### **3.2.5.2. Bulk-mRNA sequencing**

I provided Dr. Stefan Günther at the Bioinformatics core facility of MPIHLR with the RNA samples for mRNA sequencing and a 1:10 dilution for QC analysis. The following processes of cDNA library preparation, Quality Control analysis, and sequencing was performed by him, and he provided me with resultant DeSeq2 normalized count matrix, quality control plots and the basic Gene Ontology analysis based on the bioinformatics pipeline.

### **3.2.4.3. RNA-seq data interpretation**

Based on the data provided to me in the form of the reduced matrix, and Gene Ontology analysis, I analyzed the dataset to interpret the implications of the differentially regulated genes, the specific genes which belong to these Gene Ontologies as well as identification of potential transcriptional modulators of the genes associated with the mutant gene.

### **3.2.6. Microscopy and Image processing**

Confocal microscopy was performed using ZEISS microscopes using the ZEN software acquiring imaging files in the .czi format. Airyscan imaging was performed using the Standard Operating Procedure of the ZEISS LSM 880 advanced microscope with Airyscan 2. Second Harmonic Generation (SHG) and imaging was performed using the LEICA SP8 advanced confocal

microscope, with wavelength of laser tuned between 830 and 910 nm in 10nm steps.

### **3.2.6.1. Mounting for live embryo imaging**

Live imaging of zebrafish embryonic hearts was easily feasible from 48 hpf onwards. To image stopped hearts, embryos and larvae were mounted in 1% low gelling temperature agarose with 0.01% tricaine. Embryos were submerged into 2mL Eppendorf containing the above mounting medium at 37°C until they stopped twitching, following which they were aspirated along with some agarose using a glass pipette and a droplet containing the embryo was deposited in the thin glass bottom imaging dish. For upright microscopes, the embryos were mounted ventral side up, whereas for inverted microscopes such as the LSM 800 observer and Cell Discoverer Spinning Disk Microscope, the embryos were mounted ventral side down. The agarose with mounted embryos was permitted to solidify following which immersion medium of water with anesthesia was added to the dishes for upright microscopy. For inverted microscopy, immersion medium was applied on the objective prior to contact with the bottom glass of the imaging dish. An eyelash mounted atop the handle of a fine paintbrush was used to position the embryos for mounting. Embryos were collected from the imaging dishes using forceps and placed into 8 strip PCR tubes for genotyping post imaging.

For imaging of the beating heart in the Cell Observer Spinning Disk microscope, tricaine was omitted from the low gelling temperature agarose mounting medium and the embryos were mounted ventral side down with some force applied to the head to reveal the top part of the ventricle underneath and by lifting the tail of the embryos to reveal more of the heart.

### **3.2.6.2. Mounting for fixed samples or immunostainings**

Fixed samples were used for imaging due to direct inaccessibility of the heart earlier than 48 hpf as it is located between the head and the yolk. For imaging embryos at 36 hpf, samples were fixed in PFA for 1 hour at RT, following which the PFA was washed out with PBS and samples were transferred into a small petri plate. Samples were manually deyolked using insulin syringes, (Properly fixed samples exhibited hard yolks) and then using a scissor like motion the embryonic head was severed from the rest of the body. These severed heads were then immersed in 1% Low melting temperature agarose placed at 37°C and transferred with a droplet of agarose onto imaging dishes for mounting.

Mounting for the upright microscope involved positioning of the dorsal part of the severed head towards the bottom of the dish with the heart, ventral to the head directly facing the microscope objective lens. Mounting for the inverted microscope involved removing excess tissue of the yolk epidermis such that the dorsal part of the head faces up and the heart ventral to the severed head is directly positioned closest to the glass bottom of the imaging dish. Same principles apply for imaging immunostained hearts at 36 hpf. The positioning and mounting of the severed head was possible with the use of the eyelash mounted atop a thin handle of a paintbrush.

### **3.2.6.3. Slide imaging**

Slides were placed on the slide holders of the microscope with the cover slip facing the direction of the objective with sufficient immersion medium applied according to the requirement and refractive index of the objective. Careful



attention was paid during changing of objectives in upright microscopes due to possible hazards with Z positioning of objectives and size of objectives, which could lead to broken slides.

### **3.2.6.4. Image processing in ZEN and FIJI**

Images were processed directly in ZEN, or on FIJI. Linear changes to fluorescence intensity were applied to ImageJ and the same changes were applied equally within different samples and conditions of the same experiment. Quantifications were done blind prior to genotyping the samples.

### **3.2.6.5. Segmentation and image processing in IMARIS**

IMARIS from Oxford Instruments was used to perform segmentation and quantification of segmented data. Quantified data was directly exported from IMARIS as a Microsoft Excel file and imported into data analysis software. Segmentation of cardiac chamber size and surface was performed using the surfaces tool in IMARIS. Segmentation of the cardiac jelly was performed using the solids tool in IMARIS. Segmentation of cardiomyocyte nuclei was performed using the cells and nucleus tool of IMARIS and quantities such as cell number and internuclear distances were directly quantified on IMARIS and exported into the data analysis softwares.

### **3.2.6.6. Laminin and Sarcomere fluorescence intensity**

To perform measurements of fluorescence intensity of Laminin, laser settings and mounting conditions were maintained as similar as possible and samples

## CHAPTER 3 - MATERIALS AND METHODS

were quantified blind prior to genotyping. Microscopy images were imported into FIJI and the mid-sagittal plane was selected. No linear or non-linear alteration to signal intensity was performed. Ten cardiomyocytes in the mid sagittal plane were selected at random and Laminin fluorescence intensity was measured across the cardiomyocyte membrane over a distance of 5  $\mu\text{m}$  using the live signal intensity histogram tool of FIJI. Intensity data from each cardiomyocyte was averaged into a single mean intensity value per heart. Similar analysis was performed in a blind manner throughout all the images acquired. The single column signal intensity matrix for each heart was imported into GraphPad Prism for mean and SD analysis. Samples were then genotyped, and the single column intensity matrix was clustered based on genotype. Mean and Standard deviation was calculated for each position along the signal intensity matrix and plotted as mean intensity value in dark line and SD in shaded region.

Similar processing was performed for the signal intensity with live imaged hearts of *Tg(myl7:actn3b-EGFP)*. Genotyping was performed after quantifications and only used to cluster data from similar genotypes together.

### **3.2.6.7. Actin Orientation quantification**

Actin fiber orientation quantification was performed using a Macro written using the OrientationJ Plugin of FIJI. Data acquired from this plugin was imported into R and a radial plot was generated with overlay of each sample analyzed.

### **3.2.7. Miscellaneous methods**

#### **3.2.7.1. Protein Structure prediction using Alphafold2**

To predict the secondary and tertiary structures of proteins is a daunting task and has eluded researchers for a long time. Recent advances in machine learning and generation of artificial intelligence provides a unique platform for attempting to solve some of the hardest problems related to protein folding. This recently published technique for using Google's AI to solving protein structures is a very useful tool, which has been made easily accessible through the provision of an online Python notebook which only requires researchers without computer science expertise to input simple queries (<https://colab.research.google.com/github/sokrypton/ColabFold/blob/main/AlphaFold2.ipynb>) (Jumper et al., 2021; Mirdita et al., 2022).

I used this online iPython notebook to input sequences of various forms of Prelp, and other genes of interest to receive five predicted models of 3D folded structures of these Proteins. The differences in folding between these models is usually miniscule, but the differences between biologically folded proteins and these different predictions is not known. I chose the predicted models with the highest confidence (based on machine learning) and continued my analysis with these predicted models for my downstream hypotheses and analyses.

#### **3.2.7.2. Statistical analyses**

All statistical analyses in the thesis were performed on GraphPad PRISM. Normality test was performed on the data. If the data did not show normal distribution, unpaired, non-parametric, Mann Whitney U test was performed on the data. For data showing normal distribution, t-tests were performed.



## CHAPTER 4 - Results

A selection of figures and portions of this chapter are to be included in a publication titled “Extracellular Matrix Proteoglycan Prelp modulates laminin mediated cardiac chamber morphogenesis” by S. Ramkumar et. al., (manuscript currently under preparation (September 2022))

### 4.1. Mutant alleles identified

#### 4.1.1. Mutant alleles of genes specific to the heart

##### 4.1.1.1. Agrin

Based on literature review for potential domain specific activity of Agrin, sgRNA were designed targeting these domains and the following mutant alleles were obtained.

**Table. 4.1. Agrin mutant alleles recovered and respective domains.**

Domain	Activity	Allele	Source
<b>LG domain</b>	<b>Dystroglycan binding</b>	<i>p168</i>	(Gribble et al., 2018)
		Del 17	This thesis
		Ins24 Del7	This thesis
		Ins24 Del8	This thesis
<b>Nt-Agrin domain</b>	<b>Musk-LRP4 binding</b>	Del 8	This thesis
		Del 2	This thesis

## 4.1.2. Mutant alleles of genes expressed in the heart and valve

### 4.1.2.1. Decorin (*dcn*)

Decorin sgRNA were designed to target the Tgf $\beta$  binding domain (Green in Fig. 4.1). Other domains of Decorin include N-Terminal MMP2 binding domain (Blue in Fig. 4.1), RTK-Met binding domain (Yellow in Fig. 4.1), Ctgf and TLR2/4 binding domain (Brown in Fig. 4.1), and the C-Terminal ear repeat containing domain (Red in Fig. 4.1) the loss of which caused *Dcn* to behave in a Dominant Negative fashion (Bredrup et al., 2005). The following mutant alleles were recovered.



**Figure 4.1.** Decorin domains with sgRNA target sites on Tgf $\beta$  binding domain. Amino acid range for each domain indicated on figure

**Table. 4.2.** Decorin mutant alleles recovered and respective domains.

Domain	Activity	Allele	Source
Tgf $\beta$ binding domain	Ligand sequestration	Del 9 - deleterious	This Thesis
		Del 5 – PTC encoding	This Thesis

In addition to the above mutant allele, *dcn* mRNA and *DNdcn* mRNA overexpression tools were generated using the techniques mentioned in the methods section of this thesis. *DNdcn* mRNA was designed based on the

human mutation found in patients exhibiting congenital stromal corneal dystrophy (Bredrup et al., 2005).

#### 4.1.2.2. Bone Morphogenic Protein – 3 (*bmp3*)

Bmp3 is a secreted factor with a Tgfβ prodomain and can act as a direct *noggin* independent inhibitor of BMP signalling pathway. The prodomain cleavage site was targeted for mutagenesis (Fig. 4.2).

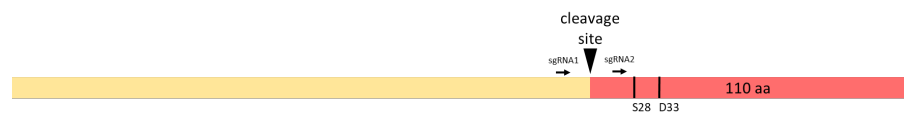


**Figure 4.2.** Schematic of Bmp3 domains with sgRNA target sites

The following mutant alleles were recovered.

**Table. 4.3. Bmp3 mutant alleles recovered and respective domains.**

Domain	Activity	Allele	Source
Tgfβ prodomain cleavage site	BMP signaling inhibition	Del 48	This Thesis
		Del 55	This Thesis
		Ins 5 Del 3	This Thesis
		Ins 11	This Thesis

#### 4.1.2.4. Proline Arginine Rich End Leucine Rich Repeat Protein

*(prelp)*

Prelp is a secreted SLRP with a heparin binding N-terminal domain, Leucine Rich Repeat domain and C-terminal dimerization domain. The most conserved domain across species was the C-Terminal domain, hence sgRNAs were designed against this domain (Fig. 4.3). The basic N-Terminal domain was also targeted with sgRNAs, but no mutant alleles were successfully recovered.

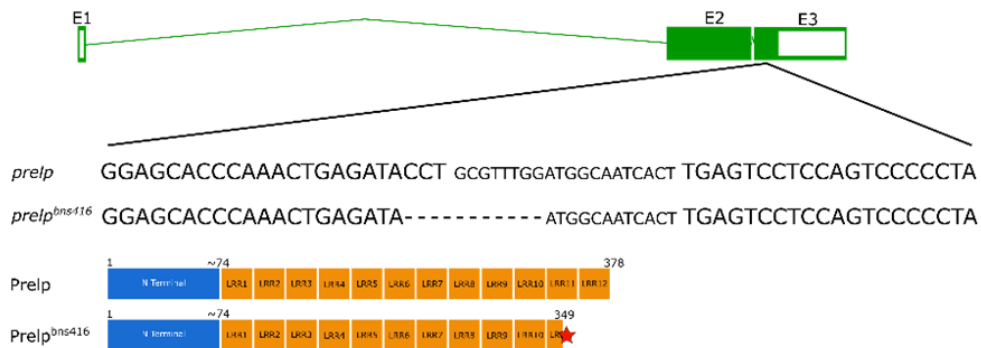


**Figure 4.3** Structure of *prelp* with target site and mutant lesion, and predicted Mutant Protein

**Table. 4.4. Prelp mutant alleles recovered and respective domains.**

Domain	Activity	Allele	Source
C-Terminal	Prelp dimerization	<i>bns416</i> – Del 11	This Thesis
		<i>bns495</i> – Ins 50	This Thesis
		<i>bns496</i> – Ins55 Del66	This Thesis
		Del 8	This Thesis
		Ins 17 Del 25	This Thesis

The deletion allele of 11nt was recovered and an established mutant allele was generated and henceforth identified as *prelp<sup>bns416</sup>* or “*prelp* mutant” throughout this thesis (Fig. 4.3).



## 4.2. Agrin in Cardiac Regeneration

Adult mutants of *agnr<sup>p168</sup>* procured from the Granato Lab (Gribble et al., 2018) were genotyped and cryoinjured using zebrafish cryoinjury protocol.

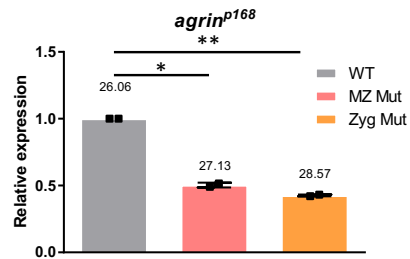


**Fig 4.4.** Relative expression of *agnr* mRNA with 2 biological replicates and 3 technical replicates averaged per biological replicate. Mean Cq values highlighted above each condition. (Statistics, Non-Parametric Mann Whitney U Test - \* - p value <0.05, \*\* - p value <0.005)

I assessed mutant mRNA levels in zebrafish *agnr<sup>p168</sup>* mutants and identified that both Maternal Zygotic *agnr<sup>p168</sup>* mutants, as well as Zygotic *agnr<sup>p168</sup>* mutants exhibit reduced mRNA levels, suggesting that mutant mRNA undergoes degradation. (Fig 4.4)

### 4.2.1. Borderzone CM proliferation is reduced in *agnr<sup>p168</sup>* mutants at 7 dpci

Cryoinjured hearts of 7 dpci WT siblings and *agnr<sup>p168</sup>* mutants were collected, fixed and cryosectioned. The cryosectioned samples were immunostained against PCNA, Mef2 and DAPI, to identify proliferating cardiomyocytes. Visual analysis of borderzone, revealed reduced number of proliferating CMs in the borderzone in *agnr<sup>p168</sup>* mutants (Fig. 4.5 A-B').

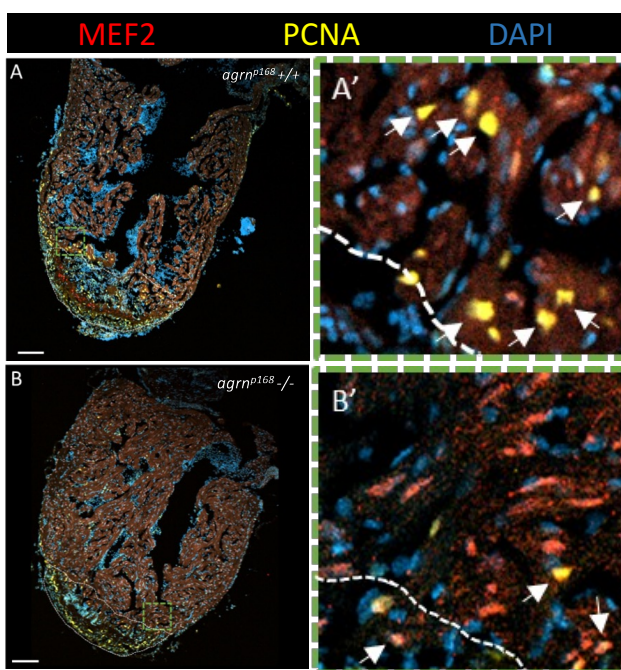
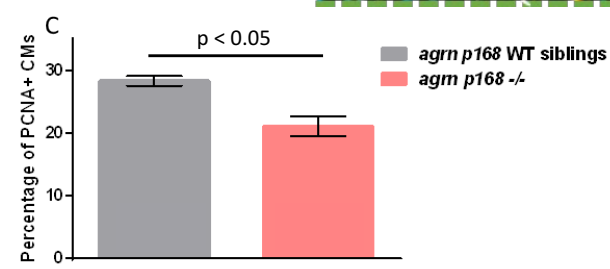


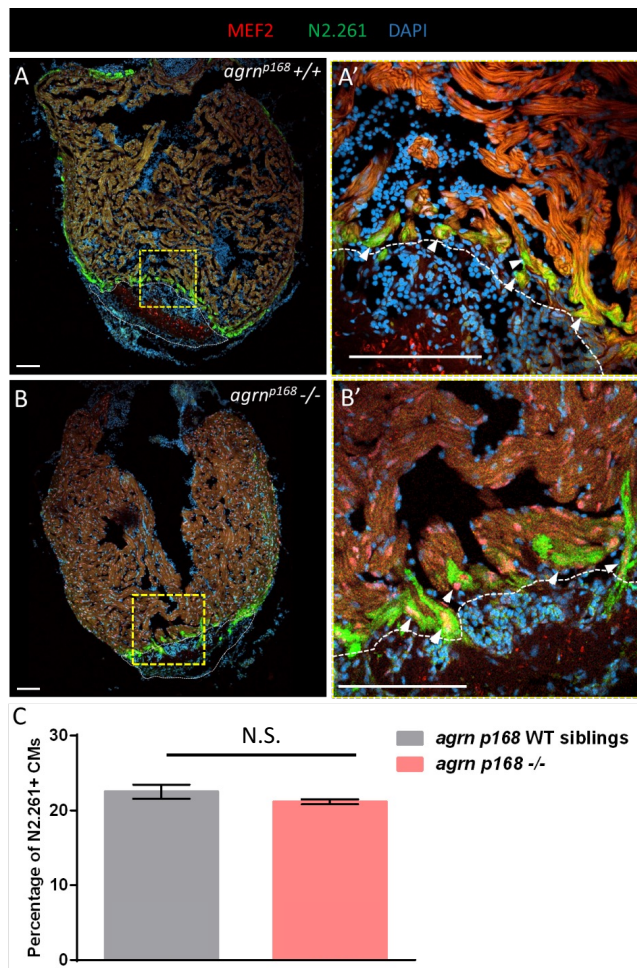
**Figure 4.5.** CM Proliferation assessed on WT siblings (A) and Agrn mutants (B) 7 dpci with colocalization of PCNA, Mef-2 and DAPI. (A'. B') Enlarged inset from A and B, respectively with PCNA+ CMs labelled with white arrows. (C) Quantification of PCNA+/Mef2+ cells in the borderzone as a ratio with Mef2+ cells in the borderzone.



Quantification revealed a reduction in proliferating CMs in *agnr<sup>p168</sup>* mutants compared to their WT siblings (Fig. 4.5 C), suggesting that agrin expression is required to maintain a strong proliferative response of CMs upon injury.

### 4.2.2. Borderzone CM dedifferentiation remains unchanged in *agrnp<sup>168</sup>* mutants at 7 dpci

Cryosectioned adult hearts were immunostained against N2.261, Mef2 and DAPI, to identify dedifferentiating cardiomyocytes. Preliminary observation of injury border revealed no major striking differences to CM dedifferentiation in the borderzone between WT and *agrnp<sup>168</sup>* mutants (Fig. 4.6 A-B').



Quantification of BZ CMs indicated no significant difference between *agrnp<sup>168</sup>* mutants and their WT siblings (Fig. 4.6 C), suggesting that Agrin is immaterial to CMs dedifferentiation upon cryoinjury.

### 4.3. Decorin in cardiac development and regeneration

Decorin mutant and overexpression tools were used to assess the role of Decorin in cardiac development and regeneration. Details of these tools have been previously described in this thesis.

#### 4.3.1. Decorin protein accumulates in collagen rich tissues and collagen rich scar post injury

Antibody staining against Decorin was performed with clone 6D6 Antibody from DSHB, which exhibited high degree of conservation between the epitope used for the antibody and zebrafish Dcn. Immunostained heart sections were compared to second harmonic generated images of cardiac valves, which exhibit highly specialized localization of fibrillar collagen (Williams et al., 2005).

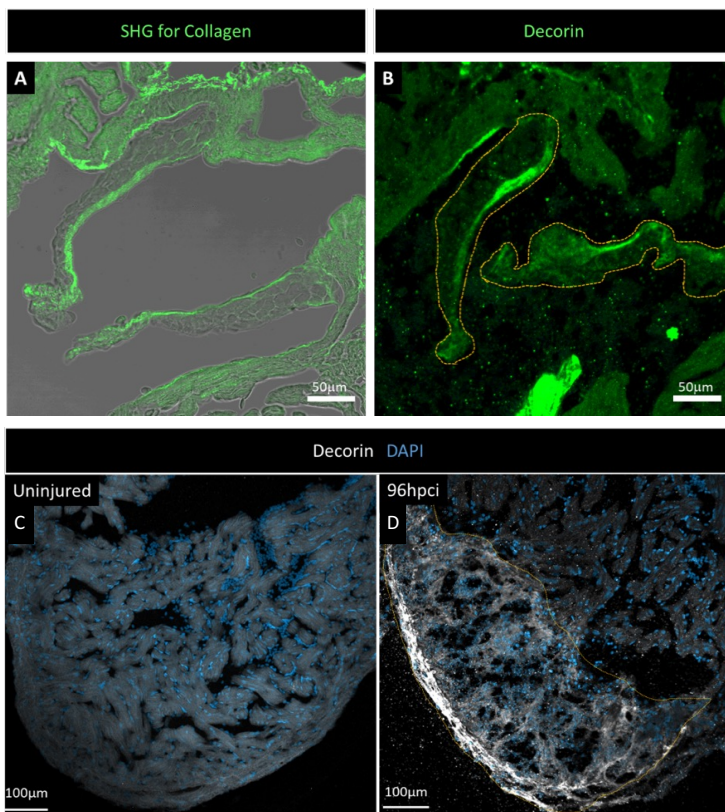


**Figure 4.7.** Second Harmonic Generated (SHG) image showing collagen fibers (A) and immunostaining with Decorin Antibody (B) of the zebrafish atrioventricular valve. Ventricular Apex of uninjured (C) and cryoinjured hearts (D) at 96 hpci, injury area outlined in gold.

## CHAPTER 4 - Results

Atrioventricular valves exhibit a striated ECM structure wherein collagen rich regions are observed in the direction of inflow to the valves, and Decorin's interaction with the collagens can be hypothesised through colocalization of Dcn and fibrillar collagen. (Fig. 4.7 A,B).

Additionally, post cardiac cryoinjury, the injury area is filled with a collagen rich scar, which acts in a transient manner to aid regeneration (González-Rosa et al., 2011). Upon cryoinjury, and immunostaining with Decorin Ab at 96 hpci, I observed that Decorin localization was high in the injured tissue (Fig. 4.7. C,D), and not detected in uninjured hearts altogether, suggesting that Decorin expression and secretion could be triggered by cardiac injury.

### 4.3.2. Decorin overexpression leads to increased myocardium thickness

40pg of Decorin mRNA was injected into zebrafish zygote in *Tg(kdrl:EGFP)* background. Spinning disk live movies and still confocal images of the heart were acquired at 80 hpf.

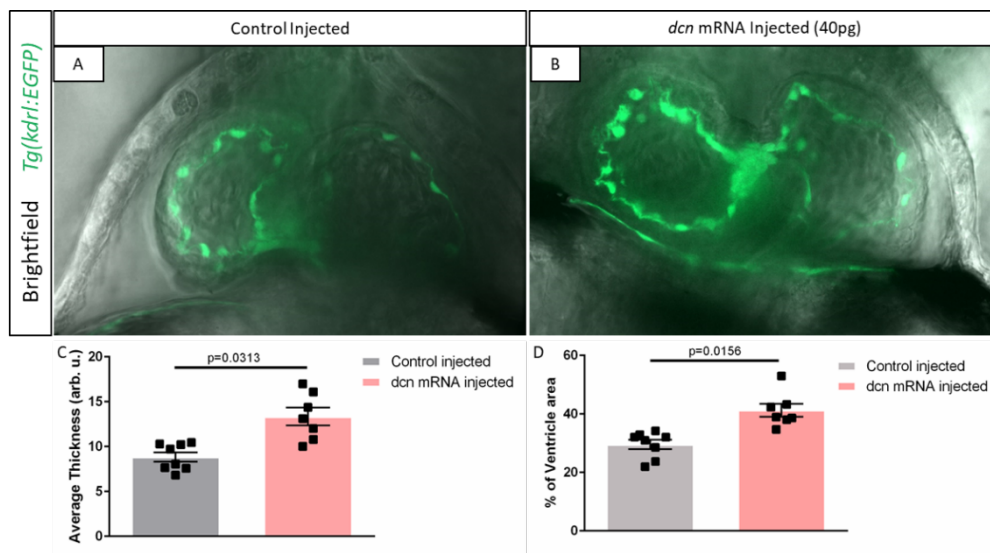


**Figure 4.8.** Mid Sagittal plane of 80 hpf hearts of Control mRNA injected (A) and whole *dcn* mRNA injected (B) larvae. Significantly increased average myocardial thickness in *dcn* mRNA injected hearts compared to control injected samples (C). Significantly increased composition of myocardial wall as a percentage of area of ventricle at diastole (D) in *dcn* mRNA injected larvae.

Assessment of cardiac contractility revealed abnormal motion of ventricle myocardium upon *dcn* overexpression (Figure 4.8. A,B) as well as thicker myocardial wall (Figure 4.8. C), which was further evident due to the increased composition of myocardium as a ratio of overall ventricle area measured at diastole (Figure 4.8. D), suggesting that *dcn* overexpression leads to an increase in myocardium thickness and affects cardiac contractility in the zebrafish.

### 4.3.3. DN Decorin overexpression leads to cardiac looping defects

Zebrafish zygotes in *Tg(kdrl:EGFP)* background were injected with 50pg of *DNdcn* mRNA, and control mRNA. Analysis of injected zebrafish larval hearts at 80 hpf revealed an increased lack of dextral looping upon *DNdcn* mRNA overexpression (Fig. 4.9 A, B).

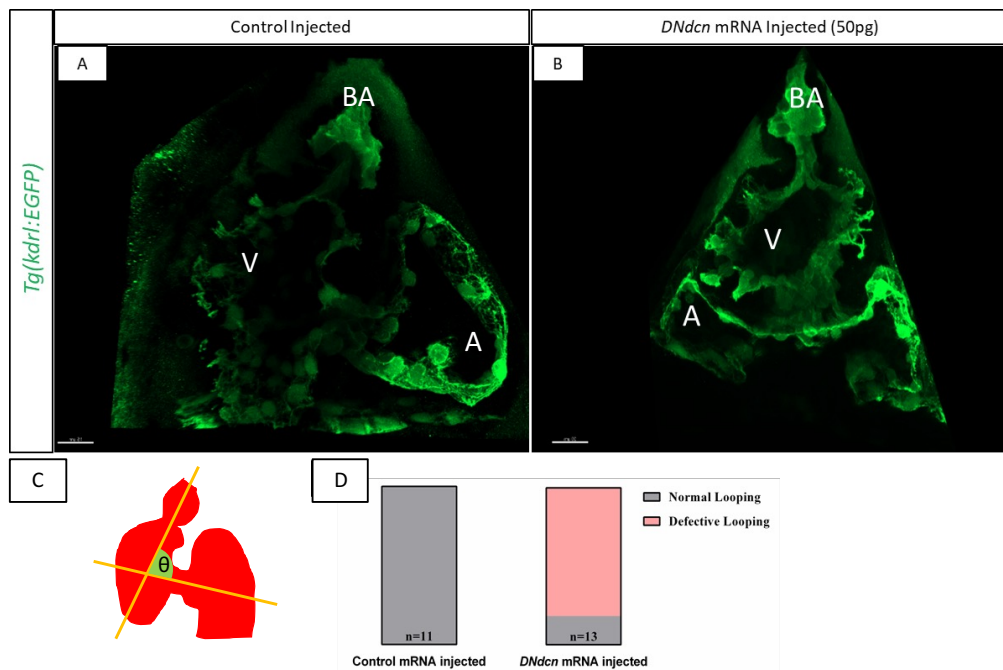


**Figure 4.9.** Mid Sagittal plane of 80 hpf hearts of Control mRNA injected (A) and *DNdcn* mRNA injected (B) larvae. Schematic for measurement of cardiac looping angle (C), Quantification of larval hearts exhibiting sinistral loop (D).

Looping angle quantification performed by measuring angle between the bulbus arteriosus – ventricle axis and the atrioventricular axis (Fig. 4.9 C), revealed an increased incidence of 180-degree angle in the *DNdcn* mRNA injected larvae (Fig. 4.9 D) suggesting potential role for native Dcn in looping morphogenesis and onset of asymmetry during development.

#### 4.4. The role of SLRP Prelp in heart development

Prelp expression and localization was analyzed through in-situ hybridization and immunofluorescence assays, to identify expression of RNA and Protein localization in developing hearts.

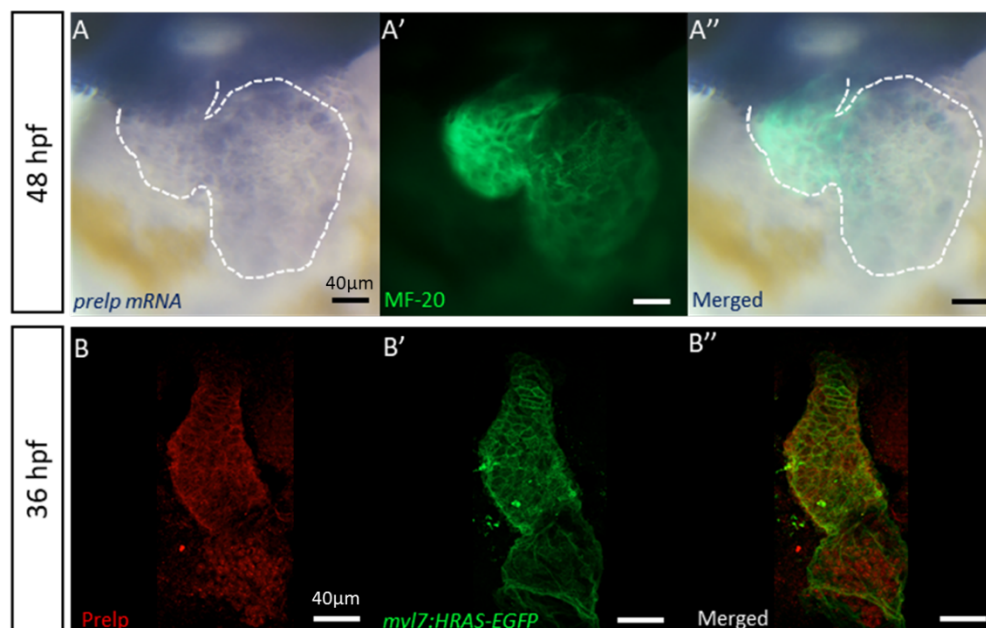


**Figure 4.10.** *in-situ* hybridization of 48 hpf zebrafish hearts (A), muscle stained with MF-20 (A') and merged (A''), Immunostaining against Prelp at 36 hpf (B), in cardiomyocyte specific myl7:HRAS-EGFP background (B') and merged (B''). Scale bars = 40  $\mu$ m.

Prelp mRNA was detected throughout the embryos at 48 hpf, notably in the head and in the myoseptum. Additionally, *prelp* expression was also detected in the heart, both in endocardial and myocardial tissues (Fig. 4.10 A-A''). Immunostainings at 36 hpf, indicated that Prelp localization in the tissue is closer to the membrane of the cardiomyocytes, and with increased intensity around the potential AV canal region (Fig. 4.10 B-B''). These data suggest that due to the nature of Prelp being primarily an ECM molecule, *prelp* expression and localization is not necessarily tissue specific in the heart during early developmental stages.



### 4.4.1. *Prelp* mutants exhibit reduced *prelp* mRNA and *Prelp* protein

*Prelp* mutant *bns416* allele was generated through CRISPR/Cas9 mutagenesis, and this encoded a premature truncation site close to the 3'-UTR, and subsequently the C-Terminal end of the protein. (Fig. 4.3).

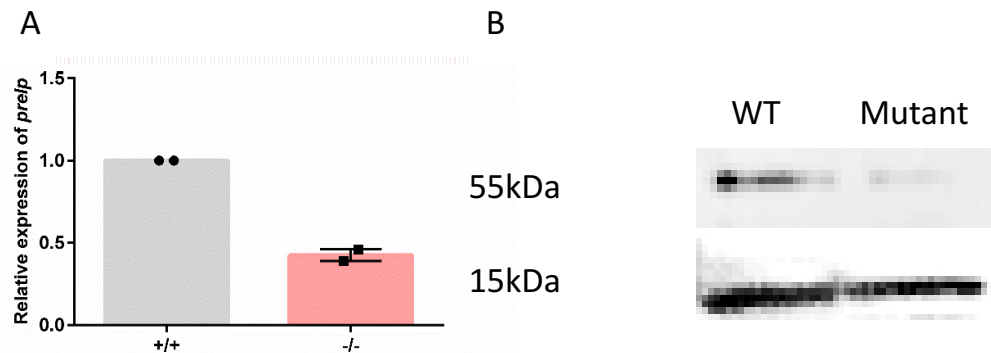


**Figure 4.11.** qPCR analysis of WT siblings and *prelp* mutants (A), Western blots of WT siblings and *prelp* mutants (B).

RT-qPCR analysis of WT siblings and *prelp*<sup>*bns416*</sup> mutants exhibited reduced levels of transcript in the mutants suggesting a potential mutant mRNA degradation (Fig. 4.11 A). To test whether the mutant protein expression was also affected, I performed a western blot analysis. Western Blots revealed that mutants still exhibited trace amounts of mutant protein, but nevertheless showed a reduction compared to WT, which can be attributed as a potential consequence of mutant mRNA degradation (Fig. 4.11 A,B).

#### 4.4.2. *Prelp* mutants exhibit increased pericardial edema and exhibit vascular defects

Single pair heterozygous parents were crossed together, and the subsequent resulting embryos were observed and genotyped post analysis. Focus was on potential cardiovascular phenotypes. I noticed that *prelp* mutants at 48 hpf exhibited a severe pericardial edema. I separated these embryos based on the severity of edema and genotyped them, to identify that a vast majority of embryos exhibiting severe edema were mutants (Fig 4.11. A, B, C).

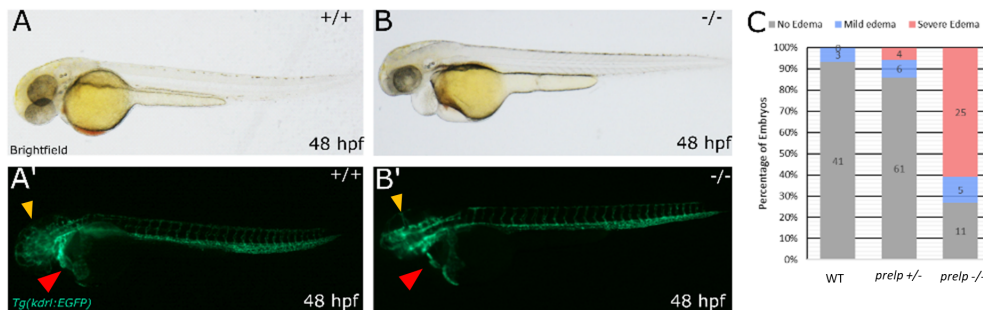
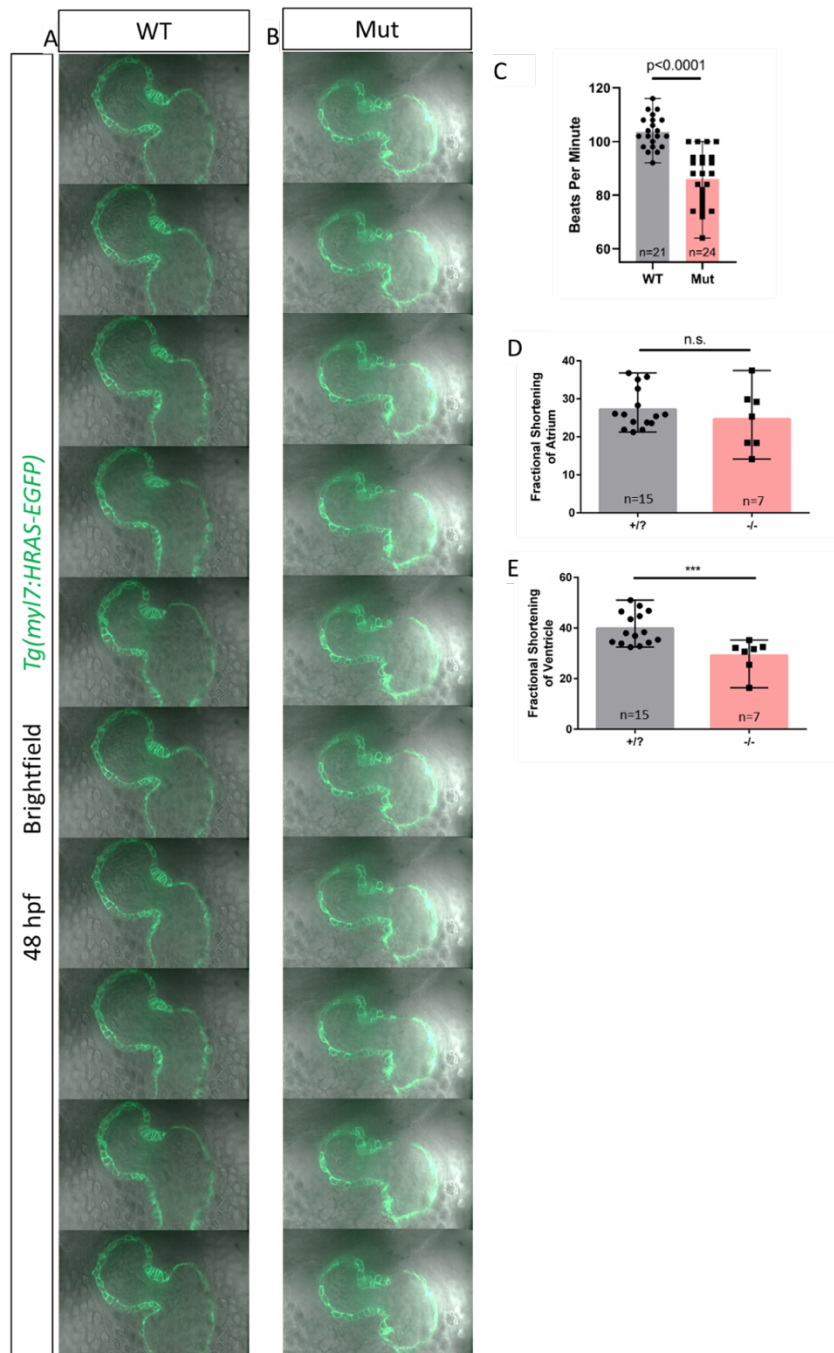


**Figure 4.12.** Brightfield embryos at 48 hpf of WT siblings (A) and *prelp* Mutants (B), and respectively in *Tg(kdrl:EGFP)* background (A',B'). Quantifications of severity of pericardial edema in mutants compared to WT and heterozygous siblings (C), with n of each quantified condition on graph.

Additionally, I noticed gross morphology defects with the thickness of the yolk extension in some of my mutants, as well as slower blood flow in the posterior cardinal vein (PCV), and hence decided to check them in the vascular background. Observing *prelp* mutants in *Tg(kdrl:EGFP)* background revealed two major preliminary findings. Mutants exhibited a severe lack of brain vasculature at 48 hpf (Yellow arrowhead, Fig. 4.12. A', B'), and additionally, mutants exhibited a less developed common cardinal vein (CCV) as well as a narrow ventricular endocardium, but an enlarged atrial endocardium, suggesting potential cardiac phenotypes. (Red arrowhead, Fig. 4.12. A', B').

### 4.4.3. Prelp mutants exhibit reduced heart rate and ventricular fractional shortening

Prelp mutants were imaged on a Zeiss® Spinning Disk microscope, at a rate of 20 frames per second, with an interval of 10 ms per frame. Average heart rate was measured at 105 beats per minute (bpm) measured at 20°C, for WT siblings, whereas mutants exhibited a reduced average heart rate of 90 bpm (Fig. 4.13 A, B, C).



## CHAPTER 4 - Results

**Figure 4.13.** Time series of one cardiac contraction with each image captured 10ms apart of WT and Mutant siblings at the Mid-sagittal plane (A,B), Heart rate calculated over a one-minute period (C), Fractional Shortening of Atrium (D), and Ventricle (E).

Additionally, contractility of atrium and ventricle were measured through fractional shortening, which revealed a reduction in fractional shortening of the ventricle in *prelp* mutants compared to their WT siblings. (Fig. 4.13 A, B, E). Interestingly, atrium contractility of *prelp* mutants exhibited a higher degree of variability (Fig. 4.13 A, B, D), suggesting that *prelp* mutant atria could potentially compensate for the reduction of ventricular contraction through variations of atrial contractility, thereby maintaining blood flow throughout the body. As previously mentioned, *prelp* mutants showed a reduction in blood flow in the PCV, but not an absence, suggesting that this reduction in blood flow could be influenced by the reduced fractional shortening of the ventricle.

#### 4.4.4. Prelp mutants exhibit enlarged atria at 48 hpf

Prelp mutant and sibling hearts were stopped and observed under an upright confocal microscope. Heart images were analysed based on mid sagittal area, surface area as well as volume. Mutants exhibited increased atrium size compared to their WT and heterozygous siblings (Fig. 4.14 A-D).

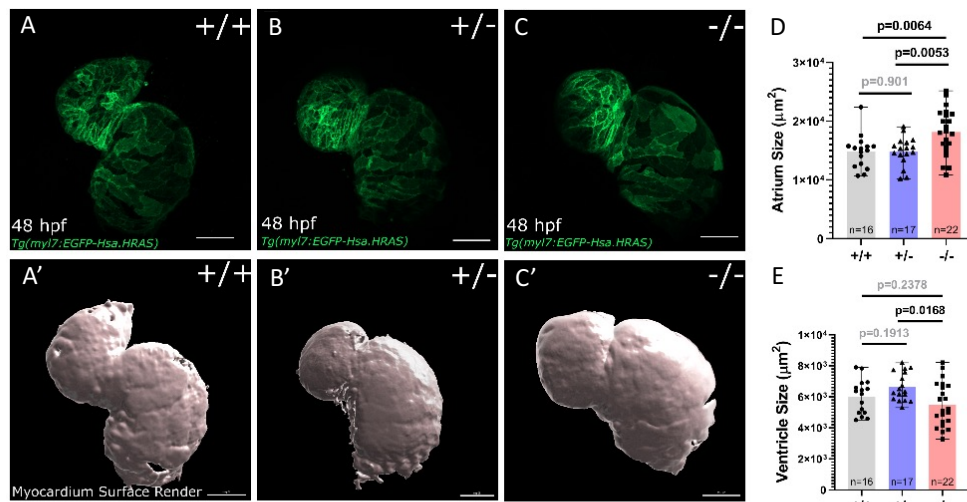


**Figure 4.14.** Maximum intensity projection of live hearts at 48 hpf in *Tg(my17:EGFP-Hsa-HRAS)* background of WT (A), Heterozygous (B) and Mutant (C). 3D surface render of hearts of WT (A'), Heterozygous (B'), and Mutant (C'). Quantification of Atrium size (D) and Ventricle Size (E) measured based on 3D surface renders. Scale bar = 50  $\mu\text{m}$ .

Mutants also exhibited a reduced ventricle size in comparison to heterozygous siblings (Fig. 4.14 A-C, E), suggesting an incomplete penetrance of the cardiac chamber size phenotype (Fig. 4.14 E). Cardiac surfaces were also analysed by 3D myocardium surface renders to detect cardiomyocytes protruding abluminally. Preliminary observation did not reveal any differences in the protrusion of CMs across the genotypes, suggesting that potential increase in size could be either due to an increased number of cardiomyocytes which remain in the cardiac wall, or due to increased size of the cardiomyocytes.

#### 4.4.5. *Prelp* mutants exhibit an enlarged atrium and reduced ventricle size at 72 hpf

I stopped and observed *prelp* WT and mutant hearts under the microscope at 72 hpf. Initial observations revealed the lack of dextral looping of the hearts (Fig. 4.15 A, B, C). Additionally, atrium and ventricle chamber size measured from mutant hearts at 72 hpf revealed that *prelp* mutants have a larger atrium but a reduced ventricle size in comparison to their WT siblings (Fig. 4.15 A-E).

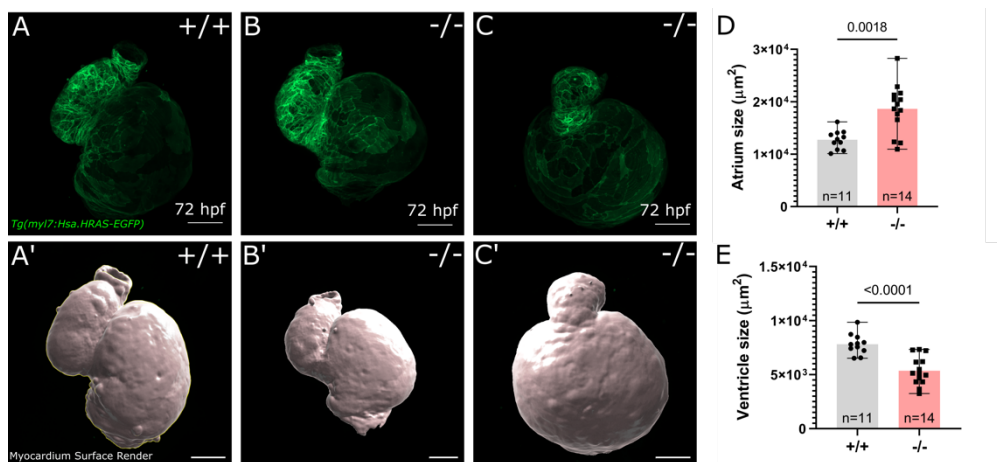


**Figure 4.15.** Maximum intensity projection of live stopped hearts at 72 hpf in *Tg(myl7:EGFP-Hsa-HRAS)* background of WT (A), Mutant (B and C). 3D surface render of hearts of WT (A'), Mutant (B' and C'). Quantification of Atrium size (D) and Ventricle Size (E) measured based on 3D surface renders. Scale bar = 50  $\mu\text{m}$ .

Upon preliminary observation of the myocardial surface renders, I noticed that *prelp* mutants appear to exhibit a slightly reduced incidence of abnormally protruding CMs (Fig. 4.15 A'-C'), suggesting that perhaps the increased chamber size could potentially be due to increased number of CMs rather than increased size of individual CMs.

#### 4.4.6. Cardiac contractility does not affect atrium size in *prelp* mutants

As previously mentioned, *prelp* mutants exhibited differences in cardiac contractility (Fig 4.13), which could lead to the cardiac chamber size differences observed (Fig 4.14, 4.15). To test this hypothesis, I injected *tnnt2a* morpholino into *prelp* mutants as an established method to stop the onset of cardiac contraction (Sehnert et al., 2002).

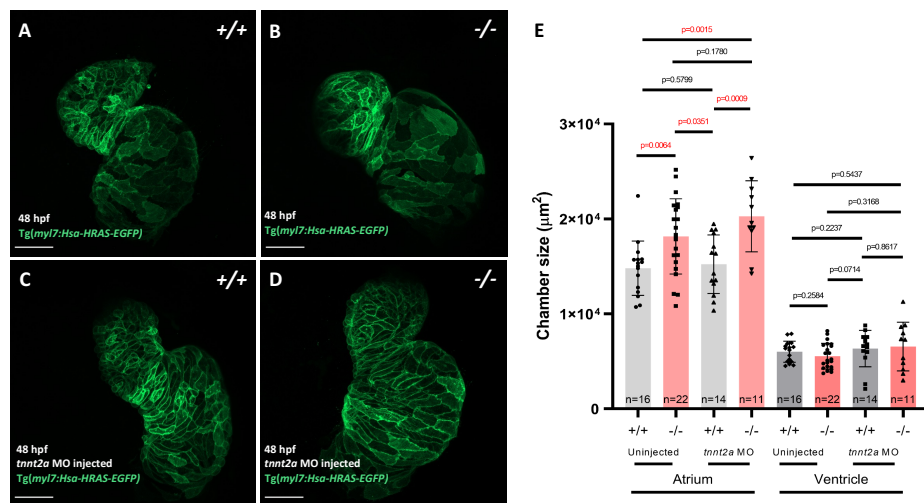


**Figure 4.16.** Maximum intensity projection of live stopped hearts at 48 hpf in Tg(my17:EGFP-Hsa-HRAS) background of uninjected WT (A), Mutant (B), *tnnt2a* Morpholino injected WT (C), and *tnnt2a* MO injected Mutant (D). Quantification of Atrium and Ventricle sizes across conditions of uninjected, and *tnnt2a* MO injected across WT and mutant hearts (E). Scale Bar = 50 μm.

Imaging and subsequent analysis of hearts at 48 hpf revealed that the atrium chamber size remained increased in mutant hearts lacking contractility (Figure 4.16. A-D), suggesting that the atrium size increase is contractility independent (Figure 4.16. B, D, E). Similarly, there was no significant change in ventricle size across the board, suggesting that the inherent changes in atrium size could be attributed to either an increased number of atrial cardiomyocytes, or an increased size of atrial cardiomyocytes.

### 4.4.7. *Prelp* mutants exhibit increased number of atrial cardiomyocytes

To test the above hypothesis, I crossed the mutant into a cardiomyocyte nuclear reporter background. I noticed that *prelp* mutants exhibited an increased number of atrial cardiomyocytes, compared to their siblings, whereas the number of ventricular cardiomyocytes remained unchanged (Fig. 4.17)

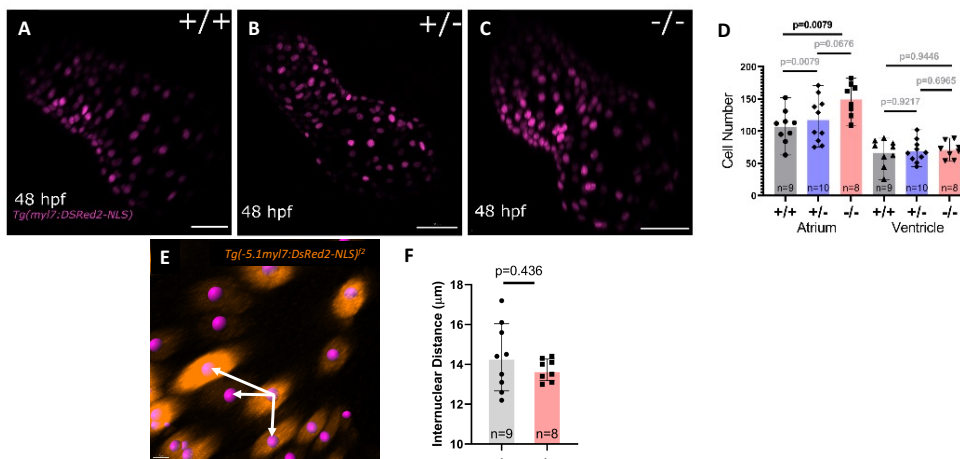


**Figure 4.17.** Maximum intensity projection of live stopped hearts at 48 hpf in *Tg(myI7:DSRed2-NLS)* background of WT (A), Heterozygous (B), and Mutant (C), Scale Bar = 50 μm. Quantification of number of atrial and ventricular cardiomyocytes (D). Schematic representation of quantification of distance to 3 nearest neighbours using nuclear centroid (E), Scale Bar = 5 μm. Average cardiomyocyte internuclear distance between WT and mutant siblings (F).

I further analysed these hearts by segmenting the nuclei using IMARIS to measure the internuclear distance as a proxy of cell size. This analysis showed no significant change in cell size in *prelp* mutants compared to their WT siblings (Fig. 4.17. E,F). These data suggest that the increase in atrium size is due to increased number of atrial cardiomyocytes in the *prelp* mutants and not due to changes in cell size. Based on this, I hypothesized that the increased number of cardiomyocytes could be due to increased proliferation, reduced apoptosis, or increased addition of cells from the second heart field, which are currently open hypotheses.



#### 4.4.8. Extracellular Laminin localization is disrupted in *prelp* mutants at 36 hpf

Prelp as a basement membrane proteoglycan, is known to interact with various proteins of the basal lamina. One such significant family of proteins is the Laminin family of proteins. I decided to check the basal lamina integrity and localization in *prelp* mutants which led me to perform immunostainings against Laminin in the hearts.

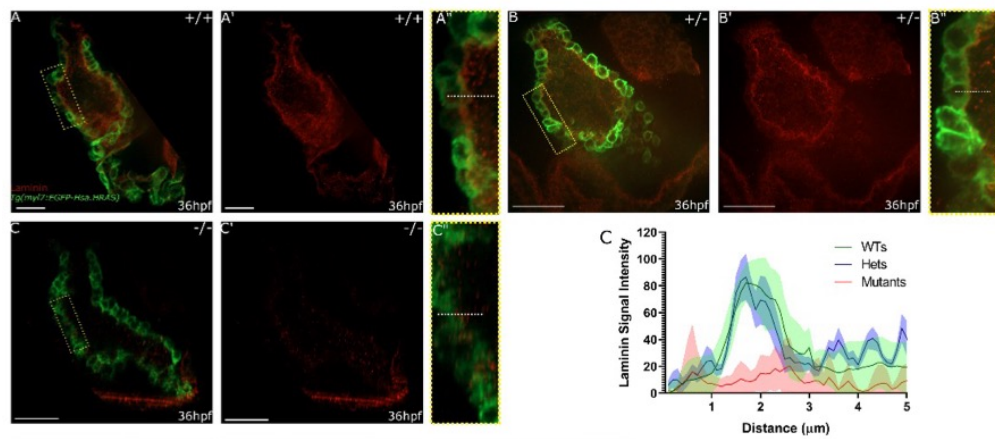


**Figure 4.18.** Mid-sagittal plane of fixed 36 hpf hearts in *Tg(myl7:EGFP-Hsa.HRAS)* background immunostained against Laminin in WT siblings (A), Heterozygous siblings (B), and *prelp* mutants (C). Corresponding single channel images of immunostaining against Laminin at the same focal plane (A',B',C'), and corresponding enlarged inset with schematic of laminin signal intensity quantification (A'',B'',C''). Mean (solid line) and SD (shaded region) of Laminin signal intensity quantification of 10 cardiomyocytes in the outer curvature averaged per heart with WT n=30, Het n=17, Mut n=29. (D). Scale Bar = 50  $\mu$ m.

Preliminary analysis post imaging revealed that *prelp* mutants exhibit a severe lack of laminin localization in the luminal side of the cardiomyocytes (Fig. 4.18 A-D). Laminin localization can be observed clearly in the WT and heterozygous siblings in the basal side of the cardiomyocytes, thereby suggesting a correlation between *prelp* mutation and the localization of laminin basal to cardiomyocytes (Fig. 4.18 A-C''). These data suggest that *prelp* expression and secretion could be important for either laminin localization post

secretion, or laminin organization, or stabilization of basal laminin. The exact process which leads to lack of laminin localization is still unknown. Surprisingly, laminin secretion is not affected in the *prelp* mutant since laminin signal can still be detected in the *prelp* mutants. But the localization is severely disrupted (Fig. 4.18 D), suggesting that Preplp may only be required for either the assembly or stability of the lamina, but not for the expression and secretion of laminins.

#### 4.4.9. Cardiac Jelly thickness and volume is increased in *prelp* mutants at 48 hpf

Based on the disrupted localization of laminin in *prelp* mutants, I hypothesized that the dynamics of the other major component of the CJ, the cardiac HA could be disrupted. To test this hypothesis, I crossed *prelp* mutants into the published HA biosensor background (Grassini et al., 2018).

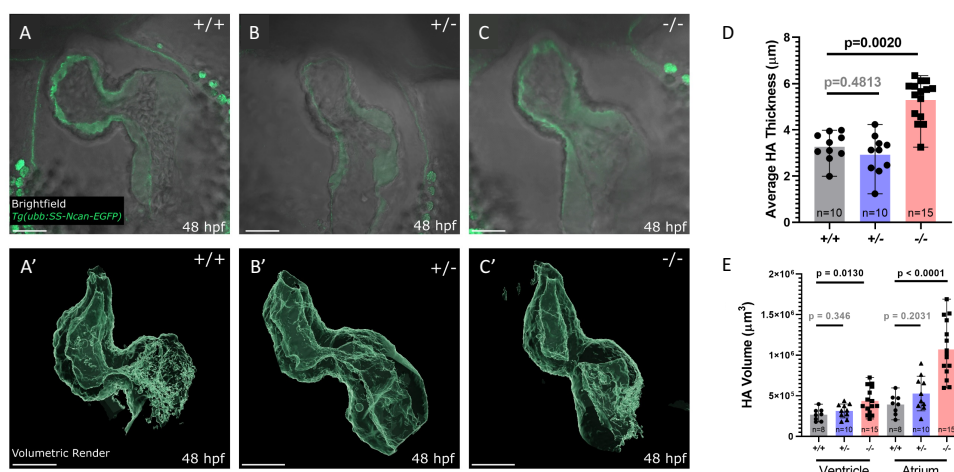


**Figure 4.19.** Brightfield images at the mid-sagittal plane of live, stopped 48 hpf hearts in *Tg(ubb:SS-Ncan-EGFP)* background of WT siblings (A), Heterozygous siblings (B), and *prelp* mutants (C). Corresponding 3D volumetric render of cardiac jelly (A'-C'). Average thickness of Cardiac HA measured as area of mid-sagittal HA over the length of the heart (D). Overall volume of ventricular HA and Atrial HA measured from the 3D volumetric render of cardiac jelly (E). Scale bar = 50 μm.

## CHAPTER 4 - Results

Preliminary observations through live imaging at 48 hpf revealed that *prelp* mutants have enlarged chamber size of the atrium (as observed in Fig. 4.14). Mutants also exhibited a reduced size of the cardiac lumen (as observed in Fig. 4.12). I then measured the average thickness of the cardiac jelly, and then genotyped the imaged embryos to reveal that *prelp* mutants exhibited an increased CJ thickness compared to their WT and heterozygous siblings. (Fig. 4.19 A, B, C, D). Since the thickness measurement was only performed in and around the mid-sagittal plane for each heart, I decided to perform a 3D volumetric rendering of the cardiac HA by segmenting the cardiac jelly using IMARIS. With this segmentation, I digitally dissected the cardiac HA volume into the atrial and ventricular volumes of cardiac HA at the midpoint center of the atrioventricular canal (AVC). Data from the segmentation revealed that both atrial and ventricular HA volumes were increased in the *prelp* mutants in comparison to their WT and heterozygous siblings (Fig. 4.19 A', B', C', E) suggesting that the increase in HA thickness and HA volume are due to mutation in *prelp*. I then hypothesized that this increase in thickness in the mutants could be potentially attributed to either increased expression of HA and therefore increased accumulation of water in the cardiac jelly, thereby expanding it, or due to a reduction in degradation of HA or a combination of both, thereby delaying the maturation of the CJ in the *prelp* mutants.

#### 4.4.10. Sarcomere distribution is irregular in *prelp* mutants at 48 hpf

Based on the disruption to BL localization and contractility defects observed in *prelp* mutants, I hypothesized that formation of the sarcomeres could be affected. To test this, I crossed the *prelp* mutants into the *Tg(myl7:EGFP-actn3b)* background which labels the z band of the sarcomeres.

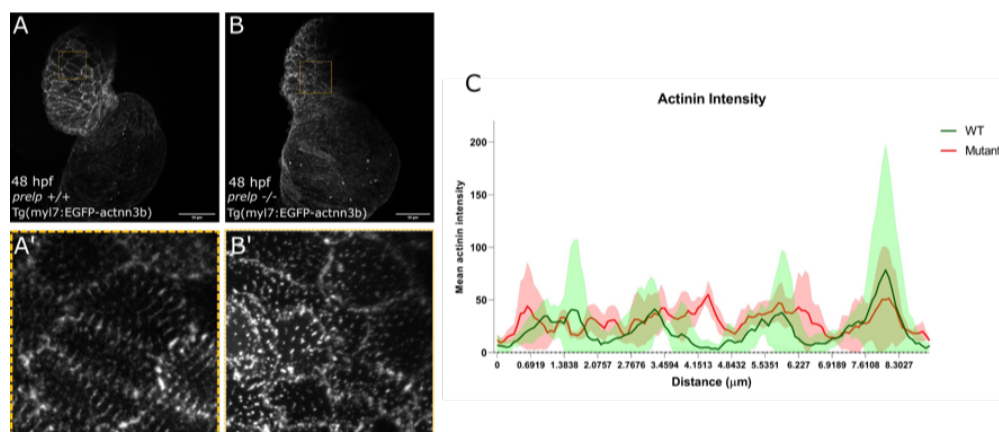


**Figure 4.20.** Maximum intensity projections of 48 hpf hearts of WT siblings (A) and *prelp* mutants (B) in *Tg(myl7:EGFP-actn3b)* background labelling sarcomeres. Enlarged inset from A (A'), and B (B'). Measurement of signal intensity regularity along sarcomeres over distance of 5µm, between WT (n=15) and Mutants (n=21) (C). Scale bar = 50 µm.

I noticed that *prelp* mutants exhibit disrupted organization of the sarcomeres (Fig. 4.20. A,B) at 48 hpf. Upon closer observation, I noticed that the sarcomere distribution was affected more than the expression and localization, suggesting that this could potentially be more of a consequence of irregular cardiac contraction of the mutants (Fig 4.20 A',B', C; Fig. 4.13). This disruption was more prominent in mutant hearts which exhibited a slower heart rate, which suggested that the reduced mutant heart rate could either be a consequence of irregular sarcomere organization, or also potentially a cause of irregular sarcomere assembly.

#### 4.4.11. Irregular sarcomere assembly can be attributed to impaired cardiac contractility in *prelp* mutants at 48 hpf

To test the hypothesis regarding sarcomere organization and cardiac contractility, I injected the *tnnt2a* MO into the mutants and WT siblings in the Z band reporter background. I noticed that the mutant sarcomere phenotype was phenocopied by the WT hearts (Fig. 4.21 A-B') suggesting that the sarcomere assembly is potentially driven by the contractility of the cardiomyocytes, and regular sarcomere organization leads to more efficient heart beating thereby suggesting a potential feedback loop.

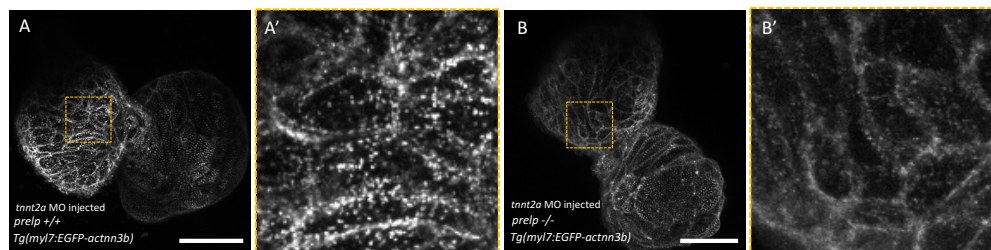


**Figure 4.21** Maximum intensity projections of *tnnt2a* MO injected 48 hpf hearts of WT siblings (A) and *prelp* mutants (B) in *Tg(myl7:EGFP-actn3b)* background labelling sarcomeres. Enlarged inset from A (A'), and B (B'). Scale bar = 50  $\mu$ m.

It remains unclear which comes first in the *prelp* mutants, the reduced heart rate, or the sarcomere assembly defects. Since the cardiac contraction is indistinguishable between WT and *prelp* mutants through Nomarski microscopy earlier than 30 hpf, we hypothesized that the setup of the sarcomeres could very well define the heart rate defects in the *prelp* mutants. This hypothesis is yet to be tested

#### 4.4.12. Actin fiber orientation is disrupted at 36 hpf in *prelp* mutants

Based on previous observations with the sarcomeres, I wanted to take a closer look at the actin fibers directly and at an earlier developmental timepoint. To test this, I stopped the hearts and fixed the embryos at 36 hpf, and then subjected them to immunostaining against Phalloidin (Fig. 4.22. A, B, A',B').

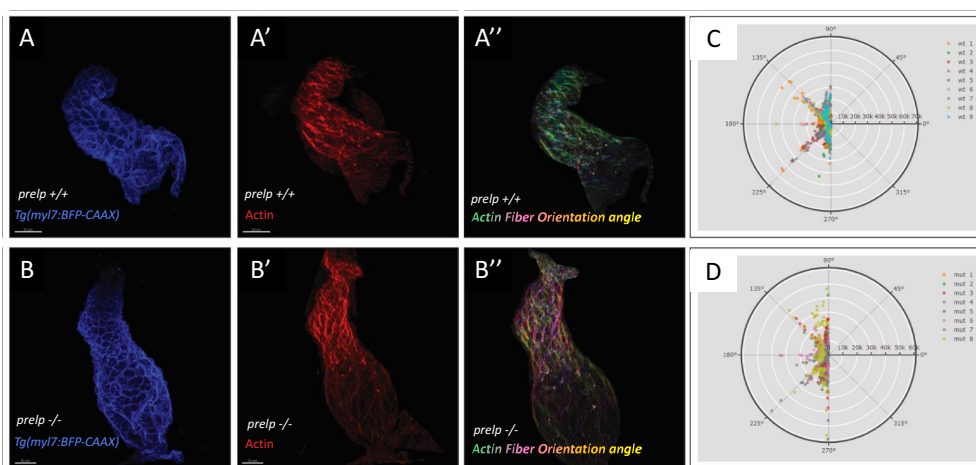


**Figure 4.22.** Stopped and fixed hearts at 36 hpf of WT sibling (A) and *prelp* (B) mutants in *Tg(myf7:BFP-CAAX)* background. Corresponding hearts treated with Phalloidin, labelling actin fibers (A',B'), and directionality analysis performed with a OrientationJ plugin on Fiji providing orientation angle at the corresponding genotypes (A'', B''). Radial plot of fiber orientation among WT (n=9) (C) and Mutant (n=8) (D). Scale bar = 30 μm.

Phalloidin, being a toxin that binds to actin fibrils (“Actin and Actin-Binding Proteins,” 2017), enables easy visualization of the actin fiber assembly and orientation in the hearts at earlier stages when used with a conjugate fluorophore. Preliminary observation revealed that the actin fibrils appeared thicker and more well defined in the WT siblings in comparison to their mutant brethren (Fig. 4.22 A',B'). More prominently, the actin fiber orientation appeared to be completely different in the mutants compared to the WT siblings (Fig 4.22 A', B', A'', B''). To visualize this more clearly, I utilized a macro

tool in FIJI using the OrientationJ Plugin, to detect the actin fiber orientation in relation to the AV axis of the heart and providing subsequent angles for each fibril. These data were then plotted on a radial plot using R, to enable quantification of this orientation of the fibrils (Fig 4.22 A'', B'', C, D). Upon plotting the angle of the fibrils, it became clear that the actin fibrils cluster along 45° angles in the WT scenario, and this was consistent across the different hearts wherein this analysis was performed. In the mutant hearts on the other hand, it was clear that many hearts still orient the actin fibrils along 45° angles, but the increased incidence of irregular orientation noted in the mutants suggest that the intracellular molecular defects observed could be an outside-in effect such that, the disrupted BL and CJ could play a role on the actin and the sarcomeres in the heart.

#### 4.4.13. Transcriptomics analysis on *prelp* mutants

Based on the above phenotypic data, I proceeded to prepare samples and submit them to the Bioinformatics and Deep Sequencing Facility of MPIHLR, to understand differences in transcriptome of *prelp* mutants and WT siblings.

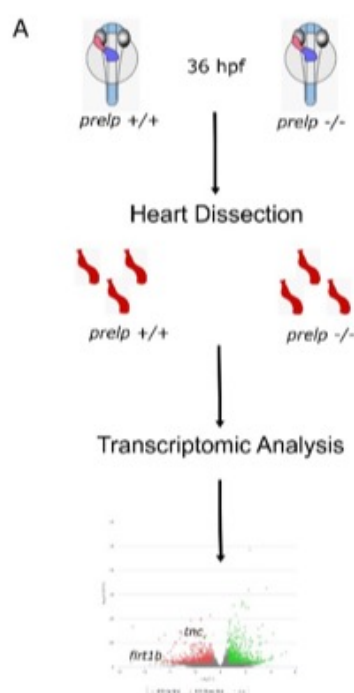


**Figure 4.23.** Schematic diagram of workflow leading to transcriptomics analysis and subsequent acquisition of RNAseq dataset. (A)

This analysis would enable deeper identification of transcriptional changes during the heart development processes, which could potentially explain the various phenotypes observed in the mutants. To this effect, I prepared the samples using the methods described in Section 3.2.5 of this

thesis. Upon receiving the sequencing results, I noticed that, samples appeared to be of a high quality and Principal Component Analysis exhibited distinct clustering of WT and Mutant samples across a major dimension of the reduced matrix, suggesting a robust dataset within which nearly 1400 genes were significantly differentially regulated between WT and Mutants, indicating that many potential processes are affected in the *prelp* mutants.

#### 4.4.14. Reactome analysis reveals multiple downregulated genes related to ECM

The RNA sequencing data was subjected to analysis through the bioinformatics pipeline of the MPIHLR sequencing facility, and the subsequent results were identified based on the above analysis.

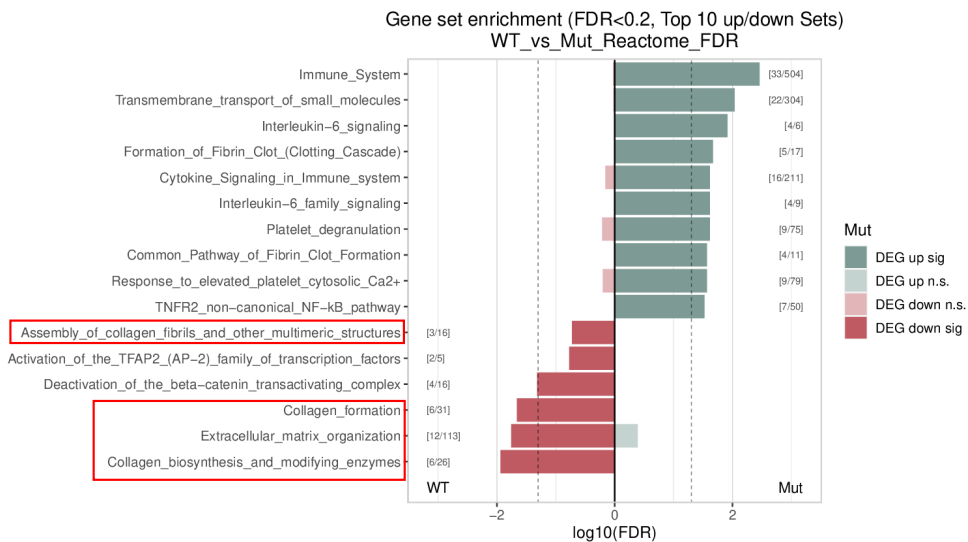


**Figure 4.24.** WT vs Mutant Reactome analysis of extracellular factors and their general family of activity identified based on gene ontology.

Differentially regulated genes were clustered based on their gene ontology, and for the reactome analysis, genes which were involved in extracellular roles were isolated. *prelp* mutant hearts exhibited an increased upregulation of genes



related to immune system and pathways related to cytokine signaling. Contrary to expectations, mutants exhibited a marked downregulation of genes related to the organization and assembly of the extracellular matrix (Fig. 4.24). Surprisingly, genes not only involved in extracellular assembly, but also in biosynthesis and modification of large ECM Proteins such as Collagens were downregulated in the mutant hearts, suggesting a potential retention of early and naïve ECM niche in the mutants in comparison to their WT siblings. Based on the reactome analysis, I also decided to take a closer look at which potential pathways were affected.

#### 4.4.15. KEGG Pathway and Gene Ontology analysis on *prelp* mutants reveals downregulated ECM-receptor interactions

KEGG Pathway analysis revealed that mutant hearts showed increased upregulation of genes related to cytokine-cytokine interactions and genes belonging to the MAPK-signaling pathway. Most interesting to me was the downregulation of genes enrichment related to the ECM-Receptor interaction (Fig 4.25 A).

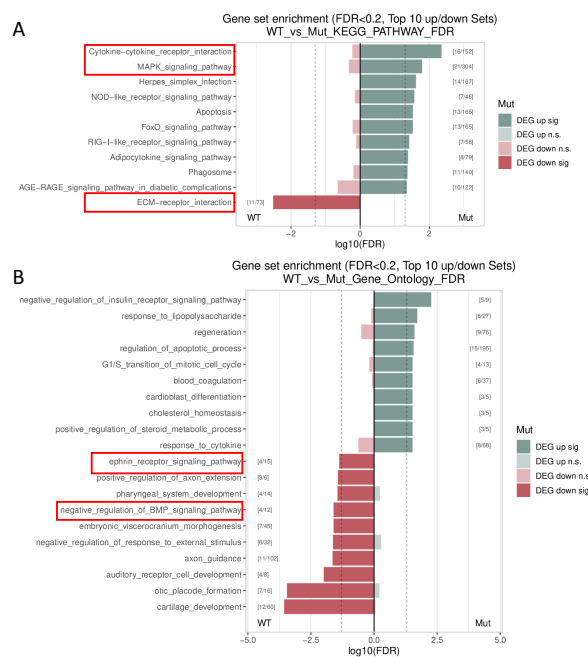


**Figure 4.25.** KEGG Pathway analysis (A) and Gene Ontology analysis (B) on mRNA from *prelp* mutant hearts compared to their WT siblings

Additionally, in the broader gene ontology context, genes related to BMP signaling pathway and ephrin receptor signaling pathway were downregulated in the mutant hearts as well (Fig 4.25 B). Overall, these data reveal a multitude of variations in the mutants, suggesting perhaps a majority of the transcriptional changes observed would be indirect effects on the heart due to extracellular changes, rather than direct effects of *prelp* mRNA or Prelp protein insufficiency. To look at the data in a more granular manner, I looked at individual genes which were differentially regulated in the mutants.

#### 4.4.16. Differentially regulated genes which potentially explain *prelp* mutant phenotypes

I previously noted that *prelp* mutants exhibit an increased volume of cardiac jelly (Fig. 4.19) and hypothesized that this could either be due to increased secretion of ECM markers, or reduced degradation of cardiac HA.

Gene	Description	Log2FC
<i>cemip</i>	Cell migration inducing hyaluronidase	-0.95
<i>mmp15b</i>	Matrix metallopeptidase 15b	-0.98
<i>tnc</i>	Tenascin – C	-1.28
<i>lama4</i>	Laminin Alpha 4	-0.37
<i>lamc3</i>	Laminin Gamma 3	-1.86
<i>podxl</i>	Podocalyxin	+0.33

**Table 4.5.** Genes related to ECM modification and organization differentially regulated in *prelp* mutant hearts

The genes *cemip* and *mmp15b* are interesting candidates downregulated in the *prelp* mutant hearts to support this hypothesis (Table 4.5). The gene Cell migration-inducing and hyaluronanidase protein (Cemip) belongs to a very well-established family of HA degrading factors during early development (de

Angelis et al., 2017; Grassini et al., 2018; Totong et al., 2011) and the downregulation of this factor suggests that perhaps *prelp* mutants are exhibiting reduced ECM degradation. This hypothesis is further supported by the downregulation of the Matrix Metalloproteinase 15b (*mmp15b*), another factor which is involved in degradation of various ECM genes (O.-H. Kim et al., 2019; Tao et al., 2011). Additionally, the laminin organization phenotype observed in the *prelp* mutant could potentially be assisted by the fact that the endothelial specific laminin gene, Laminin alpha-4 (*lama4*) is downregulated. Additionally, the multimerization of laminins depends on the beta and gamma chains which enable the formation of the lamina, which could be impacted in the *prelp* mutants due to downregulated expression of Laminin gamma-3 (*lamc3*). Furthermore, a significant ECM maturation factor Tenascin-C (*tnc*) is significantly downregulated in the *prelp* mutant hearts suggesting that the extracellular niche of the mutants retain an immature state for a longer in the developmental process. Surprisingly, the apical polarity marker of cells Podocalyxin (*podxl*) was slightly upregulated in the *prelp* mutants which suggested that the mutant hearts, which lack basal lamina organization and increased cardiac hyaluronan could potentially exhibit polarization defects of the epithelial myocardium.

#### 4.4.17. Cardiomyocytes in *prelp* mutants exhibit lack of apical polarization

To test the hypothesis regarding polarity of cardiomyocytes, I took a closer look at the mutant hearts crossed into a previously published cardiomyocyte polarity reporter transgenic background (Jiménez-Amilburu et al., 2016).

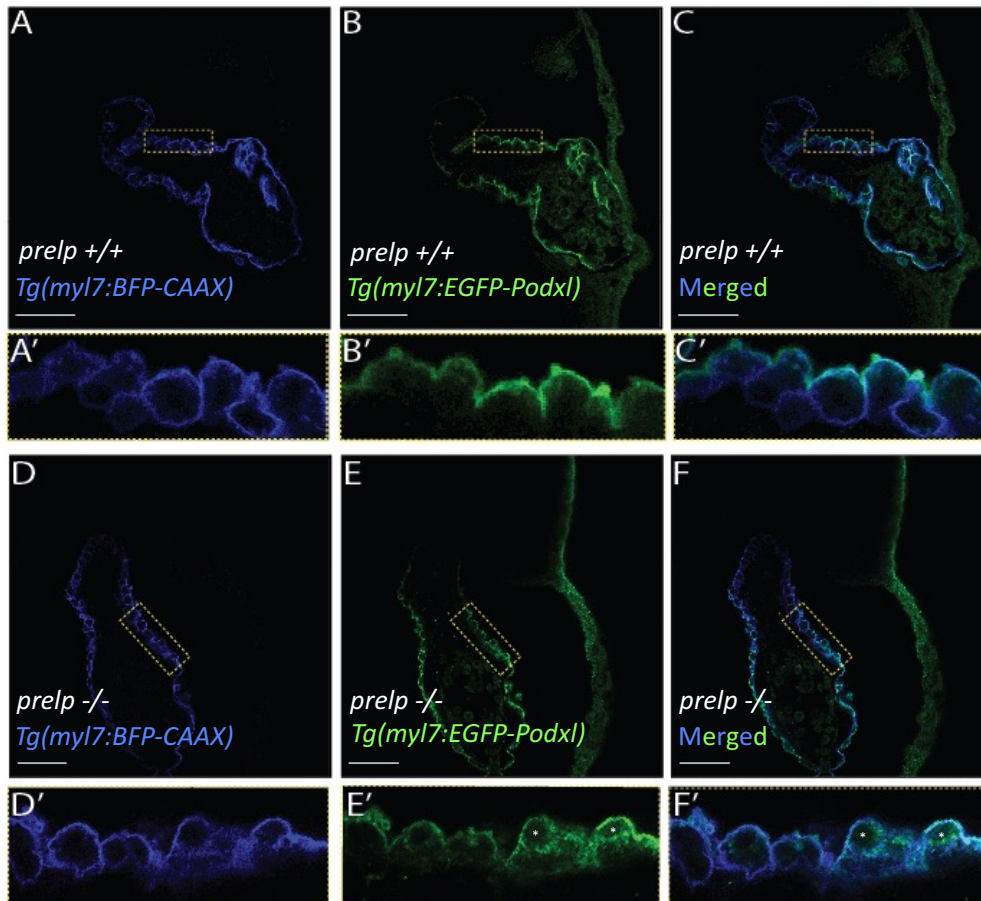


**Figure 4.26.** Mid-sagittal planes of fixed and immunostained 36 hpf hearts of WT (A, B, C) and *prelp* mutants (D, E, F) in the *Tg(myI7:BFP-CAAX)* background (A,D), *Tg(myI7:EGFP-Podxl)* background (B,E) and merged (C,F). Corresponding enlarged inset of A-F (A'-F'). Scale bar = 30  $\mu$ m.

I noticed that *prelp* mutant hearts exhibit an increased number of cardiomyocytes which were rounded up around the region of the atrioventricular canal (Fig 4.26 A-F'), and these rounded cells exhibited an increased localization of Podxl throughout the cell membrane suggesting loss of apical polarity. This could also be an outside-in signaling effect due to the

basal lamina disorganization in the *prelp* mutants. This raises the question whether these cardiomyocytes are potentially losing their epithelial identity, and this remains yet to be answered.

#### 4.4.18. Mutant cardiomyocytes exhibit increased sharp abluminal protrusions

I wanted to observe mutant and WT cardiomyocytes in high magnification and resolution to identify potential morphological differences to answer the question regarding the epithelial identity loss of the cardiomyocytes. Hence, I performed high resolution and high contrast imaging of the cardiomyocytes in the *Tg(myI7:EGFP-Hsa.HRAS)* membrane background utilizing the Airyscan technique in a Zeiss® LSM880 confocal microscope.

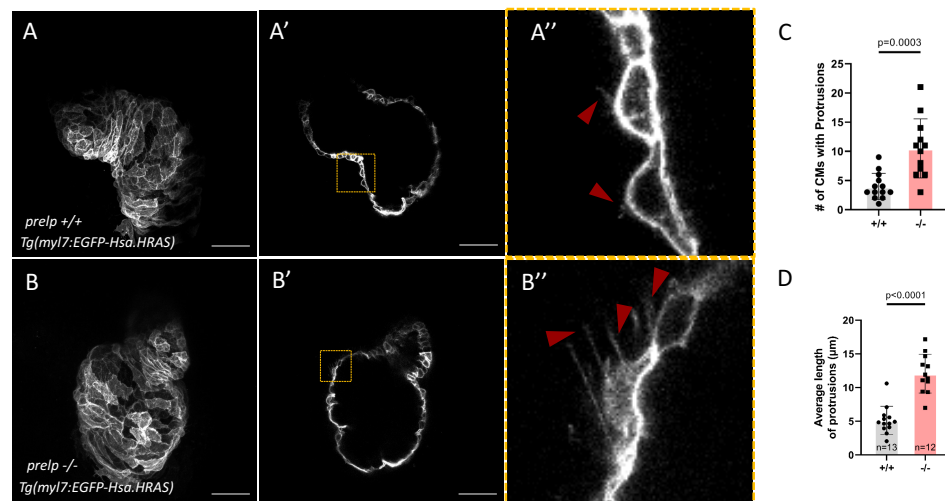


**Figure 4.27.** Maximum intensity projections of 48 hpf live stopped hearts of WT (A), and *prelp* mutants (B), mid sagittal plane of WT (A') and mutants (B') and respective enlarged inset (A'', B''). Quantification of number of cardiomyocytes exhibiting abluminal protrusions (C), Quantification of the average length of each protrusion (D). Scale Bar = 50  $\mu\text{m}$ .

This technique provided the ability to observe previously obscure details of specific long abluminal protrusions extending from the cardiomyocytes (Red arrows in Fig. 4.27 A'', B''). Upon screening individual cardiomyocytes from

each heart, I noticed that more mutant cardiomyocytes exhibited long abluminal protrusions in comparison to their WT siblings (Fig. 4.27 C). Additionally, on average, the length of the protrusions from the cardiomyocytes in the *prelp* mutants was significantly increased compared to their WT siblings (Fig. 4.27 D), suggesting that these protrusions could be a result of cells losing their epithelial identity. Or potentially, the mutant CMs could be extending these protrusions as a search for adhesion to extracellular lamina which is disrupted.

#### 4.4.19. Truncated forms of Prelp generated to identify domain specific roles of Prelp

To test whether different domains of Prelp had different roles in the cardiac jelly and could potentially partially rescue some of the *prelp* mutant phenotypes, I generated mRNA corresponding to truncated versions of the Prelp protein according to the schematic (Fig. 4.28 A).

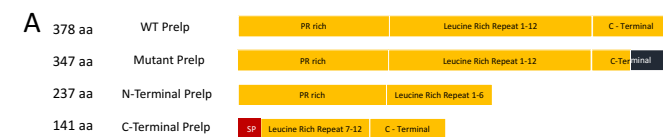
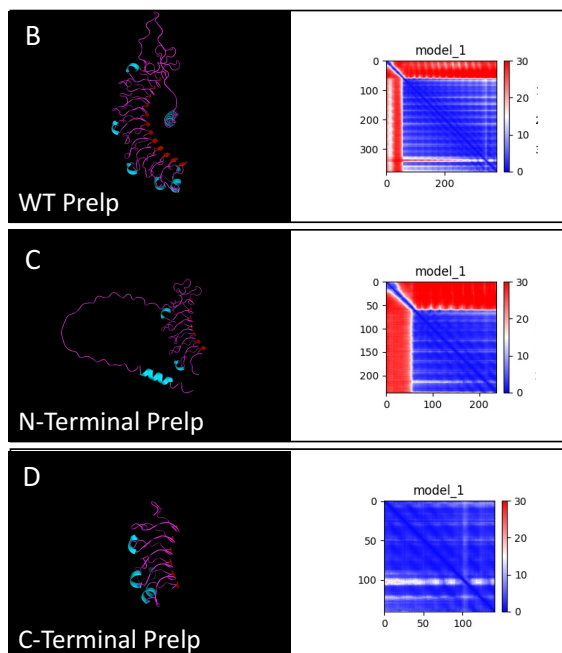


**Figure 4.28.** Schematic representation of size and Protein domains of different forms of Prelp (A), and subsequent AlphaFold predicted protein structures and prediction confidence of WT (B), N-terminal Prelp (C) and C-Terminal Prelp (D).



## CHAPTER 4 - Results

To predict potential folding of these truncated Protein structures, I took advantage of the recently released Alphafold2 program (Jumper et al., 2021). Resultant folded proteins were categorized based on prediction confidence model (Fig. 4.28 B-D). Model score was evaluated by Alphafold2, and lower number on confidence matrix suggested lower chances of potential alternative conformations of each amino acid (Fig. 4.28 B-D). Structure and confidence prediction revealed that N-terminal Prelp truncated protein would encode an open and active N-terminal domain, which is usually quenched in the WT version of the protein (Fig. 4.28 B,C) until dimerized. This prediction suggested that the N-terminal truncated version of Prelp could potentially bind to targets without homodimerization of Prelp, suggesting a potential constitutive active form of Prelp. This prediction enabled me to hypothesize and design experiments to decouple the structural roles and signaling roles of Prelp.

#### 4.4.20. Truncated forms of *Prelp* do not rescue pericardial edema exhibited by *prelp* mutants

To test the hypotheses regarding signaling roles for *prelp*, I injected the mRNA encoding these truncated forms into *prelp* mutants zygotes. The injected embryos were raised and observed under brightfield Nomarski microscopy at 36 hpf.

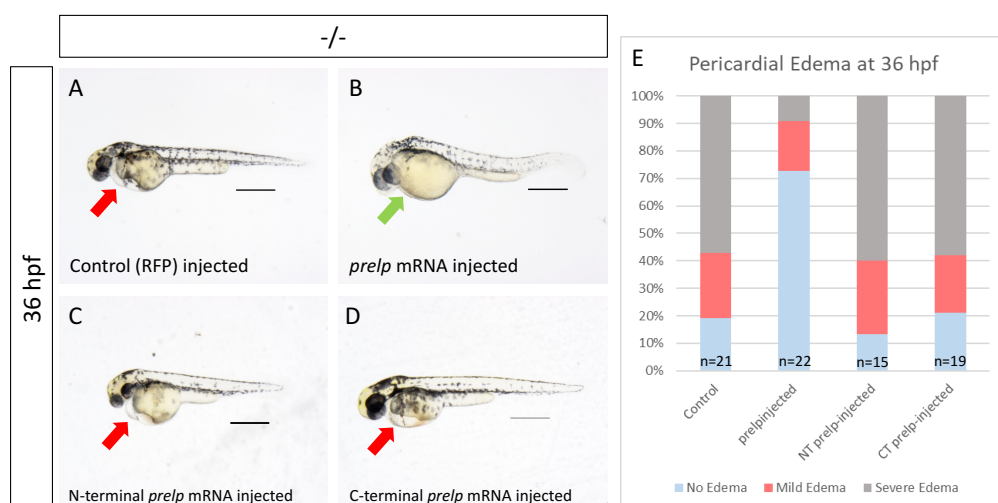


**Figure 4.29.** Whole mount brightfield images of embryos at 36 hpf of *prelp* mutants injected with Control RFP mRNA (A), whole *prelp* mRNA (B), N-terminal truncated *prelp* mRNA (C), and C-terminal truncated *prelp* mRNA (D). Quantification of edema severity across the mutants (E). Scale Bar = 500  $\mu$ m. Pericardial edema shown through Red arrows, and absence of edema Green arrow.

As previously observed, *prelp* mutants which were injected with the control RFP mRNA exhibited severe pericardial edema (Fig. 4.12) and mutants injected with the WT version of the mRNA, showed a drastic reduction in severe pericardial edema, suggesting that the pericardial edema as a gross morphological phenotype is linked to loss of *prelp* (Fig. 4.29 A, B, E). Furthermore, *prelp* mutants continued to exhibit severe pericardial edema when injected with both truncated versions of the mRNA, suggesting that these domains alone are unable to fully compensate for the loss of *prelp* (Fig. 4.29 A - E). Hence, I decided to take a closer look at the mutants injected with the



truncated forms of the mRNA, specifically at potential ECM related phenotypes, which I hypothesized to be direct consequences of loss of Prelp Protein.

#### 4.4.21. N-terminal truncated *prelp* mRNA injections partially rescue basal lamina localization in *prelp* mutants

To test the hypothesis regarding the CJ and BL phenotypes as a direct consequence of *prelp* loss, I injected zygotes with mRNA corresponding to the truncated forms (Fig. 4.28) and performed immunostaining at 36 hpf to test the laminin localization.

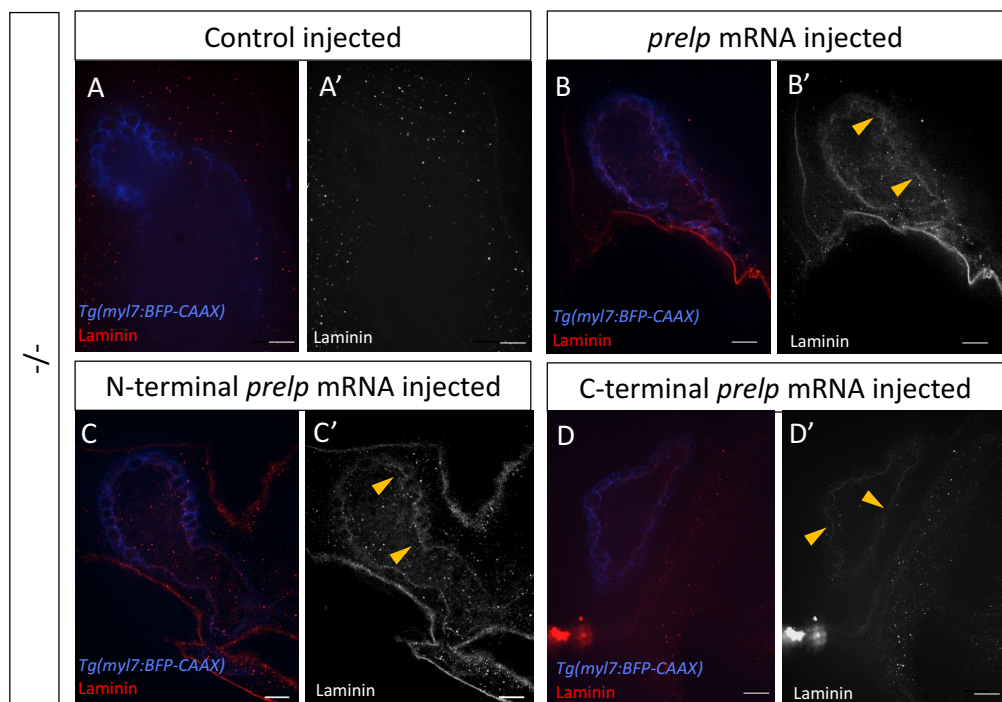


**Figure 4.30.** Mid-sagittal planes of immunostained hearts of embryos at 36 hpf of *prelp* mutants injected with Control RFP mRNA (A), whole *prelp* mRNA (B), N-terminal truncated *prelp* mRNA (C), and C-terminal truncated *prelp* mRNA (D). High contrast images at the same plane of laminin immunostainings of A-D (A'-D'). Scale Bar = 30  $\mu$ m.

Unsurprisingly, upon injection of whole *prelp* mRNA into the mutants, these mutants exhibit a marked recovery of laminin localization in the hearts (yellow arrowheads in Fig. 4.30 B'). Surprisingly, a similar recovery of BL localization

## CHAPTER 4 - Results

can be observed in *prelp* mutants injected with N-Terminal truncated form of Prelp (yellow arrowheads in Fig. 4.30 C'), suggesting that perhaps the active domain of Prelp in the N-terminal, potentially activates signaling pathways which might upregulate genes to promote ECM-receptor interaction and localization of the basal lamina and is sufficient to partially rescue the laminin organization defect observed in the *prelp* mutants. Additionally, C-terminal *prelp* injections, appear to partially enable the localization of the lamina (yellow arrowheads in Fig.4.30 D'). whereas this effect is not as pronounced as observed in the WT *prelp* injected or the N-Terminal *prelp* injected conditions (Fig.4.30 B-D) , suggesting that each domain may have more specific roles in basal lamina localization, assembly and stability. Altogether, these data suggest that potential extracellular roles of Prelp could be dissected in more detail using these truncated forms of Prelp.

#### 4.4.22. N-terminal truncated *prelp* mRNA injections rescue atrial cardiac jelly volume

To further test the hypothesis regarding the CJ and BL phenotypes as a direct consequence of *prelp* loss, I injected mutant zygotes in the HA biosensor transgenic background with mRNA corresponding to the truncated forms (Fig. 4.28) and performed live imaging at 48 hpf. The live imaged hearts were segmented using IMARIS as previously detailed (Chapter 4.4.9.).

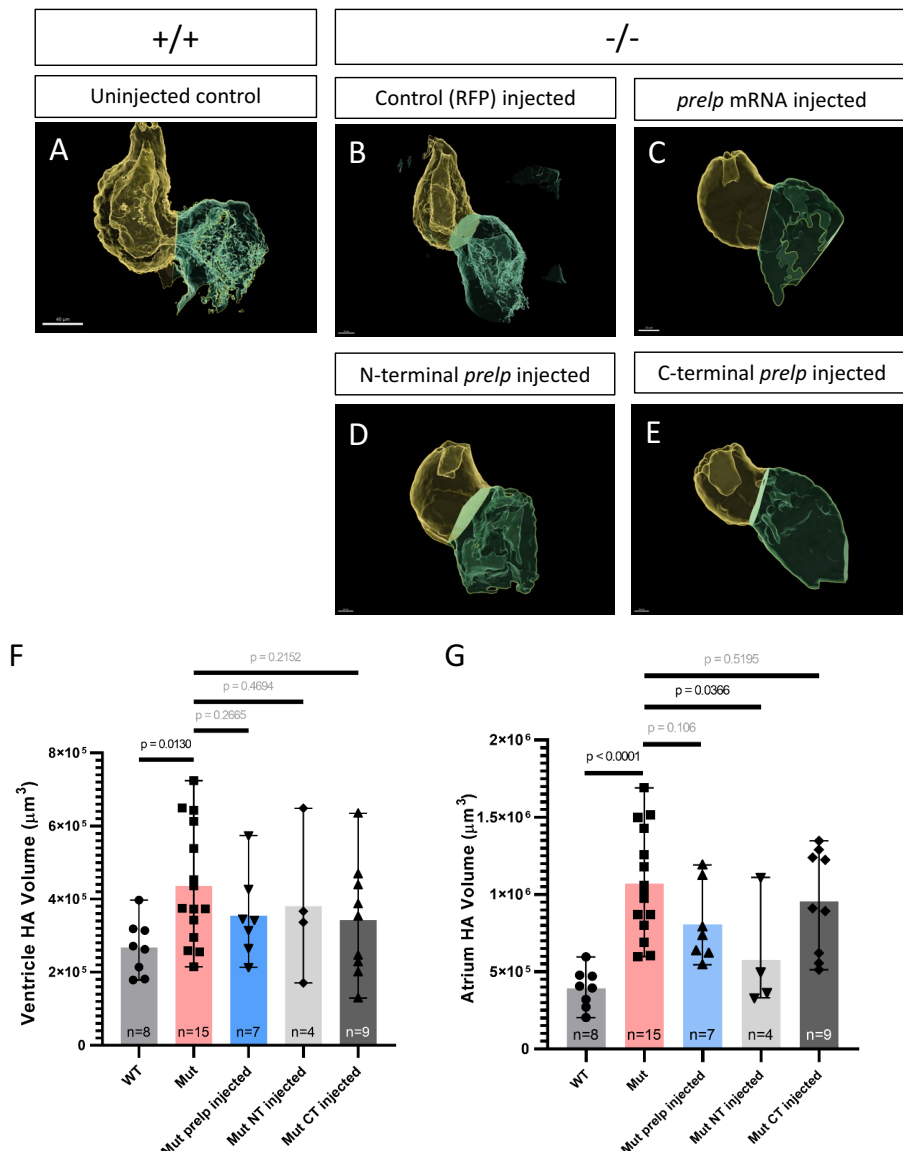


**Figure 4.31.** 3D volumetric segmentation and rendering of cardiac jelly volume from live imaged hearts at 48 hpf of WT (A) {Scale Bar = 40  $\mu\text{m}$ }; and *prelp* mutants injected with control RFP mRNA (B), *prelp* mRNA (C), N-terminal *prelp* mRNA (D) and C-terminal *prelp* mRNA (E) {Scale Bar = 20  $\mu\text{m}$ }. Quantification of segmented cardiac jelly volume of ventricle (F) and Atrium (G).

## CHAPTER 4 - Results

Surprisingly, mutants injected with WT *prelp* mRNA do not recover the Atrial or Ventricular cardiac HA volume (Fig. 4.31. A-C, F, G), raising the question whether there is a dosage dependence of *prelp* mRNA which would be required to elicit different levels of rescue of the mutant cardiac jelly phenotype. On the contrary, injecting the same number of molecules (molar concentration) of N-terminal *prelp* mRNA into the mutants, the atrial HA volume appeared to be significantly reduced, albeit the ventricle HA volume remained unchanged (Fig. 4.31. A, B, D, F, G). These data suggest that there could be a dosage dependent as well a tissue localization dependent effect of the *prelp* N-terminal domain's activity. These data also suggest that different domains of Prelp could potentially act on different parts of the cardiac jelly, during early development. The N-terminal domain of Prelp is the active domain and is highly responsible for interaction with other proteins and cell surface receptors, and upon truncation, I hypothesized that this domain becomes accessible without dimerization and enables the rescue of various mutant phenotypes that arise from a lack of whole Prelp.

#### 4.4.23. Cardiomyocyte specific *prelp* expression rescues cardiac chamber morphology in *prelp* mutants

Since *prelp* expression was detected both in the myocardium and endocardium (Fig. 4.10), albeit more in the endocardium than the myocardium (Fig. 4.32. F-H), I decided to test whether tissue specific re-establishment of *prelp* expression was sufficient to rescue different phenotypes observed in the *prelp* mutants. I generated a transgenic line for cardiomyocyte specific *prelp* expression under a shortened version of the *myl7* promoter.

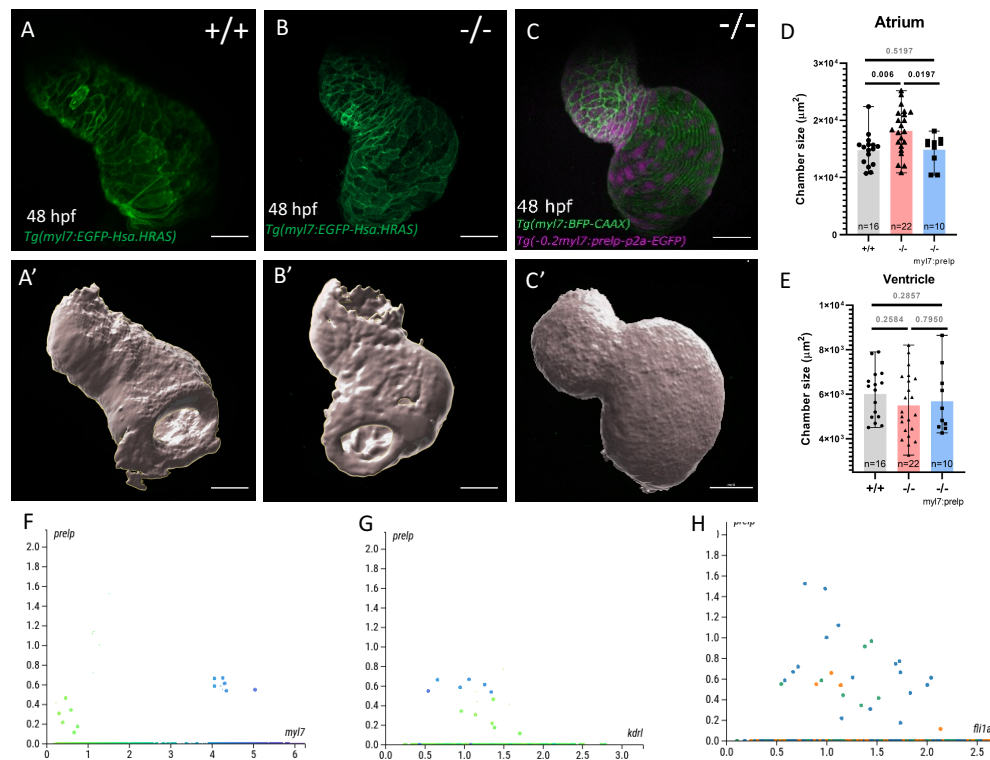


**Figure 4.32.** Maximum intensity projections of WT hearts (A), Mutant hearts (B) and mutant hearts expressing *prelp* in the myocardium (C), and corresponding 3D myocardial surface renders (A'-C'). Scale Bar = 50 µm. Chamber size quantification of Atrium (D) and Ventricle (E). Single cell RNAseq dataset from Stainier Lab showing correlative expression of *prelp* in cells expressing *myl7*<sup>+</sup> cells – myocardium (F), *kdr1*<sup>+</sup> cells – endocardium (G), *fli1a*<sup>+</sup> cells – endothelium (H) in WT hearts at 72 hpf.

I crossed this line into the *prelp* mutant background to test potential rescue of cardiac gross morphological phenotypes. Initial observation revealed very

## CHAPTER 4 - Results

surprisingly that *prelp* mutants in this rescue transgenic background do not exhibit severe pericardial edema (Data not shown). Upon closer observations, many of the *prelp* mutants continued to exhibit non cardiac specific phenotypes such as the myoseptum boundary defects (Fig. 4.12), suggesting that this rescue of *prelp* mutation is very cardiac specific and indeed due to the re-establishment of the *prelp* in the heart. The mutant hearts with the cardiomyocyte specific *prelp* expression exhibited a marked reduction in atrium chamber size, compared to mutant hearts alone (Fig. 4.32 A-E). These data suggest that since Prelp is an ECM proteoglycan, the potential role of Prelp is directly in the extracellular space and thereby does not require tissue specific expression for function activity in the CJ.

#### 4.4.24. Adult *prelp* mutants exhibit reduced survival, pericardial edema, enlarged atrium and retrograde blood flow

I genotyped embryonic *prelp* mutants and raised them to adulthood. I noticed that as development into juvenile and adult stages continued, the mortality rate was high in the *prelp* mutants (Fig. 4.33 A), suggesting that increased mortality was potentially linked to the mutation.

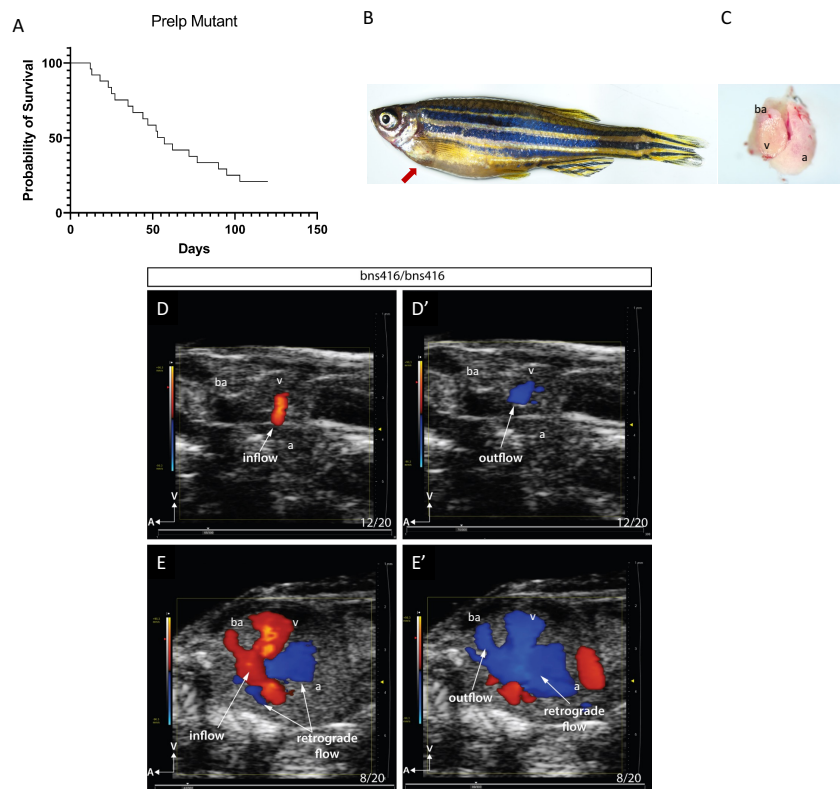


**Figure 4.33.** Survival plot indicating increased mortality of *prelp* mutants throughout development (A), Adult *prelp* mutant exhibiting pericardial edema (B), Whole mount dissected adult heart showing atrium (a), ventricle (v) and bulbus arteriosus (ba) (C). Echocardiography on adult *prelp* mutants at Ventricular diastole (D,E) and Systole (D',E').

Surprisingly, when I observed adult mutants, I noticed that some of them exhibited an increased pericardial edema (Red arrow in Fig. 4.33 B), and upon anesthesia and heart dissection, I noticed that these hearts in-fact exhibited an abnormal adult morphology, with an enlarged atrium and reduced ventricle size (Fig. 4.33 C). To check whether the mutant hearts also exhibited impaired

## CHAPTER 4 - Results

blood flow and contractility, I performed an echocardiography analysis on these mutants. Overall, over the 20 adult mutants analyzed, 8 mutants exhibited abnormal cardiac morphology as well as severe retrograde blood flow (Fig. 4.33 D,D', E, E'). These data suggest an incomplete penetrance of the mutant phenotype in the adults suggesting that mutants exhibiting severe phenotypes perhaps exhibited increased mortality and only the more resilient adults were able to develop through juvenile stages into adulthood. I hypothesized that the adult cardiac phenotypes were linked to defects of the BL in the adult heart.



#### 4.4.25. Extracellular Laminin organization is disrupted in adult *prelp* mutants

To test the hypothesis that adult *prelp* mutants exhibited cardiac morphological defects due to defects in the adult cardiac BL, I collected hearts from adult *prelp* mutants and performed cryosections and immunohistochemistry using the antibody against Laminin.

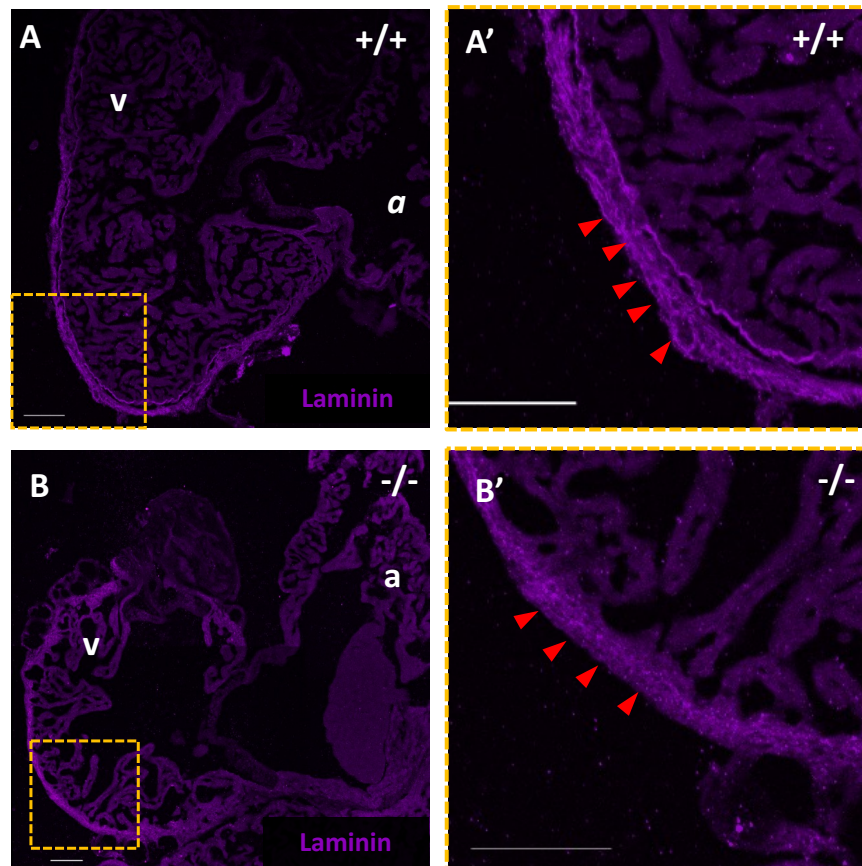


**Figure 4.34.** Cryosections of adult hearts immunostained against Laminin in WT (A) and *prelp* mutant (B) showing Atrium (a) and Ventricle (v). Enlarged inset corresponding to region marked in gold in A, B (A', B'). Scale Bar = 100  $\mu$ m.

Preliminary observation of the heart revealed a significant change in gross morphology of the hearts wherein some *prelp* mutants (8/20) exhibited a smaller ventricle compared to their WT siblings, (Fig. 4.34 v in A, B) and an enlarged atrium (Fig. 4.34 a in A, B), suggesting both resilience of zebrafish to withstand severe phenotypes and develop to adulthood, as well as a suggestion that *prelp* mutation does not lead to severe juvenile lethality. Adult WT hearts

## CHAPTER 4 - Results

revealed a neat and continuous pattern of laminin localization in the ECM rich region around the fibroblast layer luminal to the cortical layer of cardiomyocytes (Fig. 4.34 A, A', Red arrows in A'), when compared to the mutant hearts which exhibited laminin signal in the ECM rich region with a clear lack of patterning (Fig. 4.34 B,B', Red arrows in B'). These data suggest that localization of Laminin is important for optimal morphology and development of the cardiac chambers to adulthood. Additionally, this Laminin localization defects can be attributed to the potential loss of function or insufficiency of Prelp in the *prelp* mutants, thereby suggesting a causative role for Prelp towards Laminin localization in the extracellular space.

## **CHAPTER 5 - Discussion**

### **5.1. Identifying new cardiac ECM components using a combined analysis of different datasets**

At the outset of this study, I identified that combination of different datasets with the published zebrafish matrisome (Nauroy et al., 2018) enabled the identification of ECM factors and genes enriched in the cardiac developmental and regeneration landscape. Identification and categorization of ECM proteins based on their localization and function, permits targeted mutagenesis of specific domains of these proteins. I also noted ECM proteins interact in a highly promiscuous manner, with multiple binding partners and parallel interactions. Hence, dissecting direct and indirect involvement of the proteins within the various pathways continues to be a challenging task. Combination of published bulk RNAseq datasets with large single cell RNAseq datasets enables identification of correlative gene expression in the cells and tissues of interest. Due to the fluidity and dynamic nature of the ECM, the tissue where an ECM gene is expressed does not necessarily correlate with the tissue with which the same ECM protein interacts.

In the heart, during early developmental stages, the CJ is highly fluidic. Analysis of expression data in combination with proteomics datasets would enable detection of novel ECM proteoglycans which could act like signaling molecules as they provide molecular cues from the one tissue layer such as the endocardium towards the myocardium, or from the myocardium towards the developing epicardium.

## CHAPTER 5 - Discussion

When I performed this combined dataset analysis, I primarily focused on structural ECM genes due to the presumed role of ECM in providing structural stability to the developing tissue. Further analysis revealed interesting candidates such as proteoglycans/glycoproteins which modulate various extracellular signaling pathways. I was able to identify at least 13 interesting candidates expressed in the heart during early development and similarly expressed in the heart or valve during regeneration (*acanb*, *apoeb*, *agr**n*, *bgn*, *bmp3*, *coll10a1a*, *coll11a1a*, *dcn*, *fmod*, *gdf10*, *mmp14b*, *prelp*, *vc**an*). I performed mutagenesis for five of these candidates (*acanb*, *agr**n*, *bmp3*, *dcn* and *prelp*) and Agrn, Dcn and Prelp were identified as promising candidates based on their published roles in the BM and hence became the focus for further analysis in this study.

## **5.2. Understanding the role of ECM proteoglycan Agrin in cardiac regeneration**

Initial experiments with Agrin were performed with a del7ins2 mutant allele procured from the Michael Granato Lab (*agrnp<sup>168</sup>*). These mutants exhibited no gross morphological embryonic developmental phenotype, and were readily adult viable, although the mutation led to a premature truncation codon. I was unable to detect the “embryonic swimming defects” exhibited by these mutants as claimed in the publication describing the role of this mutant in neuromuscular junctions in skeletal muscle regeneration (Gribble et al., 2018). My focus was primarily on the adult heart in these mutants and upon cryoinjuries, it was noted that mutants exhibit a reduced borderzone cardiomyocyte proliferation at 7 dpci, albeit exhibiting no change in the dedifferentiation of the CMs. Previous reports in the zebrafish have suggested Agrn activity on the epicardium by induction of p53 mediated transient senescence during cardiac regeneration (Sarig et al., 2019). Studies in the murine hearts claimed a pro-regenerative myocyte proliferation response upon administration of recombinant Agrin (Bassat et al., 2017) and improved cardiac repair post ischemia in porcine hearts downstream of the Dystroglycan receptor. Additionally, Agrin was also shown to promote epicardial EMT in murine hearts during development (Sun et al., 2021) downstream of the Dystroglycan receptor as well suggesting an increased involvement of Agrn-Dag signaling axis in the heart.

To test the receptor used by Agrin in the zebrafish heart to promote myocyte proliferation observed by me, I procured mutants for Agrin receptors, Dystroglycan (*dag*), and MuSK (*musk*). Unfortunately, neither of these

## CHAPTER 5 - Discussion

mutants were adult viable and hence I was unable to perform cryoinjuries with these genetic tools. To overcome these difficulties, I devised some ideas with tissue specific overexpression of constitutively active Dag, lacking the intracellular Yap binding activity under a switch construct. Experiments with these tools could provide new insight into alternative mechanisms activated in adult heart regenerative models such as zebrafish as opposed to adult non regenerative models such as the mouse and pig hearts.

Furthermore, based on the data acquired, I tested Yap activity on the *agrn*<sup>p168</sup> mutants using a p-Yap antibody (data not included), and this suggested that once optimized, an argument could be made for the activity of Yap downstream of the Agrin-receptor interactions which would promote cardiomyocyte proliferation. An interesting approach to further validate these hypotheses would be to use tissue specific knock out alleles for Agrn receptors. Further insight into these mechanisms would enable identification of novel potential therapeutic targets for local ECM mediated signaling activation or inhibition in post MI patient care. Studies conducted in mice and pigs with intramyocardial injections of recombinant human Agrin have already shown promising results with cardiomyocyte recovery. These studies pave the way for potential clinical care with Agrin as a new means of therapy for human patients undergoing MI (Baehr et al., 2020; Bassat et al., 2017).

### 5.3. Decorin as a modulator of cardiac collagen crosslinking during development and regeneration

Decorin is a known modulator of the Tgfb $\beta$  signaling pathway by sequestration of Tgfb $\beta$  ligand. Decorin's other reported roles in cardiovascular system makes it a prime candidate to test and manipulate interactions which could modulate major molecular pathways in cardiovascular development (Factor- et al., 2009; Järveläinen et al., 2015; Miura et al., 2006; Neill et al., 2012; Weis et al., 2005; Zagris et al., 2011; Zoeller et al., 2009). Furthermore, roles for Decorin in zebrafish convergent extension suggest a potential link to early cardiac precursor migration and subsequent cardiac tube formation and elongation (Zoeller et al., 2009).

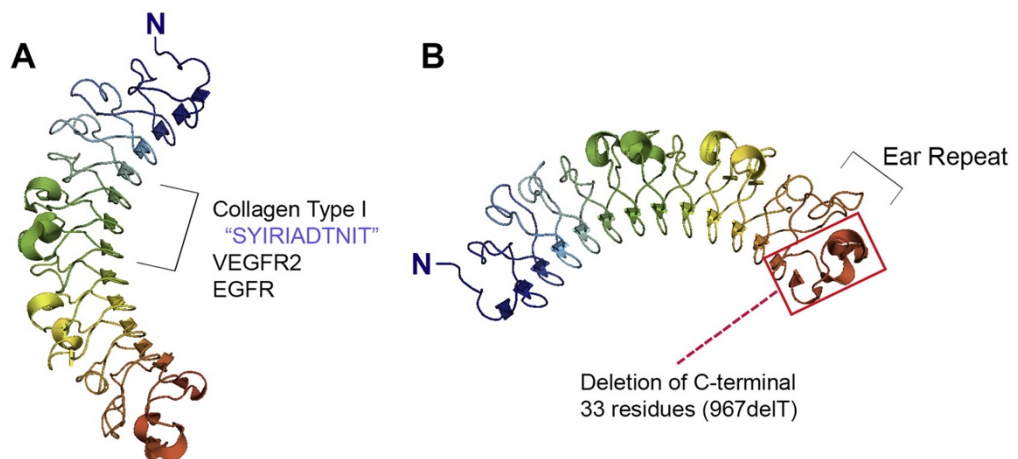


**Figure 5.1.** (A) Structure with binding domain of Decorin with Col1, Vegfr2, Egfr, (B) Mutation of Decorin marked with red box indicating dominant negative form. Published by (Gubbiotti et al., 2016). Reprint authorized under copyright license no. 5401450979121

Additionally, reported dominant negative forms of Decorin, which could inhibit Decorin's role targeting activation of VEGFR signaling and reverse the inhibition of Tgfb $\beta$  signaling through release of sequestered ligand suggested an interesting dual approach to target both pathways using a single tool (Fig. 5.1

A, B) (Gubbiotti et al., 2016). In this preliminary study with Decorin, we observed an increased thickening of the myocardial wall at 80 hpf upon overexpression of Decorin in early embryonic stages (Fig 4.8). We hypothesized that the increased thickness could be due to increased Decorin mediated collagen cross linking in the overexpression condition. This hypothesis is further supported by the observed colocalization of Decorin and fibrillar collagen in the collagen rich transient scar post cardiac cryoinjury (Fig. 4.7 D) (Chablais et al., 2011; Gamba et al., 2017; González-Rosa et al., 2011). The lack of cardiac looping observed upon injection of *DNdcn* mRNA (Fig. 4.9) suggests that genes required to induce torsion of the zebrafish linear heart tube were potentially affected (Bakkers, 2011; Maenner, 2009). One explanation of this observation is the DN-Dcn mediated disruption to the Tgf $\beta$ -BMP signaling axis of cardiovascular development (Maenner, 2009). Suppression of Tgf $\beta$  and induction of BMP signaling are essential processes which trigger expression of genes in the developing heart which regulate atrial and ventricular lineages of CMs (Marques & Yelon, 2009). The hypothesized dominant negative form of Decorin could potentially release sequestered Tgf $\beta$  ligand in the extracellular space and therefore modulate the cardiac looping process through suppression of BMP signaling and increased activation of Tgf $\beta$  signaling during early development. Future experiments in this direction with tissue specific tools and mutant alleles for *dcn* would permit identification of key extracellular factors which influence early cardiac events such as looping and chamber ballooning.



## 5.4. ECM Small Leucine Rich Proteoglycan Prelp acts as a modulator of cardiac development through the basal lamina

Small Leucine Rich Proteoglycans (SLRPs) are categorized into different classes. Class II SLRP Prelp, is a relatively obscure protein compared to other members of this family such as Class I SLRPs Decorin and Biglycan (Fig. 1.9) (Iozzo & Schaefer, 2015).

### 5.4.1. *prelp* expression correlates with tissues proximal to basement membrane

SLRPs are usually found in mammals within deep fibrillar collagen rich matrices. Prime examples of this are Class I SLRPs Decorin and Biglycan which are detected with increased interaction to fibrillar collages (Iozzo & Schaefer, 2015b; Lander & Selleck, 2000). Surprisingly, *prelp* expression and localization in different tissues is different from other related genes in this class of Proteoglycans (Fig. 1.9).

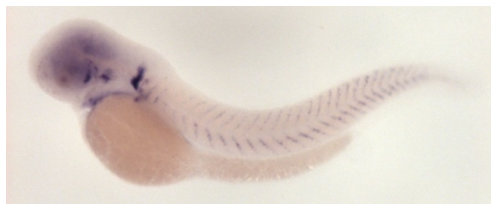


**Figure 5.2.** *in-situ* hybridization against *prelp* between Prim-15 and Prim -25 from B. Thisse et al., 2008, direct data deposit on zfin.org

Based on *in-situ* hybridization data from ZFIN *prelp* expression is detected in the brain, cornea, diencephalon, pectoral fins and in the myosepta suggests a strong link to tissues with extracellular basement membranes (Fig. 5.2) (Thisse, et.al. 2008). Accordingly, I also observed *prelp* expression in the cardiac basement membrane (Fig. 4.10). Additionally, using cardiac single cell

RNAseq datasets from the Stainier lab, expression correlation analysis revealed that *prelp* expression correlates to myocardial cells expressing *myl7* (Fig. 4.32 F), endocardial cells expressing *kdrl* (Fig 4.32. G.), as well as endothelial cells expressing *flila* (Fig 4.32. H.), suggesting a lack of tissue specificity for *prelp* expression at these early developmental stages. Immunostaining against Prelp in embryonic hearts revealed protein accumulation of Prelp in the ECM, close to the cardiomyocytes but not fully colocalizing with the membrane (Fig. 4.10 B-B'''), suggesting a potential accumulation of Prelp in the basal lamina proximal to cardiomyocytes. Prelp's reported interaction with the heparan sulphate side chains of large ECM proteoglycan Perlecan (Hspg2) (Bengtsson et al., 2002) suggests potential interaction with these partners in the CJ could contribute to modulation of the cardiac chambers during development. Further analysis with higher magnification imaging and protein colocalization studies would enable identification of potential direct interacting partners of Prelp in the CJ BL during early development.

### 5.4.2. *prelp* contributes to maintaining cardiovascular integrity

Zebrafish *prelp* mutants exhibit severe pericardial edema (Fig 4.12 A,B,C), suggesting a potential role of *prelp* in maintenance of vascular integrity in and around the heart.

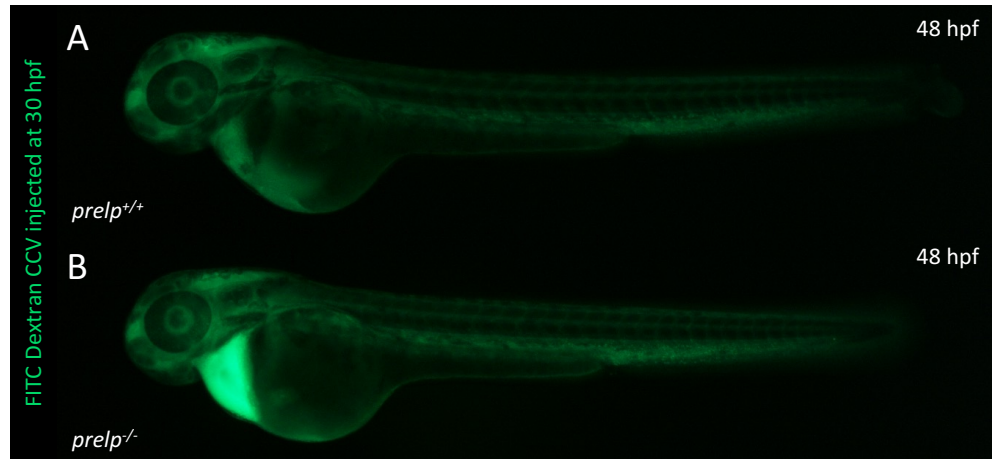


**Figure 5.3** WT (A) and *prelp* mutants (B) injected with FITC-Dextran in CCV at 30 hpf imaged at 48 hpf.

Additionally, I also noticed that *prelp* mutants exhibited an increased signal intensity of FITC-Dextran in the pericardial space upon injection into the common cardinal vein (CCV) (Fig. 5.3 A, B) suggesting potential leakiness of the vasculature leading to increased accumulation of the fluorescent dye in the pericardial space. These data together suggest a role for *prelp* in maintaining vascular integrity. In addition to the observed cardiovascular defects, *prelp* mutants also exhibited a lack of brain vasculature at 48 hpf (yellow arrows in Fig. 4.12 A', B'). These data corroborate with what has been described regarding the requirement of PRELP in maintenance of brain vasculature integrity in mice (Davaapil, 2018). Additionally, PRELP has been shown to act towards promoting tissue repair in disease conditions by inhibiting excessive inflammation through formation of the complement Membrane Attack Complex (MAC) (Birke et al., 2014; Happonen et al., 2012; Hultgårdh-

Nilsson et al., 2015). Based on these data, a hypothesis can be made regarding a potential role for zebrafish *prelp* in maintaining cardiovascular tissue integrity, through inhibition of MAC mediated membrane pore formation, or potentially through novel previously undiscovered mechanisms. Further studies describing these roles for *prelp* could provide a novel platform for therapeutic approaches against vascular diseases such as atherosclerosis or in promoting vascular repair post injury.

### **5.4.3. Proliferation, Apoptosis or SHF could contribute to increased chamber size in *prelp* mutants.**

In this study, I have shown that *prelp* mutants exhibit an increased atrium size at 48 and 72 hpf, due to increased number of atrial cardiomyocytes (Fig. 4.14, 4.15, 4.17). As a result of this, major unanswered questions remaining in this particular part of the project concern the source of this increase in the number of atrial cardiomyocytes. I plan to address these questions with future experiments using Edu-based pulse chase assays as well as using the FUCCI – (Fluorescence Ubiquitin Cell Cycle Indicator) based system as a transgenic line *Tg(myl7:mVenus-gmnn)* crossed into the *prelp* mutant background. Experiments with these tools would enable identification of potential contribution of proliferative cardiomyocytes to increase the atrial size. Alternatively, one could also argue that *prelp* mutants exhibit a reduction in apoptosis during cardiovascular development. Various studies have shown that targeted apoptosis is a critical factor for cardiovascular development and essential during processes outflow tract development as well as development of the cardiac conduction system (Fisher et al., 2000). Additional experiments

with a TUNEL assay to compare the differences in apoptosis between WT siblings and *prelp* mutants would provide insight into the above hypothesis. . A third possibility for the increased number of atrial cardiomyocytes in the heart is the addition of cells from the second heart field (SHF). If the process by which *prelp* mutant exhibit increase atrial CMs is laminin dependent, an increased second heart field (SHF) contribution to the venous pole of the heart could serve as a potential explanation. This argument leans heavily on a recent publication from the Emily Noel lab (Derrick et al., 2021) , where mutants of *lambla* exhibit an increased contribution of cells from the second heart field to the atrium of the heart but not the ventricle. As argued in this publication, this venous pole addition of SHF acts in a contractility dependent manner. This explanation for the increased number of atrial CMs in *prelp* mutants would have to be tested using the dual transgenic approach to label SHF contribution described in Derrick et al., 2021. Additionally, I noticed that the cardiac chamber size is contractility independent in *prelp* mutants (Fig. 4.16), suggesting potential differences in chamber size modulation between the *lambla* mutant and the *prelp* mutant. Further experimentation and analysis on the origin of the increased atrial CMs in *prelp* mutants could suggest novel roles for proteins in the CJ in limiting the growth of cardiac chambers.

#### **5.4.4. Delay of ECM maturation manifests as increased**

##### **Cardiac Jelly volume and loss of Laminin localization**

The earliest observed molecular phenotype in the *prelp* mutants is the loss of laminin localization at 36 hpf (Figure 4.18). I decided to characterize Laminin in the *prelp* mutants due to previously reported interactions between Laminin binding BM PG Perlecan (Hspg2) and Prelp (Bengtsson et al., 2002). Most

surprisingly, Laminin expression was not entirely lost in the *prelp* mutant based on the bulk heart RNAseq, and since the antibody recognizes the Laminin-111 trimer, a failure in multimerization of this structure in the mutant condition could be hypothesized as a leading factor which contributes to reduced antibody signal observed.

I also noticed that the *prelp* mutants exhibit an increased volume of Cardiac HA at 48 hpf (Fig. 4.19). As the heart develops, the cardiac jelly matures and loses affinity to water and cardiac hyaluronan undergoes degradation by various factors such as MMPs and ADAMTs as well as the Cell Migration inducing Hyaluronidases (CEMIPs) (de Angelis et al., 2017; Totong et al., 2011). Based on the RNAseq dataset, I noticed that *cemip* and *mmp15b* were significantly downregulated. These data in combination with the Laminin and HA volume data suggest that the dynamics of the cardiac basement membrane maturation is affected in the *prelp* mutants during early developmental stages. At both 36 hpf and 48 hpf, these extracellular dynamics could act as crucial modulators of essential processes. These processes include endocardial-myocardial signaling crosstalk, as well as regulation of mechanical signal transduction from the lumen towards the cardiomyocytes (Goddard et al., 2017; Rasouli et al., 2018; Rasouli & Stainier, 2017; Steed et al., 2016). Abrogation of these physical and chemical properties of the CJ in the *prelp* mutant can be hypothesized as the potential contributor to the observed gross morphological phenotype of the heart. Based on the above data, future analysis with mass spectrometric techniques is warranted to provide a clearer and precise understanding of the distinct roles of specific proteins in this extracellular space during early cardiovascular development. Major challenges include the decoupling of various extracellular interactors, since the ECM is

highly dynamic and requires specialized tools to distinguish different roles in an *in-vivo* setting. Studies performing endogenous tagging of these basement membrane component as shown in Keeley et al., 2020, exhibit an increased need to observe and understand these dynamic processes with a high degree of spatial and temporal resolution.

Another potential experimental approach would be to inject whole laminin trimers into the *prelp* mutants to dissect laminin independent phenotypes. These experiments still remain to be performed and could provide novel insight into more subtle phenotypes masked by the laminin dependent effects.

#### **5.4.5. Outside-In signaling affects epithelial cell polarity**

Epithelial cells exhibit certain distinct properties, one of them being distinct apico-basal polarity. Epithelial cells such as cardiomyocytes, exhibit apical localization of markers such as Podocalyxin, Crumbs2b, Tight Junctions and basolateral markers such as Marc3a, which are usually definitive to the epithelial identity of the cell. Many studies have shown that epithelial cells losing polarity to exhibit a transient proliferative or mesenchyme-like morphology also undergo rearrangement of various components of the intracellular contractile machinery (Gentile et al., 2021; Gunawan et al., 2021; Jimenez Amilburu, 2018; Jiménez-Amilburu et al., 2016; Jiménez-Amilburu & Stainier, 2019; Priya et al., 2020; Sun et al., 2021). These processes occur during essential developmental phases such as cardiac trabeculation and valvulogenesis (Jimenez Amilburu, 2018; Jiménez-Amilburu et al., 2016;

Jiménez-Amilburu & Stainier, 2019; Lee & Streuli, 2014; Rasouli & Stainier, 2017; Uribe et al., 2018; Wu, 2018).

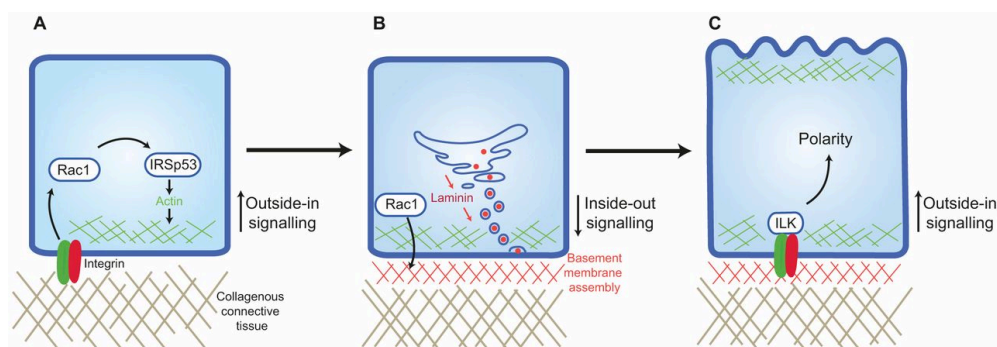


**Figure 5.4.** Signaling cascade to establish epithelial cell polarity. Figure reprinted with permission from Journal of Cell Science, Copyright License No:1273254-1

I attempted to further validate the hypothesis proposing outside-in signaling from the basal lamina to induce apico-basal polarity in the cardiomyocytes, using the *prelp* mutants. Initial observation of cardiomyocyte shape in *prelp* mutants suggest a rounded-up morphology as opposed to the traditional cuboidal shape exhibited in WT siblings (Fig. 4.13) at 48 hpf. Upon closer observations of these CMs near the AVC region, in the *Tg(myl7:EGFP-podxl)* background at 36 hpf, the earliest timepoint observed for the laminin localization phenotype, I noticed that these cardiomyocytes exhibit a lack of apical polarization and are more rounded up (Fig. 4.26.). This observation is also supported transcriptionally at 36 hpf, as *prelp* mutants exhibit increased expression of *podxl* (Table 4.5).

Furthermore, latest preliminary Laminin immunostainings performed with *prelp* mutants in the *Tg(myl7:EGFP-podxl)* background, shows that CMs abluminal to mis-localized extracellular laminin exhibit a loss of apical *podxl*, suggesting this loss of outside-in signaling in *prelp* mutants. Additionally, the role of N-terminal Prelp and its interaction with Fibronectin to induce focal adhesions could be a key contributor to this observation (Bengtsson et al.,



2016). Further experiments with immunostaining against Vinculin or Talin in *prelp* mutant background would validate this hypothesis. Experiments with re-introduction of N-Terminal Prelp along with the subsequent immunostaining against Focal Adhesion factors, would further validate the above hypothesis. A baffling behaviour observed in *prelp* mutant CMs is the extension of long and pointed protrusions (Figure 4.27). Further analysis of these protrusions is required to understand what they are and why they arise. One suggestion is that these are cytonemes extended by mutant cardiomyocytes due to inability to maintain epithelial identity. Studies have shown that extension of these long protrusions usually enable cells to reach neighboring tissues to exchange signaling molecules such as Wnt ligands (Casas-Tintó & Portela, 2019; Stanganello et al., 2015), but the direction of these protrusions in the abluminal direction suggests potential crosstalk with the pericardium or the developing epicardium rather than with the endocardium located lumenally. These data require further validation and analysis, as well as verification as potential actin-based structures. Experimental design with actin toxins could enable the dissection of the composition and potential effects of abrogation of these protrusions in the cardiac wall.

#### **5.4.6. Identification of direct binding partners of Prelp and modulators of the ECM in *prelp* mutants**

One major point of discussion is the paucity of knowledge with regard to direct binding partners of Prelp in the extracellular space as well as potential undiscovered intracellular roles for Prelp. Some studies have shown that PRELP interaction with Perlecan through heparan sulphate side chains and Collagen in a simultaneous manner through dimerization of the C-terminal

## CHAPTER 5 - Discussion

domain could be the most direct link to Laminins in the basal lamina (Bengtsson et al., 2000, 2002). More recently, CoIP analysis in ExPi293 cells has shown PRELP interaction with Fraser (FRAS) proteins (Kosuge et al., 2021), which are anchoring proteins part of the Fraser complex known to play critical roles in epithelial-mesenchyme adhesion and interaction during embryonic development (Hiroyasu & Jones, 2014; Short et al., 2007). These recent findings suggest a multitude of potential extracellular processes and targets in which Prelp might be involved. Hence, to identify zebrafish specific interactions and model specific and context specific roles, I aim to perform a Co-IP experiment with HA tagged zebrafish Prelp, as well as a novel technique of Single Cell Mass Spectrometry (Petelski et al., 2021; Specht et al., 2021) in the zebrafish with recently published tools and techniques. With these experiments, deeper understanding can be achieved towards understanding protein composition changes in the extracellular space during the early stages of heart development studied in this thesis.

## Conclusion

This thesis identifies and elucidates various extracellular matrix proteins present in the heart during cardiovascular development and regeneration. The following aims were successfully achieved.

- 1. Identification of ECM genes expressed in the heart during early development and generation of Mutant alleles** - I successfully identified various ECM genes expressed in the heart during early development and proceeded to generate various mutant alleles targeting conserved domains of these genes across species.
- 2. Identification of the Role of Agrin in cardiac regeneration in the zebrafish** – I successfully identified that Agrin mutants exhibit reduced CM proliferation during heart regeneration.
- 3. Identification of Decorin as a modulator of cardiac development** – I successfully identified zebrafish Decorin as a modulator of cardiac looping during early heart development using overexpression tools for Dcn and DNDcn.
- 4. Identification of the Role of Prelp as a modulator of basement membrane and regulator of cardiac chamber size** – I successfully demonstrated with the *prelp* mutant that Prelp is a key component of the zebrafish cardiac jelly and the basal lamina and plays a role in stabilizing multimerization of Laminins. I also successfully showed that *prelp* mutants show an increased chamber size due to increased cardiomyocyte number but failed to show why this is the case. I also successfully demonstrated that truncated N-terminal form of Prelp contains the necessary active domain and is sufficient to partially rescue the integrity of the basal lamina in the *prelp* mutants.

# BIBLIOGRAPHY

- Actin and Actin-Binding Proteins. (2017). *Cell Biology*, 575–591. <https://doi.org/10.1016/B978-0-323-34126-4.00033-5>
- Arrington, C. B., & Yost, H. J. (2009). Extra-embryonic syndecan 2 regulates organ primordia migration and fibrillogenesis throughout the zebrafish embryo. *Development*, 136(18), 3143–3152. <https://doi.org/10.1242/DEV.031492>
- Auman, H. J., Coleman, H., Riley, H. E., Olale, F., Tsai, H. J., & Yelon, D. (2007). Functional Modulation of Cardiac Form through Regionally Confined Cell Shape Changes. *PLOS Biology*, 5(3), e53. <https://doi.org/10.1371/JOURNAL.PBIO.0050053>
- Aviezer, D., Hecht, D., Safran, M., Eisinger, M., David, G., & Yayon, A. (1994). Perlecan, basal lamina proteoglycan, promotes basic fibroblast growth factor-receptor binding, mitogenesis, and angiogenesis. *Cell*, 79(6), 1005–1013. [https://doi.org/10.1016/0092-8674\(94\)90031-0](https://doi.org/10.1016/0092-8674(94)90031-0)
- Baehr, A., Umansky, K. B., Bassat, E., Jurisch, V., Klett, K., Bozoglu, T., Hornaschewitz, N., Solyanik, O., Kain, D., Ferraro, B., Cohen-Rabi, R., Krane, M., Cyran, C., Soehnlein, O., Laugwitz, K. L., Hinkel, R., Kupatt, C., & Tzahor, E. (2020). Agrin Promotes Coordinated Therapeutic Processes Leading to Improved Cardiac Repair in Pigs. *Circulation*, 142(9), 868–881. <https://doi.org/10.1161/CIRCULATIONAHA.119.045116>
- Bakkers, J. (2011). Zebrafish as a model to study cardiac development and human cardiac disease. *Cardiovascular Research*, 91(2), 279. <https://doi.org/10.1093/CVR/CVR098>
- BARRY, A. (1948). The functional significance of the cardiac jelly in the tubular heart. *The Anatomical Record*, 102(3), 289–298. <https://doi.org/10.1002/AR.1091020304>
- Bassat, E., Mutlak, Y. E., Genzelinakh, A., Shadrin, I. Y., Baruch Umansky, K., Yifa, O., Kain, D., Rajchman, D., Leach, J., Riabov Bassat, D., Udi, Y., Sarig, R., Sagi, I., Martin, J. F., Bursac, N., Cohen, S., & Tzahor, E. (2017). The extracellular matrix protein agrin promotes heart regeneration in mice. *Nature*, 547(7662), 179–184. <https://doi.org/10.1038/nature22978>
- Bengtsson, E., Aspberg, A., Heinegård, D., Sommarin, Y., & Spillmanni, D. (2000). The amino-terminal part of PRELP binds to heparin and heparan sulfate. *Journal of Biological Chemistry*, 275(52), 40695–40702. <https://doi.org/10.1074/jbc.M007917200>
- Bengtsson, E., Lindblom, K., Tillgren, V., & Aspberg, A. (2016). The leucine-rich repeat protein PRELP binds fibroblast cell-surface proteoglycans and enhances focal adhesion formation. *Biochemical Journal*, 473(9), 1153–1164. <https://doi.org/10.1042/BCJ20160095>
- Bengtsson, E., Mörgelin, M., Sasaki, T., Timpl, R., Heinegård, D., & Aspberg, A. (2002). The leucine-rich repeat protein PRELP binds perlecan and collagens and may function as a basement membrane anchor. *Journal of Biological Chemistry*, 277(17), 15061–15068. <https://doi.org/10.1074/jbc.M108285200>
- Bengtsson, E., Neame, P. J., Heinegård, D., & Sommarin, Y. (1995). The Primary Structure of a Basic Leucine-rich Repeat Protein, PRELP, Found in Connective

## BIBLIOGRAPHY

- Tissues. *Journal of Biological Chemistry*, 270(43), 25639–25644. <https://doi.org/10.1074/jbc.270.43.25639>
- Bensimon-Brito, A., Ramkumar, S., Boezio, G. L. M., Guenther, S., Kuenne, C., Helker, C. S. M., Sánchez-Iranzo, H., Iloska, D., Piesker, J., Pullamsetti, S., Mercader, N., Beis, D., & Stainier, D. Y. R. (2020). TGF- $\beta$  Signaling Promotes Tissue Formation during Cardiac Valve Regeneration in Adult Zebrafish. *Developmental Cell*, 52(1), 9–20.e7. <https://doi.org/10.1016/J.DEVCEL.2019.10.027>
- Berdougo, E., Coleman, H., Lee, D. H., Stainier, D. Y. R., & Yelon, D. (2003). Mutation of weak atrium/atrial myosin heavy chain disrupts atrial function and influences ventricular morphogenesis in zebrafish. *Development*, 130(24), 6121–6129. <https://doi.org/10.1242/DEV.00838>
- Bezakova, G., & Ruegg, M. A. (2003). New insights into the roles of agrin. *Nature Reviews Molecular Cell Biology* 2003 4:4, 4(4), 295–309. <https://doi.org/10.1038/nrm1074>
- Birke, M. T., Lipo, E., Adhi, M., Birke, K., & Kumar-Singh, R. (2014). AAV-mediated expression of human PRELP inhibits complement activation, choroidal neovascularization and deposition of membrane attack complex in mice. *Gene Therapy*, 21(5), 507–513. <https://doi.org/10.1038/gt.2014.24>
- Bredrup, C., Knappskog, P. M., Majewski, J., Rødabi, E., & Boman, H. (2005). Congenital Stromal Dystrophy of the Cornea Caused by a Mutation in the Decorin Gene. *Investigative Ophthalmology & Visual Science*, 46(2), 420–426. <https://doi.org/10.1167/IOVS.04-0804>
- Calve, S., Jacobson, K. R., Lipp, S., Acuna, A., Leng, Y., & Bu, Y. (2020). Comparative analysis of the extracellular matrix proteome across the myotendinous junction. *Journal of Proteome Research*, 19(10), 3955–3967. [https://doi.org/10.1021/ACS.JPROTEOME.0C00248/SUPPL\\_FILE/PR0C00248\\_SI\\_005.XLSX](https://doi.org/10.1021/ACS.JPROTEOME.0C00248/SUPPL_FILE/PR0C00248_SI_005.XLSX)
- Camenisch, T. D., Biesterfeldt, J., Brehm-Gibson, T., Bradley, J., & McDonald, J. A. (2001). Regulation of cardiac cushion development by hyaluronan. *Experimental & Clinical Cardiology*, 6(1), 4. /pmc/articles/PMC2858958/
- Camenisch, T. D., Spicer, A. P., Brehm-Gibson, T., Biesterfeldt, J., Augustine, M. lou, Calabro, A., Kubalak, S., Klewer, S. E., & McDonald, J. A. (2000). Disruption of hyaluronan synthase-2 abrogates normal cardiac morphogenesis and hyaluronan-mediated transformation of epithelium to mesenchyme. *The Journal of Clinical Investigation*, 106(3), 349–360. <https://doi.org/10.1172/JCI10272>
- Casas-Tintó, S., & Portela, M. (2019). Cytonemes, Their Formation, Regulation, and Roles in Signaling and Communication in Tumorigenesis. *International Journal of Molecular Sciences*, 20(22). <https://doi.org/10.3390/IJMS20225641>
- Chablais, F., Veit, J., Rainer, G., & Jawiska, A. (2011). The zebrafish heart regenerates after cryoinjury-induced myocardial infarction. *BMC Developmental Biology*, 11(1), 1–13. <https://doi.org/10.1186/1471-213X-11-21/FIGURES/8>
- Chaffin, M., Papangeli, I., Simonson, B., Akkad, A. D., Hill, M. C., Arduini, A., Fleming, S. J., Melanson, M., Hayat, S., Kost-Alimova, M., Atwa, O., Ye, J., Bedi, K. C., Nahrendorf, M., Kaushik, V. K., Stegmann, C. M., Margulies, K. B., Tucker, N. R., & Ellinor, P. T. (2022). Single-nucleus profiling of human

## BIBLIOGRAPHY

- dilated and hypertrophic cardiomyopathy. *Nature* 2022 608:7921, 608(7921), 174–180. <https://doi.org/10.1038/s41586-022-04817-8>
- Chan, F. L., & Inoue, S. (1994). Lamina lucida of basement membrane: An artefact. *Microscopy Research and Technique*, 28(1), 48–59. <https://doi.org/10.1002/JEMT.1070280106>
- CHARONIS, A. S., TSILIBARY, E. C., YURCHENCO, P. D., & FURTHMAYR, H. (1985). Binding of Laminin to Type IV Collagen: A Morphological Study. *Annals of the New York Academy of Sciences*, 460(1 Biology, Chem), 401–403. <https://doi.org/10.1111/j.1749-6632.1985.tb51191.x>
- Chen, C. C., Yeh, L. K., Liu, C. Y., Kao, W. W. Y., Samples, J. R., Lin, S. J., Hu, F. R., & Wang, I. J. (2008). Morphological differences between the trabecular meshworks of zebrafish and mammals. *Current Eye Research*, 33(1), 59–72. <https://doi.org/10.1080/02713680701795026>
- Chen, D., Smith, L. R., Khandekar, G., Patel, P., Yu, C. K., Zhang, K., Chen, C. S., Han, L., & Wells, R. G. (2020). Distinct effects of different matrix proteoglycans on collagen fibrillogenesis and cell-mediated collagen reorganization. *Scientific Reports* 2020 10:1, 10(1), 1–13. <https://doi.org/10.1038/s41598-020-76107-0>
- Chen, J. N., Haffter, P., Odenthal, J., Vogelsang, E., Brand, M., van Eeden, F. J. M., Furutani-Seiki, M., Granato, M., Hammerschmidt, M., Heisenberg, C. P., Jiang, Y. J., Kane, D. A., Kelsh, R. N., Mullins, M. C., & Nüsslein-Volhard, C. (1996). Mutations affecting the cardiovascular system and other internal organs in zebrafish. *Development*, 123, 293–302. <https://doi.org/10.1242/dev.123.1.293>
- Chen, S., Sun, M., Iozzo, R. v., Kao, W. W. Y., & Birk, D. E. (2013). Intracellularly-Retained Decorin Lacking the C-Terminal Ear Repeat Causes ER Stress: A Cell-Based Etiological Mechanism for Congenital Stromal Corneal Dystrophy. *The American Journal of Pathology*, 183(1), 247–256. <https://doi.org/10.1016/J.AJPATH.2013.04.001>
- Chen, S., Sun, M., Meng, X., Iozzo, R. v., Kao, W. W. Y., & Birk, D. E. (2011). Pathophysiological Mechanisms of Autosomal Dominant Congenital Stromal Corneal Dystrophy: C-Terminal-Truncated Decorin Results in Abnormal Matrix Assembly and Altered Expression of Small Leucine-Rich Proteoglycans. *The American Journal of Pathology*, 179(5), 2409–2419. <https://doi.org/10.1016/J.AJPATH.2011.07.026>
- Choi, H. Y., Liu, Y., Tennert, C., Sugiura, Y., Karakatsani, A., Kröger, S., Johnson, E. B., Hammer, R. E., Lin, W., & Herz, J. (2013). APP interacts with LRP4 and agrin to coordinate the development of the neuromuscular junction in mice. *ELife*, 2. <https://doi.org/10.7554/ELIFE.00220>
- CNX OpenStax. (n.d.). *Figure 27 01 03.jpg - Wikimedia Commons*. Retrieved October 2, 2022, from [https://commons.wikimedia.org/wiki/File:Figure\\_27\\_01\\_03.jpg](https://commons.wikimedia.org/wiki/File:Figure_27_01_03.jpg)
- Cognato, H., & Yurchenco, P. D. (2000). *Form and Function: The Laminin Family of Heterotrimers*. [https://doi.org/10.1002/\(SICI\)1097-0177\(200006\)218:2](https://doi.org/10.1002/(SICI)1097-0177(200006)218:2)
- Costell, M., Gustafsson, E., Aszódi, A., Mörgelin, M., Bloch, W., Hunziker, E., Addicks, K., Timpl, R., & Fässler, R. (1999). Perlecan Maintains the Integrity of Cartilage and Some Basement Membranes. *Journal of Cell Biology*, 147(5), 1109–1122. <https://doi.org/10.1083/JCB.147.5.1109>
- D’Amico, L., Scott, I. C., Jungblut, B., & Stainier, D. Y. R. (2007). A Mutation in Zebrafish *hmgcr1b* Reveals a Role for Isoprenoids in Vertebrate Heart-Tube Formation. *Current Biology*, 17(3), 252–259. <https://doi.org/10.1016/J.CUB.2006.12.023>

## BIBLIOGRAPHY

- Daniels, M. P. (2012). The Role of Agrin in Synaptic Development, Plasticity and Signaling in the Central Nervous System. *Neurochemistry International*, 61(6), 848. <https://doi.org/10.1016/J.NEUINT.2012.02.028>
- Danielson, K. G., Baribault, H., Holmes, D. F., Graham, H., Kadler, K. E., & Iozzo, R. v. (1997). Targeted Disruption of Decorin Leads to Abnormal Collagen Fibril Morphology and Skin Fragility. *Journal of Cell Biology*, 136(3), 729–743. <https://doi.org/10.1083/JCB.136.3.729>
- Davaapil, H. (2018). The role of the proteoglycans OMD and PRELP in the maintenance of brain vasculature. *Doctoral Thesis, UCL (University College London)*. .
- Davis CL. (1924). The cardiac jelly of the chick embryo. *Anatomical Record*, 27, 201–202. <https://ci.nii.ac.jp/naid/10027384360/>
- de Angelis, J. E., Lagendijk, A. K., Chen, H., Tromp, A., Bower, N. I., Tunny, K. A., Brooks, A. J., Bakkers, J., Francois, M., Yap, A. S., Simons, C., Wicking, C., Hogan, B. M., & Smith, K. A. (2017). Tmem2 Regulates Embryonic Vegf Signaling by Controlling Hyaluronic Acid Turnover. *Developmental Cell*, 40(2), 123–136. <https://doi.org/10.1016/J.DEVCEL.2016.12.017>
- de Sá Schiavo Matias, G., da Silva Nunes Barreto, R., Carreira, A. C. O., Junior, M. Y. N., Fratini, P., Ferreira, C. R., & Miglino, M. A. (2022). Proteomic profile of extracellular matrix from native and decellularized chorionic canine placenta. *Journal of Proteomics*, 256, 104497. <https://doi.org/10.1016/J.JPROT.2022.104497>
- del Monte-Nieto, G., Ramialison, M., Adam, A. A. S., Wu, B., Aharonov, A., D’uva, G., Bourke, L. M., Pitulescu, M. E., Chen, H., de la Pompa, J. L., Shou, W., Adams, R. H., Harten, S. K., Tzahor, E., Zhou, B., & Harvey, R. P. (2018). Control of cardiac jelly dynamics by NOTCH1 and NRG1 defines the building plan for trabeculation. *Nature* 2018 557:7705, 557(7705), 439–445. <https://doi.org/10.1038/s41586-018-0110-6>
- Derrick, C. J., Pollitt, E. J. G., Sanchez Sevilla Uruchurtu, A., Hussein, F., Grierson, A. J., & Noël, E. S. (2021). Lamb1a regulates atrial growth by limiting second heart field addition during zebrafish heart development. *Development (Cambridge, England)*, 148(20). <https://doi.org/10.1242/DEV.199691>
- Derrick, C. J., Sánchez-Posada, J., Hussein, F., Tessadori, F., Pollitt, E. J. G., Savage, A. M., Wilkinson, R. N., Chico, T. J., van Eeden, F. J., Bakkers, J., & Noël, E. S. (2022). Asymmetric Hapln1a drives regionalized cardiac ECM expansion and promotes heart morphogenesis in zebrafish development. *Cardiovascular Research*, 118(1), 226–240. <https://doi.org/10.1093/CVR/CVAB004>
- Dzamba, B. J., & DeSimone, D. W. (2018). Extracellular Matrix (ECM) and the Sculpting of Embryonic Tissues. *Current Topics in Developmental Biology*, 130, 245–274. <https://doi.org/10.1016/BS.CTDB.2018.03.006>
- Exposito, J. Y., Valcourt, U., Cluzel, C., & Lethias, C. (2010). The Fibrillar Collagen Family. *International Journal of Molecular Sciences*, 11(2), 407. <https://doi.org/10.3390/IJMS11020407>
- Factor-, G., Yan, W., & Wang, P. (2009). Decorin Gene Delivery Inhibits Cardiac Fibrosis in Spontaneously Hypertensive Rats by Modulation. 1199(October), 1190–1199.
- Ferdous, Z., Peterson, S. B., Tseng, H., Anderson, D. K., Iozzo, R. v., & Grande-Allen, K. J. (2010). A role for decorin in controlling proliferation, adhesion, and

## BIBLIOGRAPHY

- migration of murine embryonic fibroblasts. *Journal of Biomedical Materials Research Part A*, 93A(2), 419–428. <https://doi.org/10.1002/JBM.A.32545>
- Fisher, S. A., Langille, B. L., & Srivastava, D. (2000). Apoptosis During Cardiovascular Development. *Circulation Research*, 87(10), 856–864. <https://doi.org/10.1161/01.RES.87.10.856>
- Frantz, C., Stewart, K. M., & Weaver, V. M. (2010). The extracellular matrix at a glance. *Journal of Cell Science*, 123(123), 4195–4200. <https://doi.org/10.1242/jcs.023820>
- Freire, E., & Coelho-Sampaio, T. (2000). Self-assembly of Laminin Induced by Acidic pH. *Journal of Biological Chemistry*, 275(2), 817–822. <https://doi.org/10.1074/JBC.275.2.817>
- Fukuda, K., Kanazawa, H., Aizawa, Y., Ardell, J. L., & Shivkumar, K. (2015). Cardiac Innervation and Sudden Cardiac Death. *Circulation Research*, 116(12), 2005–2019. <https://doi.org/10.1161/CIRCRESAHA.116.304679>
- Gad Armony. (2017, March 27). *An illustration of the Laminin-111 complex*. Wikimedia Commons. <https://commons.wikimedia.org/wiki/File:Laminin111.png>
- Gamba, L., Amin-Javaheri, A., Kim, J., Warburton, D., & Lien, C. L. (2017). Collagenolytic Activity Is Associated with Scar Resolution in Zebrafish Hearts after Cryoinjury. *Journal of Cardiovascular Development and Disease*, 4(1). <https://doi.org/10.3390/JCDD4010002>
- Gamer, L. W., Ho, V., Cox, K., & Rosen, V. (2008). Expression and function of BMP3 during chick limb development. *Developmental Dynamics*, 237(6), 1691–1698. <https://doi.org/10.1002/dvdy.21561>
- Gentile, A., Bensimon-Brito, A., Priya, R., Maischein, H. M., Piesker, J., Guenther, S., Gunawan, F., & Stainier, D. Y. R. (2021). The EMT transcription factor Snail maintains myocardial wall integrity by repressing intermediate filament gene expression. *ELife*, 10. <https://doi.org/10.7554/ELIFE.66143>
- Glicman Holtzman, N., Schoenebeck, J. J., Tsai, H. J., & Yelon, D. (2007). Endocardium is necessary for cardiomyocyte movement during heart tube assembly. *Development*, 134(12), 2379–2386. <https://doi.org/10.1242/dev.02857>
- Goddard, L. M., Duchemin, A. L., Ramalingan, H., Wu, B., Chen, M., Bamezai, S., Yang, J., Li, L., Morley, M. P., Wang, T., Scherrer-Crosbie, M., Frank, D. B., Engleka, K. A., Jameson, S. C., Morrisey, E. E., Carroll, T. J., Zhou, B., Vermot, J., & Kahn, M. L. (2017). Hemodynamic Forces Sculpt Developing Heart Valves through a KLF2-WNT9B Paracrine Signaling Axis. *Developmental Cell*, 43(3), 274–289.e5. <https://doi.org/10.1016/j.devcel.2017.09.023>
- González-Rosa, J. M., Martín, V., Peralta, M., Torres, M., & Mercader, N. (2011). Extensive scar formation and regression during heart regeneration after cryoinjury in zebrafish. *Development*, 138(9), 1663–1674. <https://doi.org/10.1242/DEV.060897>
- Grassini, D. R., Lagendijk, A. K., de Angelis, J. E., da Silva, J., Jeanes, A., Zettler, N., Bower, N. I., Hogan, B. M., & Smith, K. A. (2018). Nppa and nppb act redundantly during zebrafish cardiac development to confine AVC marker expression and reduce cardiac jelly volume. *Development (Cambridge)*, 145(12). <https://doi.org/10.1242/DEV.160739/VIDEO-2>
- Gribble, Gribble, K. D., Walker, L. J., Saint-Amant, L., Kuwada, J. Y., & Granato, M. (2018). The synaptic receptor Lrp4 promotes peripheral nerve regeneration. In



## BIBLIOGRAPHY

- Nature Communications* (Vol. 9, Issue 1). Nature Publishing Group. <https://doi.org/10.1038/s41467-018-04806-4>
- Grover, J., & Roughley, P. J. (2001). Characterization and expression of murine PRELP. *Matrix Biology*, 20(8), 555–564. [https://doi.org/10.1016/S0945-053X\(01\)00165-2](https://doi.org/10.1016/S0945-053X(01)00165-2)
- Gubbiotti, M. A., Vallet, S. D., Ricard-Blum, S., & Iozzo, R. v. (2016). Decorin interacting network: A comprehensive analysis of decorin-binding partners and their versatile functions. *Matrix Biology*, 55, 7–21. <https://doi.org/10.1016/J.MATBIO.2016.09.009>
- Guerra, A., Germano, R. F. V., Stone, O., Arnaout, R., Guenther, S., Ahuja, S., Uribe, V., Vanhollebeke, B., Stainier, D. Y. R., & Reischauer, S. (2018). Distinct myocardial lineages break atrial symmetry during cardiogenesis in zebrafish. *ELife*, 7. <https://doi.org/10.7554/ELIFE.32833>
- Gunawan, F., Gentile, A., Fukuda, R., Tsedeke, A. T., Jiménez-Amilburu, V., Ramadass, R., Iida, A., Sehara-Fujisawa, A., & Stainier, D. Y. R. (2019). Focal adhesions are essential to drive zebrafish heart valve morphogenesis. *Journal of Cell Biology*, 218(3), 1039–1054. <https://doi.org/10.1083/JCB.201807175/VIDEO-4>
- Gunawan, F., Gentile, A., Gauvrit, S., Stainier, D. Y. R., & Bensimon-Brito, A. (2020). Nfatc1 Promotes Interstitial Cell Formation During Cardiac Valve Development in Zebrafish. *Circulation Research*, 968–984. <https://doi.org/10.1161/CIRCRESAHA.119.315992>
- Gunawan, F., Priya, R., & Stainier, D. Y. R. (2021). Sculpting the heart: Cellular mechanisms shaping valves and trabeculae. *Current Opinion in Cell Biology*, 73, 26–34. <https://doi.org/10.1016/J.CEB.2021.04.009>
- Haffter, P., Granato, M., Brand, M., Mullins, M. C., Hammerschmidt, M., Kane, D. A., Odenthal, J., van Eeden, F. J. M., Jiang, Y. J., Heisenberg, C. P., Kelsh, R. N., Furutani-Seiki, M., Vogelsang, E., Beuchle, D., Schach, U., Fabian, C., & Nüsslein-Volhard, C. (1996). The identification of genes with unique and essential functions in the development of the zebrafish, *Danio rerio*. *Development*, 123, 1–36. <https://doi.org/10.1242/dev.123.1.1>
- Hällgren, R., Gerdin, B., Tengblad, A., & Tufveson, G. (1990). Accumulation of hyaluronan (hyaluronic acid) in myocardial interstitial tissue parallels development of transplantation edema in heart allografts in rats. *The Journal of Clinical Investigation*, 85(3), 668–673. <https://doi.org/10.1172/JCI114490>
- Happonen, K. E., Fürst, C. M., Saxne, T., Heinegård, D., & Blom, A. M. (2012). PRELP Protein Inhibits the Formation of the Complement Membrane Attack Complex. *Journal of Biological Chemistry*, 287(11), 8092–8100. <https://doi.org/10.1074/jbc.M111.291476>
- Heinegård, D. (2009). Proteoglycans and more - From molecules to biology. *International Journal of Experimental Pathology*, 90(6), 575–586. <https://doi.org/10.1111/J.1365-2613.2009.00695.X>
- Heineghrd, D., Larsson, T., Sommarin, Y., Franzen, A., Paulsson, M., & Hedbom, E. (1986). Two Novel Matrix Proteins Isolated from Articular Cartilage Show Wide Distributions among Connective Tissues\*. *The Journal of Biological Chemistry*, 261(29), 13866–13872.
- Hiroyasu, S., & Jones, J. C. R. (2014). A New Component of the Fraser Complex. *The Journal of Investigative Dermatology*, 134(5), 1192. <https://doi.org/10.1038/JID.2013.514>

## BIBLIOGRAPHY

- Ho, Y. L., Lin, Y. H., Tsai, I. J., Hsieh, F. J., & Tsai, H. J. (2007). In Vivo Assessment of Cardiac Morphology and Function in Heart-specific Green Fluorescent Zebrafish. *Journal of the Formosan Medical Association*, 106(3), 181–186. [https://doi.org/10.1016/S0929-6646\(09\)60238-2](https://doi.org/10.1016/S0929-6646(09)60238-2)
- Hocking, A. M., Shinomura, T., & McQuillan, D. J. (1998). Leucine-rich repeat glycoproteins of the extracellular matrix. In *Matrix Biology* (Vol. 17, Issue 1, pp. 1–19). Elsevier B.V. [https://doi.org/10.1016/S0945-053X\(98\)90121-4](https://doi.org/10.1016/S0945-053X(98)90121-4)
- Hopf, C., & Hoch, W. (1996). *Agrin Binding to  $\alpha$ -Dystroglycan DOMAINS OF AGRIN NECESSARY TO INDUCE ACETYLCHOLINE RECEPTOR CLUSTERING ARE*. 271(9), 5231–5236.
- Hulin, A., Hortells, L., Gomez-Stallons, M. V., O'Donnell, A., Chetal, K., Adam, M., Lancellotti, P., Oury, C., Potter, S. S., Salomonis, N., & Yutzey, K. E. (2019). Maturation of heart valve cell populations during postnatal remodeling. *Development (Cambridge)*, 146(12). <https://doi.org/10.1242/DEV.173047/264834/AM/MATURATION-OF-HEART-VALVE-CELL-POPULATIONS-DURING>
- Hultgårdh-Nilsson, A., Borén, J., & Chakravarti, S. (2015). The small leucine-rich repeat proteoglycans in tissue repair and atherosclerosis. *Journal of Internal Medicine*, 278(5), 447–461. <https://doi.org/10.1111/joim.12400>
- Hynes, R. O. (2009). The extracellular matrix: Not just pretty fibrils. In *Science* (Vol. 326, Issue 5957, pp. 1216–1219). <https://doi.org/10.1126/science.1176009>
- Iozzo, R. v., & Schaefer, L. (2015a). Proteoglycan form and function: A comprehensive nomenclature of proteoglycans. *Matrix Biology*, 42, 11–55. <https://doi.org/10.1016/J.MATBIO.2015.02.003>
- Iozzo, R. v., & Schaefer, L. (2015b). Proteoglycan form and function: A comprehensive nomenclature of proteoglycans. *Matrix Biology*, 42, 11–55. <https://doi.org/10.1016/J.MATBIO.2015.02.003>
- Järveläinen, H., Puolakkainen, P., Pakkanen, S., Brown, E. L., Höök, M., Iozzo, R. v., Sage, E. H., & Wight, T. N. (2006). A role for decorin in cutaneous wound healing and angiogenesis. *Wound Repair and Regeneration*, 14(4), 443–452. <https://doi.org/10.1111/J.1743-6109.2006.00150.X>
- Järveläinen, H., Sainio, A., & Wight, T. N. (2015). Pivotal role for decorin in angiogenesis. *Matrix Biology*, 43, 15–26. <https://doi.org/10.1016/j.matbio.2015.01.023>
- Järvinen, T. A. H., & Prince, S. (2015). Decorin: A Growth Factor Antagonist for Tumor Growth Inhibition. *BioMed Research International*, 2015. <https://doi.org/10.1155/2015/654765>
- Jayadev, R., & Sherwood, D. R. (2017). Basement membranes. *Current Biology*, 27(6), R207–R211. <https://doi.org/10.1016/J.CUB.2017.02.006>
- Jimenez Amilburu, V. (2018). *Cardiomyocyte apicobasal polarity during cardiac trabeculation in zebrafish*. <http://publikationen.uni-frankfurt.de/frontdoor/index/index/docId/51385>
- Jiménez-Amilburu, V., Rasouli, S. J., Staudt, D. W., Nakajima, H., Chiba, A., Mochizuki, N., & Stainier, D. Y. R. (2016). In Vivo Visualization of Cardiomyocyte Apicobasal Polarity Reveals Epithelial to Mesenchymal-like Transition during Cardiac Trabeculation. *Cell Reports*, 17(10), 2687–2699. <https://doi.org/10.1016/J.CELREP.2016.11.023>
- Jiménez-Amilburu, V., & Stainier, D. Y. R. (2019). The transmembrane protein Crb2a regulates cardiomyocyte apicobasal polarity and adhesion in zebrafish.

## BIBLIOGRAPHY

- Development* (Cambridge, England), 146(9).  
<https://doi.org/10.1242/DEV.171207>
- Jin, S. W., Beis, D., Mitchell, T., Chen, J. N., & Stainier, D. Y. R. (2005). Cellular and molecular analyses of vascular tube and lumen formation in zebrafish. *Development*, 132(23), 5199–5209. <https://doi.org/10.1242/DEV.02087>
- Jumper, J., Evans, R., Pritzel, A., Green, T., Figurnov, M., Ronneberger, O., Tunyasuvunakool, K., Bates, R., Židek, A., Potapenko, A., Bridgland, A., Meyer, C., Kohl, S. A. A., Ballard, A. J., Cowie, A., Romera-Paredes, B., Nikolov, S., Jain, R., Adler, J., ... Hassabis, D. (2021). Highly accurate protein structure prediction with AlphaFold. *Nature*, 596(7873), 583–589. <https://doi.org/10.1038/s41586-021-03819-2>
- Keegan, B. R., Meyer, D., & Yelon, D. (2004). Organization of cardiac chamber progenitors in the zebrafish blastula. *Development (Cambridge, England)*, 131(13), 3081–3091. <https://doi.org/10.1242/DEV.01185>
- Keeley, D. P., Hastie, E., Jayadev, R., Kelley, L. C., Chi, Q., Payne, S. G., Jeger, J. L., Hoffman, B. D., & Sherwood, D. R. (2020). Comprehensive Endogenous Tagging of Basement Membrane Components Reveals Dynamic Movement within the Matrix Scaffolding. *Developmental Cell*, 54(1), 60-74.e7. <https://doi.org/10.1016/J.DEVCEL.2020.05.022>
- Kim, J. H., Ko, J. M., Lee, I., Kim, J. Y., Kim, M. J., & Tchah, H. (2011). A novel mutation of the decorin gene identified in a korean family with congenital hereditary stromal dystrophy. *Cornea*, 30(12), 1473–1477. <https://doi.org/10.1097/ICO.0B013E3182137788>
- Kim, K. H., Nakaoka, Y., Augustin, H. G., & Koh, G. Y. (2018). Myocardial Angiopoietin-1 Controls Atrial Chamber Morphogenesis by Spatiotemporal Degradation of Cardiac Jelly. *Cell Reports*, 23(8), 2455–2466. <https://doi.org/10.1016/J.CELREP.2018.04.080>
- Kim, M. J., Liu, I. H., Song, Y., Lee, J. A., Halfter, W., Balice-Gordon, R. J., Linney, E., & Cole, G. J. (2007). Agrin is required for posterior development and motor axon outgrowth and branching in embryonic zebrafish. *Glycobiology*, 17(2), 231–247. <https://doi.org/10.1093/GLYCOB/CWL069>
- Kim, O.-H., An, H. S., & Choi, T.-Y. (2019). Generation of mmp15b Zebrafish Mutant to Investigate Liver Diseases. *Development & Reproduction*, 23(4), 385–390. <https://doi.org/10.12717/DR.2019.23.4.385>
- Kimmel, C. B., Ballard, W. W., Kimmel, S. R., Ullmann, B., & Schilling, T. F. (1995). Stages of embryonic development of the zebrafish. *Developmental Dynamics : An Official Publication of the American Association of Anatomists*, 203(3), 253–310. <https://doi.org/10.1002/AJA.1002030302>
- Kokabu, S., & Rosen, V. (2018). BMP3 expression by osteoblast lineage cells is regulated by canonical Wnt signaling. *FEBS Open Bio*, 8(2), 168–176. <https://doi.org/10.1002/2211-5463.12347>
- Komuro, I., & Izumo, S. (1993). Csx: a murine homeobox-containing gene specifically expressed in the developing heart. *Proceedings of the National Academy of Sciences of the United States of America*, 90(17), 8145. <https://doi.org/10.1073/PNAS.90.17.8145>
- Kosuge, H., Nakakido, M., Nagatoishi, S., Fukuda, T., Bando, Y., Ohnuma, S. I., & Tsumoto, K. (2021). Proteomic identification and validation of novel interactions of the putative tumor suppressor PRELP with membrane proteins

## BIBLIOGRAPHY

- including IGFI-R and p75NTR. *Journal of Biological Chemistry*, 296, 100278. <https://doi.org/10.1016/J.JBC.2021.100278>
- Kupperman, E., An, S., Osborne, N., Waldron, S., & Stainier, D. Y. R. (2000a). A sphingosine-1-phosphate receptor regulates cell migration during vertebrate heart development. *Nature*, 406(6792), 192–195. <https://doi.org/10.1038/35018092>
- Kupperman, E., An, S., Osborne, N., Waldron, S., & Stainier, D. Y. R. (2000b). A sphingosine-1-phosphate receptor regulates cell migration during vertebrate heart development. *Nature* 2000 406:6792, 406(6792), 192–195. <https://doi.org/10.1038/35018092>
- Kyprianou, C., Christodoulou, N., Hamilton, R. S., Nahaboo, W., Boomgaard, D. S., Amadei, G., Migeotte, I., & Zernicka-Goetz, M. (2020). Basement membrane remodelling regulates mouse embryogenesis. *Nature* 2020 582:7811, 582(7811), 253–258. <https://doi.org/10.1038/s41586-020-2264-2>
- Lai, S.-L., Marín-Juez, R., Luís Moura, P., Kuenne, C., Kuan Han Lai, J., Taddese Tsedeke, A., Guenther, S., Looso, M., & Stainier, D. Y. (2017). *Reciprocal analyses in zebrafish and medaka reveal that harnessing the immune response promotes cardiac regeneration*. <https://doi.org/10.7554/eLife.25605.001>
- Lander, A. D., & Selleck, S. B. (2000). The elusive functions of proteoglycans: In vivo veritas. *Journal of Cell Biology*, 148(2), 227–232. <https://doi.org/10.1083/jcb.148.2.227>
- Laurie, G. W., Leblond, C. P., & Martin, G. R. (1983). Light microscopic immunolocalization of type IV collagen, laminin, heparan sulfate proteoglycan, and fibronectin in the basement membranes of a variety of rat organs. *The American Journal of Anatomy*, 167(1), 71–82. <https://doi.org/10.1002/aja.1001670107>
- Lee, J. L., & Streuli, C. H. (2014). Integrins and epithelial cell polarity. *Journal of Cell Science*, 127(15), 3217–3225. <https://doi.org/10.1242/JCS.146142/259771/AM-INTEGRINS-AND-EPITHELIAL-CELL-POLARITY>
- Lewis, M. (2003). PRELP, collagen, and a theory of Hutchinson-Gilford progeria. *Ageing Research Reviews*, 2(1), 95–105. [https://doi.org/10.1016/S1568-1637\(02\)00044-2](https://doi.org/10.1016/S1568-1637(02)00044-2)
- Li, J., Ma, J., Zhang, Q., Gong, H., Gao, D., Wang, Y., Li, B., Li, X., Zheng, H., Wu, Z., Zhu, Y., & Leng, L. (2022). Spatially resolved proteomic map shows that extracellular matrix regulates epidermal growth. *Nature Communications* 2022 13:1, 13(1), 1–16. <https://doi.org/10.1038/s41467-022-31659-9>
- Lints, T. J., Parsons, L. M., Hartley, L., Lyons, I., & Harvey, R. P. (1993). Nkx-2.5: a novel murine homeobox gene expressed in early heart progenitor cells and their myogenic descendants. *Development*, 119(2), 419–431. <https://doi.org/10.1242/DEV.119.2.419>
- Little, C. D., Piquet, D. M., Davis, L. A., Walters, L., & Drake, C. J. (1989). Distribution of laminin, collagen type IV, collagen type I, and fibronectin in chicken cardiac jelly/basement membrane. *The Anatomical Record*, 224(3), 417–425. <https://doi.org/10.1002/AR.1092240310>
- Liu, G., Ermert, D., Johansson, M. E., Singh, B., Su, Y.-C., Paulsson, M., Riesbeck, K., & Blom, A. M. (2017). PRELP Enhances Host Innate Immunity against the Respiratory Tract Pathogen *Moraxella catarrhalis*. *The Journal of Immunology*, 198(6), 2330–2340. <https://doi.org/10.4049/jimmunol.1601319>

## BIBLIOGRAPHY

- Lockhart, M., Wirrig, E., Phelps, A., & Wessels, A. (2011). Extracellular matrix and heart development. In *Birth Defects Research Part A - Clinical and Molecular Teratology* (Vol. 91, Issue 6, pp. 535–550). <https://doi.org/10.1002/bdra.20810>
- Maenner, J. (2009). The anatomy of cardiac looping: A step towards the understanding of the morphogenesis of several forms of congenital cardiac malformations. *Clinical Anatomy*, 22(1), 21–35. <https://doi.org/10.1002/CA.20652>
- Mak, K. M., & Mei, R. (2017). Basement Membrane Type IV Collagen and Laminin: An Overview of Their Biology and Value as Fibrosis Biomarkers of Liver Disease. *The Anatomical Record*, 300(8), 1371–1390. <https://doi.org/10.1002/AR.23567>
- Männer, J., & Yelbuz, T. M. (2019). Functional Morphology of the Cardiac Jelly in the Tubular Heart of Vertebrate Embryos. *Journal of Cardiovascular Development and Disease* 2019, Vol. 6, Page 12, 6(1), 12. <https://doi.org/10.3390/JCDD6010012>
- Marques, S. R., & Yelon, D. (2009). Differential requirement for BMP signaling in atrial and ventricular lineages establishes cardiac chamber proportionality. *Developmental Biology*, 328(2), 472–482. <https://doi.org/10.1016/J.YDBIO.2009.02.010>
- Mauviel, A., Santra, M. an jan, Chen, Y. Q., Uitto, J., & Iozzo, R. v. (1995). Transcriptional Regulation of Decorin Gene Expression. *Journal of Biological Chemistry*, 270(19), 11692–11700. <https://doi.org/10.1074/jbc.270.19.11692>
- Menter, D. G., & Dubois, R. N. (2012). Prostaglandins in cancer cell adhesion, migration, and invasion. *International Journal of Cell Biology*. <https://doi.org/10.1155/2012/723419>
- Merline, R., Moreth, K., Beckmann, J., Nastase, M. v., Zeng-Brouwers, J., Tralhão, J. G., Lemarchand, P., Pfeilschifter, J., Schaefer, R. M., Iozzo, R. v., & Schaefer, L. (2011). Signaling by the matrix proteoglycan decorin controls inflammation and cancer through PDCD4 and microRNA-21. *Science Signaling*, 4(199). [https://doi.org/10.1126/SCISIGNAL.2001868/SUPPL\\_FILE/4\\_RA75\\_SM.PDF](https://doi.org/10.1126/SCISIGNAL.2001868/SUPPL_FILE/4_RA75_SM.PDF)
- Mirdita, M., Schütze, K., Moriwaki, Y., Heo, L., Ovchinnikov, S., & Steinegger, M. (2022). ColabFold: making protein folding accessible to all. *Nature Methods* 2022 19:6, 19(6), 679–682. <https://doi.org/10.1038/s41592-022-01488-1>
- Miura, T., Kishioka, Y., Wakamatsu, J., Hattori, A., Hennebry, A., Berry, C. J., Sharma, M., Kambadur, R., & Nishimura, T. (2006). Decorin binds myostatin and modulates its activity to muscle cells. *Biochemical and Biophysical Research Communications*, 340(2), 675–680. <https://doi.org/10.1016/j.bbrc.2005.12.060>
- Moorehead, C., Prudnikova, K., & Marcolongo, M. (2019). The regulatory effects of proteoglycans on collagen fibrillogenesis and morphology investigated using biomimetic proteoglycans. *Journal of Structural Biology*, 206(2), 204–215. <https://doi.org/10.1016/J.JSB.2019.03.005>
- Naba, A., Clauser, K. R., Ding, H., Whittaker, C. A., Carr, S. A., & Hynes, R. O. (2016). The extracellular matrix: Tools and insights for the “omics” era. In *Matrix Biology* (Vol. 49, pp. 10–24). Elsevier B.V. <https://doi.org/10.1016/j.matbio.2015.06.003>
- Nakajima, Y., Morishima, M., Nakazawa, M., Momma, K., & Nakamura, H. (1997). Distribution of fibronectin, type I collagen, type IV collagen, and laminin in the cardiac jelly of the mouse embryonic heart with retinoic acid-induced complete

## BIBLIOGRAPHY

- transposition of the great arteries. *The Anatomical Record*, 249(4), 478–485. [https://doi.org/10.1002/\(sici\)1097-0185\(199712\)249:4<478::aid-ar7>3.3.co;2-f](https://doi.org/10.1002/(sici)1097-0185(199712)249:4<478::aid-ar7>3.3.co;2-f)
- Nakamura, A., & Manasek, F. J. (1978). Experimental studies of the shape and structure of isolated cardiac jelly. *Development*, 43(1), 167–183. <https://doi.org/10.1242/DEV.43.1.167>
- Nakamura, A., & Manasek, F. J. (1981). An experimental study of the relation of cardiac jelly to the shape of the early chick embryonic heart. *Development*, 65(1), 235–256. <https://doi.org/10.1242/DEV.65.1.235>
- Nauroy, P., Hughes, S., Naba, A., & Ruggiero, F. (2018). The in-silico zebrafish matrisome: A new tool to study extracellular matrix gene and protein functions. *Matrix Biology*, 65, 5–13. <https://doi.org/10.1016/J.MATBIO.2017.07.001>
- Neill, T., Schaefer, L., & Iozzo, R. v. (2012). Decorin: A guardian from the matrix. *American Journal of Pathology*, 181(2), 380–387. <https://doi.org/10.1016/j.ajpath.2012.04.029>
- Neill, T., Schaefer, L., & Iozzo, R. v. (2016). Decorin as a multivalent therapeutic agent against cancer. *Advanced Drug Delivery Reviews*, 97, 174–185. <https://doi.org/10.1016/j.addr.2015.10.016>
- Ocken, A. R., Ku, M. M., Kinzer-Ursem, T. L., & Calve, S. (2020). Perlecan knockdown significantly alters extracellular matrix composition and organization during cartilage development. *Molecular and Cellular Proteomics*, 19(7), 1220–1235. <https://doi.org/10.1074/mcp.RA120.001998>
- Osborne, N., Brand-Arzamendi, K., Ober, E. A., Jin, S. W., Verkade, H., Holtzman, N. G., Yelon, D., & Stainier, D. Y. R. (2008). The Spinster Homolog, Two of Hearts, Is Required for Sphingosine 1-Phosphate Signaling in Zebrafish. *Current Biology*, 18(23), 1882–1888. <https://doi.org/10.1016/J.CUB.2008.10.061>
- Pakshir, P., Alizadehgiashi, M., Wong, B., Coelho, N. M., Chen, X., Gong, Z., Shenoy, V. B., McCulloch, C., & Hinz, B. (2019). Dynamic fibroblast contractions attract remote macrophages in fibrillar collagen matrix. *Nature Communications* 2019 10:1, 10(1), 1–17. <https://doi.org/10.1038/s41467-019-09709-6>
- Pang, X., Li, W., Chang, L., Gautrot, J. E., Wang, W., & Azevedo, H. S. (2021). Hyaluronan (HA) Immobilized on Surfaces via Self-Assembled Monolayers of HA-Binding Peptide Modulates Endothelial Cell Spreading and Migration through Focal Adhesion. *ACS Applied Materials and Interfaces*, 13(22), 25792–25804. [https://doi.org/10.1021/ACSAMI.1C05574/SUPPL\\_FILE/AM1C05574\\_SI\\_001.PDF](https://doi.org/10.1021/ACSAMI.1C05574/SUPPL_FILE/AM1C05574_SI_001.PDF)
- Petelski, A. A., Emmott, E., Leduc, A., Huffman, R. G., Specht, H., Perlman, D. H., & Slavov, N. (2021). Multiplexed single-cell proteomics using SCoPE2. *Nature Protocols* 2021 16:12, 16(12), 5398–5425. <https://doi.org/10.1038/s41596-021-00616-z>
- Pokhilko, A., Brezzo, G., Handunnetthi, L., Heilig, R., Lennon, R., Smith, C., Allan, S. M., Granata, A., Sinha, S., Wang, T., Markus, H. S., Naba, A., Fischer, R., van Aghtmael, T., Horsburgh, K., & Cader, M. Z. (2021). Global proteomic analysis of extracellular matrix in mouse and human brain highlights relevance to cerebrovascular disease. *Journal of Cerebral Blood Flow and Metabolism*, 41(9), 2423–2438. [https://doi.org/10.1177/0271678X211004307/ASSET/IMAGES/LARGE/10.1177\\_0271678X211004307-FIG2.JPEG](https://doi.org/10.1177/0271678X211004307/ASSET/IMAGES/LARGE/10.1177_0271678X211004307-FIG2.JPEG)

## BIBLIOGRAPHY

- Priya, R., Allanki, S., Gentile, A., Mansingh, S., Uribe, V., Maischein, H. M., & Stainier, D. Y. R. (2020). Tension heterogeneity directs form and fate to pattern the myocardial wall. *Nature*, *588*(7836), 130–134. <https://doi.org/10.1038/S41586-020-2946-9>
- Qi, J., Rittershaus, A., Priya, R., Mansingh, S., Stainier, D. Y. R., & Helker, C. S. M. (2022). Apelin signaling dependent endocardial protrusions promote cardiac trabeculation in zebrafish. *ELife*, *11*. <https://doi.org/10.7554/ELIFE.73231>
- Qu, X., Harmelink, C., & Scott Baldwin, H. (2019). Tie2 regulates endocardial sprouting and myocardial trabeculation. *JCI Insight*, *4*(13). <https://doi.org/10.1172/JCI.INSIGHT.96002>
- Rasouli, S. J., El-Brolosy, M., Tsedeke, A. T., Bensimon-Brito, A., Ghanbari, P., Maischein, H. M., Kuenne, C., & Stainier, D. Y. (2018). The flow responsive transcription factor Klf2 is required for myocardial wall integrity by modulating Fgf signaling. *ELife*, *7*. <https://doi.org/10.7554/ELIFE.38889>
- Rasouli, S. J., & Stainier, D. Y. R. (2017). Regulation of cardiomyocyte behavior in zebrafish trabeculation by Neuregulin 2a signaling. *Nature Communications*, *8*. <https://doi.org/10.1038/NCOMMS15281>
- Ribeiro, C., Petit, V., & Affolter, M. (2003). Signaling systems, guided cell migration, and organogenesis: Insights from genetic studies in *Drosophila*. *Developmental Biology*, *260*(1), 1–8. [https://doi.org/10.1016/S0012-1606\(03\)00211-2](https://doi.org/10.1016/S0012-1606(03)00211-2)
- Rienks, M., Papageorgiou, A. P., Frangogiannis, N. G., & Heymans, S. (2014). Myocardial extracellular matrix: An ever-changing and diverse entity. *Circulation Research*, *114*(5), 872–888. <https://doi.org/10.1161/CIRCRESAHA.114.302533>
- Rohr, S., Bit-Avragim, N., & Abdelilah-Seyfried, S. (2006). Heart and soul/PRKCi and nagie oko/Mpp5 regulate myocardial coherence and remodeling during cardiac morphogenesis. *Development*, *133*(1), 107–115. <https://doi.org/10.1242/DEV.02182>
- Rohr, S., Otten, C., & Abdelilah-Seyfried, S. (2008). Asymmetric involution of the myocardial field drives heart tube formation in zebrafish. *Circulation Research*, *102*(2). <https://doi.org/10.1161/CIRCRESAHA.107.165241>
- Rosenthal, N., & Harvey, R. P. (2010). Heart Development and Regeneration. *Heart Development and Regeneration*. <https://doi.org/10.1016/C2009-1-62569-7>
- Rottbauer, W., Saurin, A. J., Lickert, H., Shen, X., Burns, C. G., Wo, Z. G., Kemler, R., Kingston, R., Wu, C., & Fishman, M. (2002). Reptin and Pontin Antagonistically Regulate Heart Growth in Zebrafish Embryos. *Cell*, *111*(5), 661–672. [https://doi.org/10.1016/S0092-8674\(02\)01112-1](https://doi.org/10.1016/S0092-8674(02)01112-1)
- Rozario, T., & DeSimone, D. W. (2010). The extracellular matrix in development and morphogenesis: A dynamic view. *Developmental Biology*, *341*(1), 126–140. <https://doi.org/10.1016/J.YDBIO.2009.10.026>
- Rucci, N., Rufo, A., Alamanou, M., Capulli, M., del Fattore, A., Åhrman, E., Capece, D., Iansante, V., Zazzeroni, F., Alesse, E., Heinegård, D., & Teti, A. (2009). The glycosaminoglycan-binding domain of PRELP acts as a cell type-specific NF- $\kappa$ B inhibitor that impairs osteoclastogenesis. *Journal of Cell Biology*, *187*(5), 669–683. <https://doi.org/10.1083/jcb.200906014>
- Rühland, C., Schönherr, E., Robenek, H., Hansen, U., Iozzo, R. v., Bruckner, P., & Seidler, D. G. (2007). The glycosaminoglycan chain of decorin plays an important role in collagen fibril formation at the early stages of fibrillogenesis.

## BIBLIOGRAPHY

- The FEBS Journal*, 274(16), 4246–4255. <https://doi.org/10.1111/J.1742-4658.2007.05951.X>
- Sakaguchi, T., Kikuchi, Y., Kuroiwa, A., Takeda, H., & Stainier, D. Y. R. (2006). The yolk syncytial layer regulates myocardial migration by influencing extracellular matrix assembly in zebrafish. *Development*, 133(20), 4063–4072. <https://doi.org/10.1242/DEV.02581>
- Sarig, R., Rimmer, R., Bassat, E., Zhang, L., Umansky, K. B., Lendengolts, D., Perlmoter, G., Yaniv, K., & Tzahor, E. (2019). Transient p53-Mediated Regenerative Senescence in the Injured Heart. *Circulation*, 139(21), 2491–2494. <https://doi.org/10.1161/CIRCULATIONAHA.119.040125>
- Schoenebeck, J. J., Hutchinson, S. A., Byers, A., Beale, H. C., Carrington, B., Faden, D. L., Rimbault, M., Decker, B., Kidd, J. M., Sood, R., Boyko, A. R., Fondon, J. W., Wayne, R. K., Bustamante, C. D., Ciruna, B., & Ostrander, E. A. (2012). Variation of BMP3 Contributes to Dog Breed Skull Diversity. *PLOS Genetics*, 8(8), e1002849. <https://doi.org/10.1371/JOURNAL.PGEN.1002849>
- Schönherr, E., Levkau, B., Schaefer, L., Kresse, H., & Walsh, K. (2001). Decorin-mediated signal transduction in endothelial cells. Involvement of Akt/protein kinase B in up-regulation of p21(WAF1/CIP1) but not p27(KIP1). *The Journal of Biological Chemistry*, 276(44), 40687–40692. <https://doi.org/10.1074/jbc.M105426200>
- Scott, J. E. (1988). Proteoglycan-fibrillar collagen interactions. *Biochemical Journal*, 252(2), 313. <https://doi.org/10.1042/BJ2520313>
- Scott, P. G., McEwan, P. A., Dodd, C. M., Bergmann, E. M., Bishop, P. N., & Bella, J. (2004). Crystal structure of the dimeric protein core of decorin, the archetypal small leucine-rich repeat proteoglycan. *Proceedings of the National Academy of Sciences of the United States of America*, 101(44), 15633–15638. [https://doi.org/10.1073/PNAS.0402976101/SUPPL\\_FILE/IMAGE290.GIF](https://doi.org/10.1073/PNAS.0402976101/SUPPL_FILE/IMAGE290.GIF)
- Sehnert, A. J., Huq, A., Weinstein, B. M., Walker, C., Fishman, M., & Stainier, D. Y. R. (2002). Cardiac troponin T is essential in sarcomere assembly and cardiac contractility. *Nature Genetics* 2002 31:1, 31(1), 106–110. <https://doi.org/10.1038/ng875>
- Shao, X., Taha, I. N., Clauser, K. R., Gao, Y. (Tom), & Naba, A. (2020). MatrisomeDB: the ECM-protein knowledge database. *Nucleic Acids Research*, 48(D1), D1136–D1144. <https://doi.org/10.1093/NAR/GKZ849>
- Short, K., Wiradjaja, F., & Smyth, I. (2007). Let's stick together: The role of the Fras1 and Frem proteins in epidermal adhesion. *IUBMB Life*, 59(7), 427–435. <https://doi.org/10.1080/15216540701510581>
- Specht, H., Emmott, E., Petelski, A. A., Huffman, R. G., Perlman, D. H., Serra, M., Kharchenko, P., Koller, A., & Slavov, N. (2021). Single-cell proteomic and transcriptomic analysis of macrophage heterogeneity using SCoPE2. *Genome Biology*, 22(1), 1–27. <https://doi.org/10.1186/S13059-021-02267-5/TABLES/2>
- Stainier, D. Y. R., Fouquet, B., Chen, J. N., Warren, K. S., Weinstein, B. M., Meiler, S. E., Mohideen, M. A. P. K., Neuhaus, S. C. F., Solnica-Krezel, L., Schier, A. F., Zwartkruis, F., Stemple, D. L., Malicki, J., Driever, W., & Fishman, M. C. (1996). Mutations affecting the formation and function of the cardiovascular system in the zebrafish embryo. *Development*, 123, 285–292. <https://doi.org/10.1242/dev.123.1.285>



## BIBLIOGRAPHY

- Stainier, D. Y. R., Lee, R. K., & Fishman, M. C. (1993). Cardiovascular development in the zebrafish. I. Myocardial fate map and heart tube formation. *Development*, *119*(1), 31–40. <https://doi.org/10.1242/DEV.119.1.31>
- Stanganello, E., Hagemann, A. I. H., Mattes, B., Sinner, C., Meyen, D., Weber, S., Schug, A., Raz, E., & Scholpp, S. (2015). Filopodia-based Wnt transport during vertebrate tissue patterning. *Nature Communications* *2015 6:1*, *6*(1), 1–14. <https://doi.org/10.1038/ncomms6846>
- Steed, E., Faggianelli, N., Roth, S., Ramsbacher, C., Concordet, J. P., & Vermot, J. (2016). *klf2a* couples mechanotransduction and zebrafish valve morphogenesis through fibronectin synthesis. *Nature Communications* *2016 7:1*, *7*(1), 1–14. <https://doi.org/10.1038/ncomms11646>
- Sun, X., Malandraki-Miller, S., Kennedy, T., Bassat, E., Klaourakis, K., Zhao, J., Gamen, E., Vieira, J. M., Tzahor, E., & Riley, P. R. (2021). The extracellular matrix protein agrin is essential for epicardial epithelial-to-mesenchymal transition during heart development. *Development (Cambridge, England)*, *148*(9). <https://doi.org/10.1242/DEV.197525>
- Tao, G., Levay, A. K., Gridley, T., & Lincoln, J. (2011). *Mmp15* is a direct target of *Snai1* during endothelial to mesenchymal transformation and endocardial cushion development. *Developmental Biology*, *359*(2), 209–221. <https://doi.org/10.1016/J.YDBIO.2011.08.022>
- Tezuka, T., Inoue, A., Hoshi, T., Weatherbee, S. D., Burgess, R. W., Ueta, R., & Yamanashi, Y. (2014). The MuSK activator agrin has a separate role essential for postnatal maintenance of neuromuscular synapses. *Proceedings of the National Academy of Sciences of the United States of America*, *111*(46), 16556–16561. [https://doi.org/10.1073/PNAS.1408409111/SUPPL\\_FILE/PNAS.201408409SI.PDF](https://doi.org/10.1073/PNAS.1408409111/SUPPL_FILE/PNAS.201408409SI.PDF)
- Thisse, et. al. (n.d.). *ZFIN Figures - Prelp Expression, Thisse et al., 2008*. Retrieved September 27, 2022, from <https://zfin.org/action/figure/all-figure-view/ZDB-PUB-080227-22?probeZdbID=ZDB-EST-080327-14>
- Thisse, B., Thisse, C., & Wright, G. J. (2008). *Embryonic and Larval Expression Patterns from a Large Scale Screening for Novel Low Affinity Extracellular Protein Interactions*. . ZFIN Direct Data Submission. <https://zfin.org/ZDB-PUB-080227-22>
- Thureson-Klein, Å., & Klein, R. L. (1971). Cation distribution and cardiac jelly in early embryonic heart: A histochemical and electron microscopic study. *Journal of Molecular and Cellular Cardiology*, *2*(1), 31–40. [https://doi.org/10.1016/0022-2828\(71\)90076-9](https://doi.org/10.1016/0022-2828(71)90076-9)
- Totong, R., Schell, T., Lescroart, F., Ryckebüsch, L., Lin, Y. F., Zygmunt, T., Herwig, L., Krudewig, A., Gershoony, D., Belting, H. G., Affolter, M., Torres-Vázquez, J., & Yelon, D. (2011). The novel transmembrane protein *tmem2* is essential for coordination of myocardial and endocardial morphogenesis. *Development*, *138*(19), 4199–4205. <https://doi.org/10.1242/DEV.064261/-/DC1>
- Trinh, L. A., & Stainier, D. Y. R. (2004). Fibronectin regulates epithelial organization during myocardial migration in zebrafish. *Developmental Cell*, *6*(3), 371–382. [https://doi.org/10.1016/S1534-5807\(04\)00063-2](https://doi.org/10.1016/S1534-5807(04)00063-2)
- Tsedeke, A. T., Allanki, S., Gentile, A., Jimenez-Amilburu, V., Rasouli, S. J., Guenther, S., Lai, S. L., Stainier, D. Y. R., & Marín-Juez, R. (2021). Cardiomyocyte heterogeneity during zebrafish development and regeneration.

## BIBLIOGRAPHY

- Developmental Biology*, 476, 259–271.  
<https://doi.org/10.1016/J.YDBIO.2021.03.014>
- Uribe, V., Ramadass, R., Dogra, D., Rasouli, S. J., Gunawan, F., Nakajima, H., Chiba, A., Reischauer, S., Mochizuki, N., & Stainier, D. Y. R. (2018). In vivo analysis of cardiomyocyte proliferation during trabeculation. *Development (Cambridge, England)*, 145(14). <https://doi.org/10.1242/DEV.164194>
- Varadi, M., Anyango, S., Deshpande, M., Nair, S., Natassia, C., Yordanova, G., Yuan, D., Stroe, O., Wood, G., Laydon, A., Zidek, A., Green, T., Tunyasuvunakool, K., Petersen, S., Jumper, J., Clancy, E., Green, R., Vora, A., Lutfi, M., ... Velankar, S. (2022). AlphaFold Protein Structure Database: massively expanding the structural coverage of protein-sequence space with high-accuracy models. *Nucleic Acids Research*, 50(D1), D439–D444. <https://doi.org/10.1093/NAR/GKAB1061>
- Waardenberg, A. J., Ramialison, M., Bouvere, R., & Harvey, R. P. (2014). Genetic Networks Governing Heart Development. *Cold Spring Harbor Perspectives in Medicine*, 4(11). <https://doi.org/10.1101/CSHPERSPECT.A013839>
- Wagner, D. E., Weinreb, C., Collins, Z. M., Briggs, J. A., Megason, S. G., & Klein, A. M. (2018). Single-cell mapping of gene expression landscapes and lineage in the zebrafish embryo. *Science*, 360(6392), 981–987. [https://doi.org/10.1126/SCIENCE.AAR4362/SUPPL\\_FILE/AAR4362\\_WAGNER\\_SM.PDF](https://doi.org/10.1126/SCIENCE.AAR4362/SUPPL_FILE/AAR4362_WAGNER_SM.PDF)
- Walker, L. J., Roque, R. A., Navarro, M. F., & Granato, M. (2021). Agrin/Lrp4 signal constrains MuSK-dependent neuromuscular synapse development in appendicular muscle. *Development (Cambridge)*, 148(21). <https://doi.org/10.1242/DEV.199790/VIDEO-1>
- Walsh, E. C., & Stainier, D. Y. R. (2001). UDP-glucose dehydrogenase required for cardiac valve formation in zebrafish. *Science (New York, N.Y.)*, 293(5535), 1670–1673. <https://doi.org/10.1126/SCIENCE.293.5535.1670>
- Weis, S. M., Zimmerman, S. D., Shah, M., Covell, J. W., Omens, J. H., Ross, J., Dalton, N., Jones, Y., Reed, C. C., Iozzo, R. v., & McCulloch, A. D. (2005). A role for decorin in the remodeling of myocardial infarction. *Matrix Biology*, 24(4), 313–324. <https://doi.org/10.1016/j.matbio.2005.05.003>
- Williams, R. M., Zipfel, W. R., & Webb, W. W. (2005). Interpreting Second-Harmonic Generation Images of Collagen I Fibrils. *Biophysical Journal*, 88(2), 1377–1386. <https://doi.org/10.1529/BIOPHYSJ.104.047308>
- Wittig, J. G., & Münsterberg, A. (2016). The Early Stages of Heart Development: Insights from Chicken Embryos. *Journal of Cardiovascular Development and Disease*, 3(2). <https://doi.org/10.3390/JCDD3020012>
- Wittig, J. G., & Münsterberg, A. (2020). The Chicken as a Model Organism to Study Heart Development. *Cold Spring Harbor Perspectives in Biology*, 12(8), a037218. <https://doi.org/10.1101/CSHPERSPECT.A037218>
- Wu, M. (2018). Mechanisms of trabecular formation and specification during cardiogenesis. *Pediatric Cardiology*, 39(6), 1082. <https://doi.org/10.1007/S00246-018-1868-X>
- Wu, M., Chen, G., & Li, Y. P. (2016). TGF- $\beta$  and BMP signaling in osteoblast, skeletal development, and bone formation, homeostasis and disease. *Bone Research*, 4(March). <https://doi.org/10.1038/boneres.2016.9>
- Yamashita, K., Mikawa, S., & Sato, K. (2016). BMP3 expression in the adult rat CNS. *Brain Research*, 1643, 35–50. <https://doi.org/10.1016/j.brainres.2016.04.057>

## BIBLIOGRAPHY

- Yelon, D., Horne, S. A., & Stainier, D. Y. R. (1999). Restricted Expression of Cardiac Myosin Genes Reveals Regulated Aspects of Heart Tube Assembly in Zebrafish. *Developmental Biology*, 214(1), 23–37. <https://doi.org/10.1006/DBIO.1999.9406>
- Zagris, N., Gilipathi, K., Soulintzi, N., & Konstantopoulos, K. (2011). Decorin developmental expression and function in the early avian embryo. *International Journal of Developmental Biology*, 55(6), 633–639. <https://doi.org/10.1387/ijdb.113321nz>
- Zhang, W., Liu, Y., & Zhang, H. (2021). Extracellular matrix: an important regulator of cell functions and skeletal muscle development. *Cell & Bioscience* 2021 11:1, 11(1), 1–13. <https://doi.org/10.1186/S13578-021-00579-4>
- Zhao, Q., Liu, X., & Collodi, P. (2001). Identification and characterization of a novel fibronectin in zebrafish. *Experimental Cell Research*, 268(2), 211–219. <https://doi.org/10.1006/excr.2001.5291>
- Zoeller, J. J., Pimpong, W., Corby, H., Goldoni, S., Iozzo, A. E., Owens, R. T., Ho, S.-Y., & Iozzo, R. v. (2009). A Central Role for Decorin during Vertebrate Convergent Extension. *Journal of Biological Chemistry*, 284(17), 11728–11737. <https://doi.org/10.1074/jbc.M808991200>

# APPENDIX

## I. List of Abbreviations

<b>Abbreviation</b>	<b>Expansion</b>
<b>ALPM</b>	Anterior Lateral Plate Mesoderm
<b>amhc</b>	atrial myosin heavy chain
<b>AV</b>	Atrioventricular
<b>BA</b>	Bulbus Arteriosus
<b>BFP</b>	Blue Fluorescence Protein
<b>BL</b>	Basal Lamina
<b>BM</b>	Basement membrane
<b>BMP</b>	Bone Morphogenic Protein
<b>BZ</b>	Borderzone
<b>CBL</b>	Cardiac Basal Lamina
<b>CBM</b>	Cardiac Basement Membrane
<b>CCV</b>	Common Cardinal Vein
<b>CJ</b>	Cardiac Jelly
<b>CM</b>	Cardiomyocyte
<b>cmlc</b>	cardiac myosin light chain
<b>CRISPR</b>	Clustered Regularly Interspaced Short Palindromic Repeats
<b>CS</b>	Chondroitin Sulphate
<b>DNA</b>	Deoxyribonucleic Acid
<b>dpab</b>	days post ablation
<b>dpci</b>	days post cryoinjury
<b>dpf</b>	days post fertilization
<b>DS</b>	Dermatan Sulphate
<b>DSHB</b>	Developmental Studies Hybridoma Bank
<b>EC</b>	Endothelial Cell

APPENDIX

<b>ECM</b>	Extracellular Matrix
<b>EDTA</b>	Ethylene Diamine Tetra Acetate
<b>EGFP</b>	Enhanced Green Fluorescence Protein
<b>EMT</b>	Epithelial to Mesenchymal Transition
<b>FIJI</b>	FIJI is just ImageJ
<b>Fn</b>	Fibronectin
<b>GAG</b>	Glycosaminoglycan
<b>HA</b>	Hyaluronic Acid / Hyaluronan
<b>hpab</b>	hours post ablation
<b>hpci</b>	hours post cryoinjury
<b>hpf</b>	hours post fertilization
<b>HS</b>	Heparan Sulphate
<b>HSPG</b>	Heparan Sulphate proteoglycan
<b>IDT</b>	Integrated DNA Technologies
<b>IGF1R</b>	Insulin Growth Factor 1 Receptor
<b>KS</b>	Keratan Sulphate
<b>LB</b>	Lysogeny Broth
<b>LG</b>	Laminin Globular
<b>LRP</b>	Low Density Lipoprotein receptor
<b>MAC</b>	Membrane Attack Complex
<b>MAPK</b>	Mitogen Activated Protein K
<b>MI</b>	Myocardial Infarction
<b>MMP</b>	Matrix metalloprotease / Matrix metallopeptidase
<b>MO</b>	Morpholino
<b>MPIHLR</b>	Max Planck Institute for Heart and Lung Research
<b>MuSK</b>	Muscle Specific Kinase
<b>MYH</b>	Myosin heavy Chain
<b>MYL</b>	Myosin light chain
<b>NLS</b>	Nuclear localization signal
<b>NMJ</b>	Neuromuscular junction
<b>PBS</b>	Phosphate buffered Saline

APPENDIX

<b>PCNA</b>	Proliferating Cell Nuclear Antigen
<b>PCR</b>	Polymerase Chain Reaction
<b>PCV</b>	Posterior Cardinal Vein
<b>PFA</b>	Paraformaldehyde
<b>PG</b>	Proteoglycan
<b>Podxl</b>	Podocalyxin
<b>Prelp</b>	proline arginine rich ends leucine rich repeat protein
<b>RFP</b>	Red Fluorescence Protein
<b>RL</b>	Reticular Lamina
<b>RNA</b>	Ribonucleic Acid
<b>RTK</b>	Receptor Tyrosine Kinase
<b>SLRP</b>	Small Leucine rich Proteoglycan
<b>SOC</b>	Super Optimal broth with Catabolite repression
<b>TBE</b>	Tris Boric Acid - EDTA
<b>Tgf<math>\beta</math></b>	Transforming growth factor beta
<b>TL</b>	Tüpfel Longfin
<b>Tnf<math>\alpha</math></b>	Tumor necrosis factor alpha
<b>VEGF</b>	vascular endothelial growth factor
<b>vmhc</b>	ventricular myosin heavy chain
<b>WT</b>	Wild Type
<b>YAP</b>	Yes-associated protein
<b>ZFIN</b>	Zebrafish Information Network

## II. Acknowledgements

I find writing the acknowledgements part to be the most difficult and emotionally challenging part of this Thesis. Primarily because it indicates that I'm at the end of the PhD as a journey but more importantly because I look back at the entire journey, many memories and emotions come to light. A PhD isn't a lonesome road, many people come along and change your life forever.

At first, I would like to thank Didier, for initially accepting me for my master's thesis, and then giving me the option to come back and start my doctoral research as well. Thanks a lot for giving me this opportunity and the freedom to develop an idea and run with it. Thanks a lot for providing an environment with an abundance of resources and scientific help. When I think about how I started this PhD, and where I am today, I realize that I have taken many different turns with the projects, and how I've been molded to think like a scientist. My approach to science has changed and matured from jelly like thoughts to structured and linked thoughts, just like the cardiac ECM and I would like to thank Didier for helping me reach this point.

A major reason for me to want to do a PhD, was because of the mentorship and guidance from Anabela. She made me see the beauty in data (especially microscopy) and in science. I would like to thank her for everything, especially for putting up with my constant puns and silly jokes, with a suitable eye roll, and then setting me off on the path to identify problem areas, try to solve them on my own, and giving me the freedom to make mistakes and learn from these mistakes. I really appreciate her answer "What do you think?" to questions I raised as this made me start to use my brain as opposed to let it sit around idle. I appreciate how she took me under her wing and taught me how to work and how not to work in the lab. I would also like to thank her for being a mentor in every sense of the term, not just in science, but also in life. A special thanks to her for putting up with my extremely short notice requests and my style of working last minute to finish things. I really appreciate all the effort she put into showing me how to do scientific research in the lab. I hope I make her proud wherever I go next.

Next, I would like to thank all the people over the many years who have impacted my life and career in this lab. A first round of thanks to Sharon Meaney-Gardian and Franziska Hainer for helping me a lot with the administrative stuff over the years. A round of thanks to Dr. Bilge Reischauer for organizing the TAC meetings and my external TAC member Prof. Virginie Lecaudey for her input on my work over the years. Special thanks to Dr. Simon Perathoner for help with documentations and for introducing me to the saving grace "ZebraBase". A round of thanks to former PhDs from the lab Deepika, Javad, Teja, Claudia, Giulia, Mohamed, Srinivas, Alessandra, Hadil, Ayele and many more (I'm sorry I'm sure I've forgotten someone here) as well as the

## APPENDIX

current PhDs Yanli, Shengnan, Marga, Agatha, Pinelopi, Armaan, Preethi, Savita for discussions, sharing reagents and creating a nice workplace environment. Special thanks to a dear friend and neighbour Kenny for being my go-to person with gene editing and for indulging me in crazy discussions over a variety of topics. I would like to thank all current and former Postdocs in the lab for all the discussions, sharing of ideas and reagents, especially Ryuichi and Carol for their straightforward no-nonsense approach to personal interactions. I would also like to thank Felix for his input and feedback on my project. I would like to thank Radhan for his crucial help with microscopy.

A special round of thanks to my Bay 8 family, especially to Hadil, Paolo, Thomas, Barbara and Agatha for dealing with my silly humor and chaotic bench. You guys made working in Bay 8 enjoyable. Special thanks to Paolo for discussion on many topics especially on things related to life and careers in academia and to Hadil for being the one person who actually laughed at my stupid jokes even though they were facepalm moments.

As a student, I learnt from everyone who had experience around me. Nobody describes experience better than Hans-Martin Maischein. Although sometimes I may not agree with him on the way he approaches things, I really learnt a lot from him about working with zebrafish embryos, and popular music of the 20<sup>th</sup> century during our microinjection sessions and I would like to thank him a lot for that. I would like to especially thank him for being a friend in need and for providing support even when waking up early in the morning is not really his thing. I would also like to thank Nana for teaching me how to CRISPR and for showing me that endless optimism and energy is not a myth. I would also like to thank all the technical support staff of the lab, Carmen Büttner, Sarah Howard, Petra Neeb, Marianne Ploch, Carmen Kremser, as well as the late Beate Grohmann for all their support over the years.

A PhD is enriched by the friends who come along with you. I would like to thank a few special people who really changed my definition of friendship. First of all, I would like to mention Martin Laszczyk, a true friend and fellow football enthusiast and my first friend outside the lab, thanks a lot for being available to me whenever I needed you and showing me that life outside the lab can be fun too. I would like to mention Leonie, for being the person to push me out of my comfort zone (especially with eating healthy) and making me look at life from different perspectives. Your influence on me is immense and I would like to thank you for putting up with my constant nonsense, hopefully also in the future. I would like to thank my primary fitness motivator Vahan, for all the long scientific and political discussions and showing me how to deal with adversity with a positive outlook. I would also like to thank João, Inês, Adriana, Marco, Pooja and Malarvizhi for being very supportive and encouraging especially in my many moments of need throughout this journey. A quick shout out to Luv and Kush for showing me the lighter side of life and demonstrating that mischief and unpredictability are the purest sources of humour.

I would also like to thank my PhDnet family, especially my dear Offspring team. You all showed me the joy of collaboration and collective thinking and showed me how to be organized and I cannot thank you enough for that. A special shout out to my brother in arms Nikolai Hörmann for coming along for



## APPENDIX

the ride with the Podcast and taking part alongside me in the journey through the vast administrative wilderness of the MPG.

Finally, I would like to thank my family for being very supportive and encouraging throughout this journey. I would like to especially thank my parents Ramkumar Ranganathan and Kamakshi Srinivasan for being my emotional rock throughout my life and career. Since childhood, I know that I've been a difficult person to deal with, especially by the way I used to question everything and try to explore and take apart every new thing that I came across. You let me explore a life and career in asking questions and trying to take apart and reassemble the very essence of life by letting me pursue Biology (although I know that you would have preferred that I studied something that pays well like computer science) and I would really like to thank you for that. I can only hope that I make you proud.

In case you have read this far, I would like to thank you for doing that as well.

The things I learnt most from doing science was patience, and prioritization. Hence I would like to leave you all with one of my favourite quotes from Albert Einstein

*“The only reason for time, is so that everything  
doesn't happen at once”.*

## III. Curriculum Vitae

### Srinath Ramkumar

#### Personal details

Nationality: Indian

Gender: Male

#### Language Proficiency

English (Native), Tamil (Native), German (B1-B2), Hindi (Colloquial Spoken), Sanskrit (A1), Kannada (Colloquial Spoken)

#### Technical Proficiency

MatLab, PyMOL, C, C++, AutoCAD, HTML, Python (basic), IMARIS, Fiji, R

#### Education

August 2013 – July 2018

**Master of Science (Hons.)** in Biological Sciences from Birla Institute of Technology and Science, Pilani, K K Birla Goa Campus, India

Thesis Title: “Immune Response during cardiac valve regeneration of the Zebrafish”

**Bachelor of Engineering (Hons.)** in Chemical Engineering from Birla Institute of Technology and Science, Pilani, K K Birla Goa Campus, India

Thesis Title: “Fluid dynamics of blood flow during zebrafish cardiac valve regeneration”

#### Conferences

12-14 May 2022 Poster Presentation at “Weinstein cardiovascular conference” – Marseille, France

## APPENDIX

Poster title: “Extracellular Matrix Proteoglycan Prelp modulates laminin mediated cardiac morphogenesis”

### Scientific publications

1. **Srinath Ramkumar**, Anabela Bensimon-Brito, Stefan Günther, Didier Stainier, “Extracellular Matrix Proteoglycan Prelp modulates laminin mediated cardiac chamber morphogenesis”, *manuscript in preparation*
2. Bensimon-Brito, Anabela, **Srinath Ramkumar**, Giulia LM Boezio, Stefan Guenther, Carsten Kuenne, Christian SM Helker, Héctor Sánchez-Iranzo et al. "TGF- $\beta$  signaling promotes tissue formation during cardiac valve regeneration in adult zebrafish." *Developmental cell* 52, no. 1 (2020): 9-20.
3. Bensimon-Brito, Anabela, Giulia LM Boezio, João Carneira-da-Silva, Astrid Wietelmann, **Srinath Ramkumar**, Pia R. Lundegaard, Christian SM Helker et al. "Integration of multiple imaging platforms to uncover cardiovascular defects in adult zebrafish." *Cardiovascular Research* (2021).
4. Tarasco, Marco, Paulo J. Gavaia, Anabela Bensimon-Brito, João Carneira-da-Silva, **Srinath Ramkumar**, Fabrice P. Cordelières, Stefan Günther et al. "New insights into benzo [ $\alpha$ ] pyrene osteotoxicity in zebrafish." *Ecotoxicology and Environmental Safety* 226 (2021): 112838.
5. Ramachandran, Ramya, Swetha Ramesh, **Srinath Ramkumar**, Arunaloke Chakrabarti, and Utpal Roy. "Calcium alginate bead-mediated enhancement of the selective recovery of a lead novel antifungal bacillomycin variant." *Applied biochemistry and biotechnology* 186, no. 4 (2018): 917-936.

### Certifications

- FELASA (Federation of European Laboratory Animal Science Association) accreditation for fish (2019) and rodent (2021).

### Scientific Technical proficiencies

- Molecular biology techniques
- Genome engineering using CRISPR/Cas9
- Advanced microscopy using ZEISS LSM Confocal Microscopes and Leica SP confocal microscopes
- Histology: in situ hybridization, immunohistochemistry
- Embryological techniques: zebrafish husbandry and maintenance, microinjection
- Animal handling and experimentations: Zebrafish adult: heart cryoinjury, dissection, IP injections, RO injections,

## APPENDIX

Echocardiography, genotyping; Mouse : IP injections, IV injections, surgery, and dissection

### Extracurriculars

Coordinator and Editor in Chief of Offspring Magazine– Max Planck PhDnet (January 2019 – December 2021)

- Organization, Writing and Publication of official annual magazine of the Max Planck PhDnet.
  - Notable Example :  
[https://www.phdnet.mpg.de/121484/20191028\\_CRISPR?c=22833](https://www.phdnet.mpg.de/121484/20191028_CRISPR?c=22833)
  - Magazine Example:  
<https://www.phdnet.mpg.de/outreach/offspring-blog>
- Production, Hosting, Editing and Publishing of the weekly science communication podcast of the Max Planck PhDnet.
  - Founded the Podcast
  - Hosted 34 episodes, and Produced
  - Notable Example: Interview with Dr. Neil DeGrasse Tyson :  
<https://youtu.be/kv0Eb8DvzPc>
  - Other episodes: <https://podfollow.com/offspring-podcast/view>

Managed and organized a team of 25 PhDs involved in production of weekly podcast episodes and design and layout of annual magazine.